Dissertation zur Erlangung des akademischen Grades eines Doktors der Ingenieurwissenschaften (Dr.-Ing.)
im
Fachbereich Elektrotechnik/Informatik der Universität Kassel

Simulation and Design of a high speed Solid State Switch for Excimer Laser

UNIVERSITÄT KASSEL
FB 16 Elektrische Energieversorgungssysteme

by
Dipl. Ing. (FH), MEng Claus Strowitzki

First Director: Prof. Dr.-Ing. Peter Zacharias
Second Director: Prof. Dr.-Ing. Albert Claudi

Submitted: August 2008

Disputation: 9.March2009

Acknowledgement

The practical work was done during my employment with Coherent GmbH subsidiary Munich.
For the success of this work I want to thank several people:

First of all, my tutor in the University of Kassel, Prof. Dr. Peter Zacharias for his very good supervision and enthusiasm for this subject,

my supervisor at Coherent Dr. Sebastian Spörlein for his encouragement,

my colleagues in the department Laser Discharge Unit Munich, Dr. Andreas Görtler, Michael Baumann, Ansgar Matern, Sacha Djordjevic, Dr. Jochen Wieser and Michael Bauer who always supported me,

Karl Auwärter for his linguistic help and

my wife Karola Strowitzki for her patience and understanding.

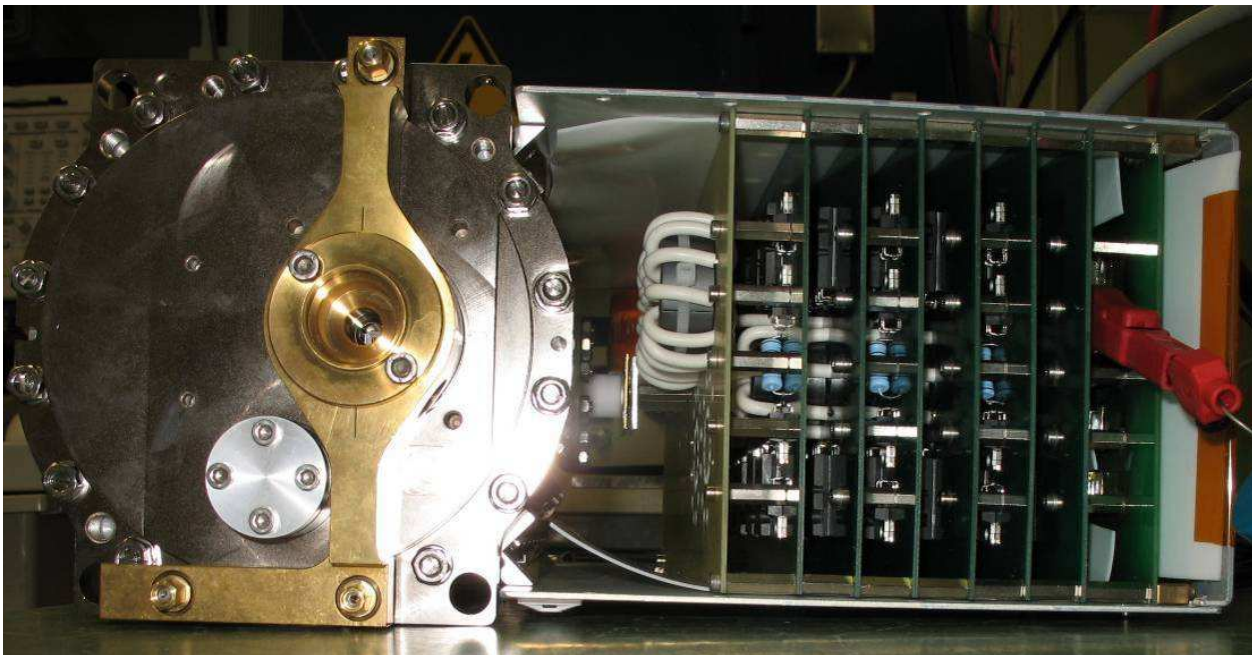

Fig. 1: The topic of this work: Solid state switch for Excimer laser

Erklärung

Hiermit versichere ich, dass ich die vorliegende Dissertation selbständig und ohne unerlaubte Hilfe angefertigt und andere als die in der Dissertation angegebenen Hilfsmittel nicht benutzt habe. Alle Stellen, die wörtlich oder sinngemäß aus veröffentlichten oder unveröffentlichten Schriften entnommen sind, habe ich als solche kenntlich gemacht. Kein Teil dieser Arbeit ist in einem anderen Promotions- oder Habilitationsverfahren verwendet worden.

……

Dipl. Ing. (FH), MEng Claus Strowitzki

Zusammenfassung

Excimerlaser sind gepulste Gaslaser, die Laseremission in Form von Linienstrahlung – abhängig von der Gasmischung – im UV erzeugen. Der erste entladungsgepumpte Excimerlaser wurde 1977 von Ischenko demonstriert. Alle kommerziell verfügbaren Excimerlaser sind entladungsgepumpte Systeme.
Um eine Inversion der Besetzungsdichte zu erhalten, die notwendig ist, um den Laser zum Anschwingen zu bekommen, muss aufgrund der kurzen Wellenlänge sehr stark gepumpt werden. Diese Pumpleistung muss von einem Impulsleistungsmodul erzeugt werden. Als Schaltelement gebräuchlich sind Thyratrons, Niederdruckschaltröhren, deren Lebensdauer jedoch sehr limitiert ist. Deshalb haben sich seit Mitte der 1990iger Jahre Halbleiterschalter mit Pulskompressionsstufen auch in dieser Anwendung mehr und mehr durchgesetzt.
In dieser Arbeit wird versucht, die Pulskompression durch einen direkt schaltenden Halbleiterstapel zu ersetzen und dadurch die Verluste zu reduzieren sowie den Aufwand für diese Pulskompression einzusparen. Zudem kann auch die maximal mögliche Repetitionsrate erhöht werden.
Um die Belastung der Bauelemente zu berechnen, wurden für alle Komponenten möglichst einfache, aber leistungsfähige Modelle entwickelt. Da die normalerweise verfügbaren Daten der Bauelemente sich aber auf andere Applikationen beziehen, mussten für alle Bauteile grundlegende Messungen im Zeitbereich der späteren Applikation gemacht werden.
Für die nichtlinearen Induktivitäten wurde ein einfaches Testverfahren entwickelt um die Verluste bei sehr hohen Magnetisierungsgeschwindigkeiten zu bestimmen. Diese Messungen sind die Grundlagen für das Modell, das im Wesentlichen eine stromabhängige Induktivität beschreibt. Dieses Modell wurde für den „magnetic assist“ benützt, der die Einschaltverluste in den Halbleitern reduziert.
Die Impulskondensatoren wurden ebenfalls mit einem in der Arbeit entwickelten Verfahren nahe den späteren Einsatzparametern vermessen. Dabei zeigte sich, dass die sehr gebräuchlichen Class II Keramikkondensatoren für diese Anwendung nicht geeignet sind. In der Arbeit wurden deshalb Class I Hochspannungs- Vielschicht- Kondensatoren als Speicherbank verwendet, die ein deutlich besseres Verhalten zeigen.
Die eingesetzten Halbleiterelemente wurden ebenfalls in einem Testverfahren nahe den späteren Einsatzparametern vermessen. Dabei zeigte sich, dass nur moderne Leistungs-MOSFET´s für diesen Einsatz geeignet sind. Bei den Dioden ergab sich, dass nur Siliziumkarbid (SiC) Schottky Dioden für die Applikation einsetzbar sind.
Für die Anwendung sind prinzipiell verschiedene Topologien möglich. Bei näherer Betrachtung zeigt sich jedoch, dass nur die C-C Transfer Anordnung die gewünschten Ergebnisse liefern kann.
Diese Topologie wurde realisiert. Sie besteht im Wesentlichen aus einer Speicherbank, die vom Netzteil aufgeladen wird. Aus dieser wird dann die Energie in den Laserkopf über den Schalter transferiert.
Aufgrund der hohen Spannungen und Ströme müssen 24 Schaltelemente in Serie und je 4 parallel geschaltet werden. Die Ansteuerung der Schalter wird über hochisolierende „Gate“-Transformatoren erreicht.
Es zeigte sich, dass eine sorgfältig ausgelegte dynamische und statische Spannungsteilung für einen sicheren Betrieb notwendig ist.
In der Arbeit konnte ein Betrieb mit realer Laserkammer als Last bis 6 kHz realisiert werden, der nur durch die maximal mögliche Repetitionsrate der Laserkammer begrenzt war.

Table of Figures

Table of Contents

1 Introduction

1.1 History of Excimer Laser

The theoretical basis for the laser was established in 1917 when Einstein[1] postulated the theoretical concept of stimulated emission.
It took 43 years to prove this theoretical work by Mainman with the building of the first ruby laser, the first visible laser.
The first Excimer laser was built 1971 by Basow[2]. The early Excimer lasers were very sensitive devices. This changed in the last decade dramatically. Nowadays Excimer lasers are working horses in many applications.
Excimer laser are discharge pumped gas lasers which emit laser light in the UV-range of the spectrum. Compared to other UV Lasers the efficiencies are quite good in the range of one to five percent.
Due to the high operation voltage, the high gas pressure, the reactive gas and the very intense UV beam Excimer lasers are still expensive and technological demanding devices.
The development of the lasers is still in progress to reduce operating cost and improve performance. Several technological breakthroughs happened in the last 20 years. The introduction of dust remover system in the tube, the replacement of all-plastic by ceramics, corona pre ionization, solid state pulsed power modules, optic purging, metal sealing and calcium fluoride optics, to address some of the important events.

1.2 Laser basics

The word “LASER” itself is a shortcut of **L**ight **A**mplification by **S**timulated **E**mission of **R**adiation. The understanding in this work is a source of an intensive coherent light field.
The laser has a close analogy to an electric amplifier which has a positive feedback loop. It is well known that this arrangement tents to start oscillation, if the feedback is positive and the amplification is higher than the losses.

Oscillation condition: Amplification > losses

The same happens in a laser. The light is amplified by a light amplifying medium.
A light amplifying medium is called inverted, because normally the lower levels are more populated than the upper levels. Under certain conditions, it is possible to change this. Then the upper levels are more populated than the lower levels.
Such a medium amplifies light by stimulated emission. The feedback is realized by two mirrors forming a resonator. One mirror has a 100 % reflection (or very close to that) and the other has a transmission of some percent (or less than 100 % reflection).
The optical properties of the laser beam, for example the bandwidth, are mainly determined by the optical resonator.

1.3 Pumping requirements

For laser operation inversion is needed. This requires not only the pumping of the upper lever but also depletion of the lower level. Otherwise due to the operation itself the lower level will get highly populated and the inversion will be destroyed and only a very short laser pulse is possible. This happens in nitrogen lasers.
Houtermans[3] proposed in 1960 to use molecules that can exist in an upper level but are unstable in the lower level as a laser medium.
One family can be formed with a combination of rare gas and a halogen. The first rare gas - halogen laser was the electron pumped XeBr- laser from Searles and Hart[4] in 1975. The name Excimer is the short form of excited dimer because it can only exist in excited state. The first discharged pumped Excimer laser, a XeCl - laser was constructed in 1977 by Ischenko et al..
A discharged pumped Excimer laser has many advantages compared to an electron beam pumped laser. Electron beam pumped laser can produce very high energy but are single pulse devices. These lasers are huge and were used for fusion research and military applications.
All commercial used Excimer lasers are discharged pumped.

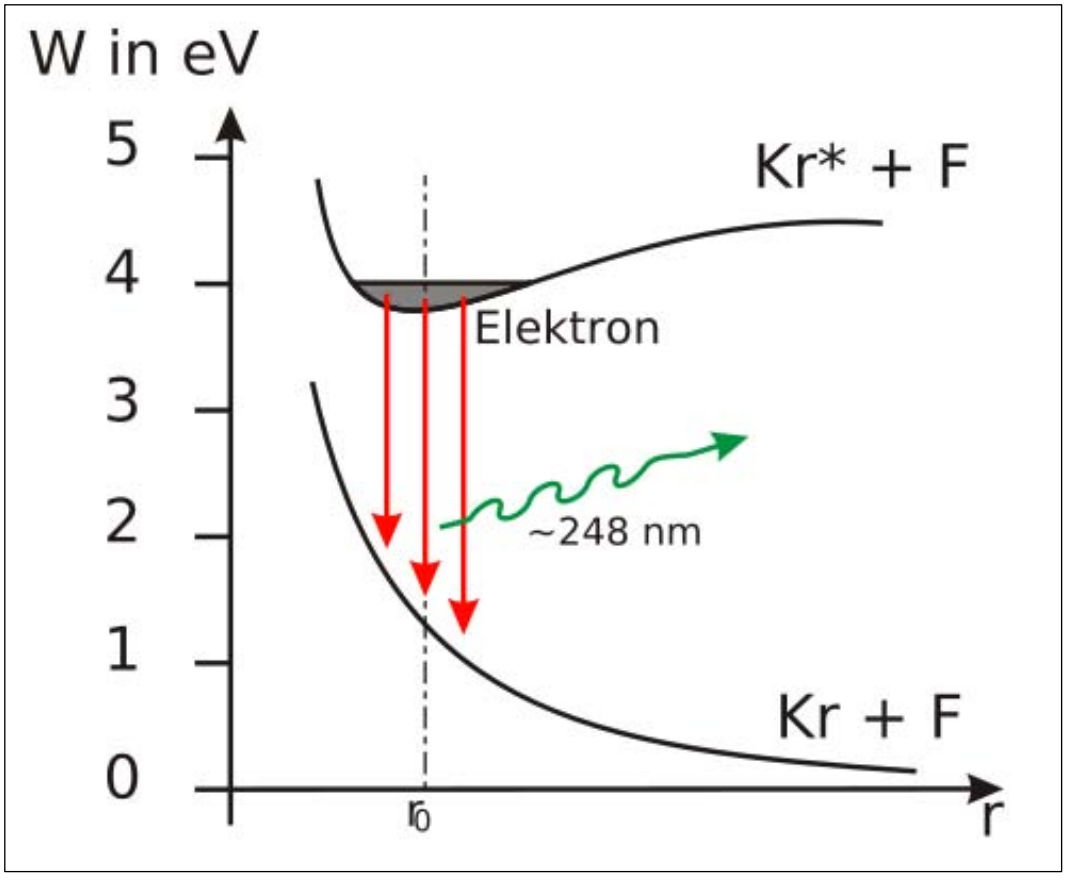

Fig. 2: Energy level in a KrF* molecule (Wikipedia "Excimer laser")

The potential energy of the lower level decreases with larger inter-nuclear distance. This means that the rare gas atom and the halogen atom repel each other and the molecule falls apart. Actually KrF is loosely bonded in the X-state (around 1 eV). However, thermal vibrations are already strong enough to break this weak bound.
Excimer lasers have high quantum efficiency. The radiant transition is directly related to the ground level. For the most important formation channel at least one Kr^+ is needed to create a KrF* molecule. The theoretical maximum obtainable quantum efficiency is ca 33 % (12 eV ionization, 4 eV radiations). In practice, the highest reported efficiency for a discharge pumped KrF* Laser is ca 4 %. In the test laser system used in this thesis, the maximum efficiency is ca 2 %.
Due to the short wavelength the pumping density in an Excimer laser has to be very high. It is ca 100 J/l. Due to the very short pumping time the pumping power density is remarkably high, in the range of 10 GW/l.
To provide such a high power density a capacitor discharge circuit is used. The challenges of the laser head design are the low inductivity of the laser head (20 nH down to 1 nH), the gas tightness and the cleanness.

1.4 Requirements for the pulsed power module

The capacitors which are located directly to the laser head are traditionally called peaking capacitors. The purpose of the pulsed power module is to charge up these peaking capacitors. For best laser performance it is necessary to charge the peaking capacitors in less than 100 ns. One reason is that due to the fast voltage rise time the peak voltage is high (due to ignition delay) and so the pump energy is high. Another reason is that the pre-ionization of the laser works at the same time frame as the charging time of the peaking capacitors and has to be fast, too. The pre-ionization produces electrons in the discharge region to ensure a stable homogenous glow discharge.
Pulsed power modules for Excimer lasers are quite challenging (see Tab. 1).

Energy:	0.2 J up to 50 J
Voltage:	8 kV up to 40 kV
Charge Time:	50 ns up to 150 ns
Peaking Capacity	2 nF up to 100 nF
Average Power	up to 50 kW
Repetition Rate:	up to 10 kHz
Laser Energy	2 mJ up to 2 J

Tab. 1: Typical requirements for the pulsed power of an Excimer laser

Apart from these facts, a perfect matching of the pulsed power module to the laser head is not possible due to the extreme non linear behavior of the discharge (open to close to a short circuit). Hence a fraction of the energy (up to 50%) is reflected by the laser head and has to be handled by the pulsed power module. This reflected energy can lead to destruction of components or tends to causes ringing in the circuit with the result of additional wear of the laser tube.
The control of the reflected energy is one key to a reliable operation of the laser.

1.5 Standard technology for the pulsed power module

The classic approach is a C-C transfer circuit with a Thyratron switch[5]. The schematic circuit is shown in Fig. 3.
The bank is charged by a capacitor charger. By triggering the Thyratron the energy of the bank is transferred to the peaking capacitors. The peaking capacitors are charged up to the point where the discharge ignites and the energy is transferred in the plasma of the laser discharge.

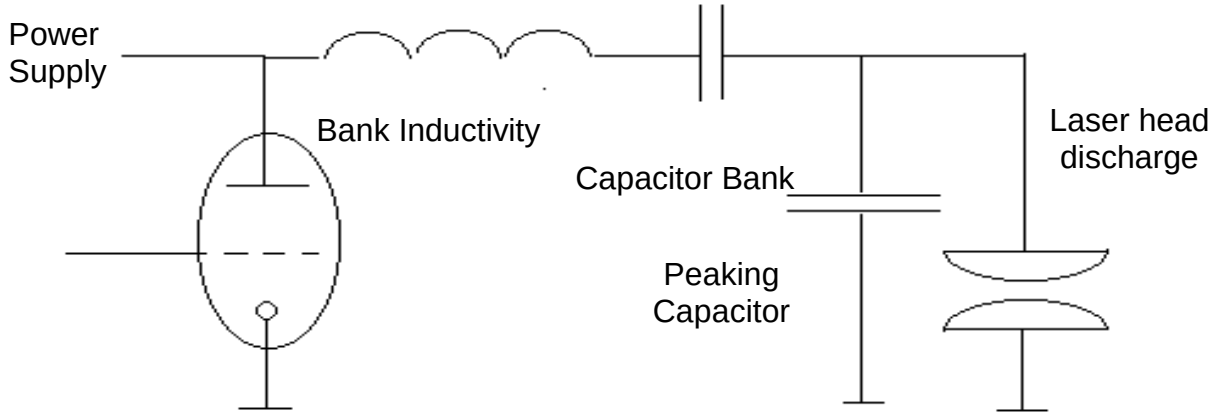

Fig. 3: Schematic of an C-C transfer Thyratron circuit

Pros:	Cons:
Very simple design	Limited life time and repetition rates
Low trigger-to-light delay and jitter	No energy recovery
Low investment	Warm-up time

Tab. 2: Typical characteristics of a Thyratron pulser

The main advantage is a very simple design and the low investment (Tab. 2). This design is still used in lasers, however better solutions are available even there even there.
The modern approach is a solid state switch with magnetic pulse compression. These circuits consist of much more components because the switching capability of the solid state switches does not fulfill the requirements of this application. The voltage and current rise is typically a factor of 100 to 1000 smaller than needed to ignite the laser discharge. A pulse transformer is needed to match the voltage. Several magnetic pulse compression stages match the time frame of the pulse. Fig. 4 shows a typical configuration for a solid state pulser with magnetic pulse compression. The basic properties of such a circuit are shown in Tab.3.

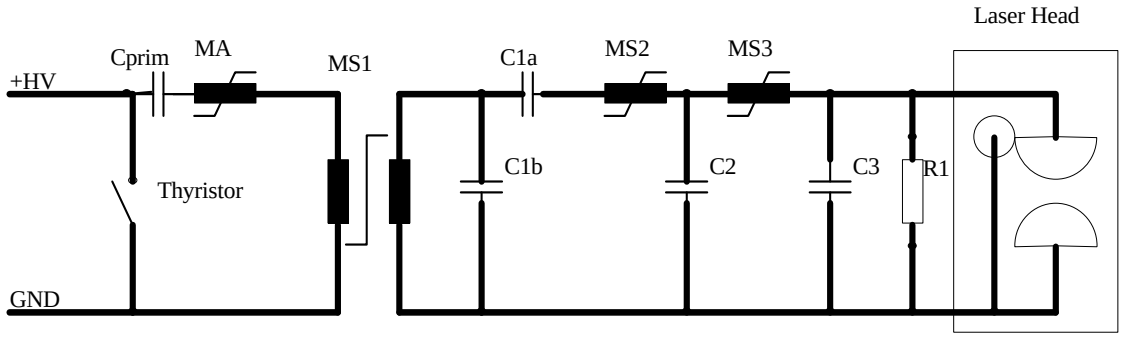

Fig. 4: Schematic of a Solid state circuit with magnetic pulse compression

Pros:	Cons:
Very high life time (>10G pulses)	Complex design
Energy recovery (tube life time!)	Long trigger-to-light delay (5µs)
Low charging voltage (1.5kV)	High trigger-to-light delay, drift and jitter
	Moderate efficiency (70%)

Tab. 3: Typical characteristic of a solid state circuit with magnetic pulse compression

One important feature of these solid state pulsers is the energy capability to recover. The energy which is reflected by the discharge swapped back in the capacitor bank and could there stored to be re used in the next pulse. Due to the store in the bank ringing tendencies are avoided and hence stress for all components is reduced including the laser head.

1.6 Motivation

Solid state pulsed power modules are the standard in many types of Excimer lasers for several applications.
Due to the progress in semiconductors switching, it is possible to overcome the pulse transformer and magnetic pulse compression, by a one to one replacement of a Thyratron with a semiconductor stack.
First basic calculations indicate that such a solution is possible and economical for very small and extremely high repetition rate Excimer laser (Tab. 4).

Bank energy:	0.2 J
Voltage:	15 kV
Charge Time:	100 ns
Peaking Capacity	2 nF
Average Power	2 kW
Repetition Rate:	10 kHz
Laser Energy	2 mJ

Tab. 4: Overview of the proposed circuit

The benefits are extremely good timing control, very good efficiencies of the pulsed power module (up to 90%) and nearly unlimited repetition rates.

A first attempt was done by Claudia Hartmann[6]. This first work was not successful because of wrong circuit topology and the lack of appropriate diodes.
The principle design is quite simple but the amount of components, due to the stacked semiconductors, are comparable to a solid state circuit with magnetic pulse compression.
Possible applications of such a small Excimer laser are inspection and detection systems for wafers and masks in the optical lithography.
In this thesis one seeks to get a basic understanding of such a circuit and the related components.
Different semiconductors are tested in a test circuit and simulation models are built. With these results a real stack is built up and compared with the calculated results.
The passive components are often neglected in power electronics. It turns out that in pulsed power the behavior and the technology of passive components is as demanding as of the active components.

2 Simulation of the components

To calculate the stress of the components simulations are a very helpful tool. The basis of the simulation is the models for the components.
The development of reliable models of the components is the most critical part of the simulation. A golden middle has to be found between accuracy and complexity.
In this work it is tried to develop very simple models to accelerate optimization speed.
Because nonlinear magnetic components have in pulsed power a very important role special focus is taken on these parts. It is amazing what is possible with such parts. It starts from magnetic diodes, magnetic assist to magnetic pulse compression. The proposed model covers all the applications without adaptations.
The models are made from a phenomenological point of view. This helps to reduce efforts and it shows that the accuracy is high enough for our simulation.

2.1 Nonlinear cores and coils

On the markets an enormous amount of different materials for magnetic components are available. There a two main categories of material, the ferrites and the metallic materials.
The ferrites are easy to form to very odd shapes and generally used in small and medium power application. The metallic components are used in high power applications and could be produced only in toroid or cut cores. Between these categories there are the metal powder cores which are not considered in this work.
The ferrite can be also divided into two categories. The commonly used manganese zinc ferrites and the nickel zinc ferrites.
The nickel zinc ferrites are mainly used for EMI suppression and high frequency application. Manganese zinc ferrites are conductive, so eddy current play a big role and causes high losses at high frequencies and high flux densities. Zinc ferrites have nearly insulating properties and showing very low losses even at very high frequencies.
The metallic materials can be divided into three sub categories:

- the amorphous material;
- the nano-crystalline materials;
- the classic crystalline materials (Permaloy).

The nano-crystalline material shows the best performance and is less expensive due to the high iron content (amorphous material consists of mainly cobalt and nickel).
This work will only focus on nickel zinc ferrites and nano crystalline cores. The results could be easily transferred to all other available materials.
Silicon iron (transformer) cores are also not considered (not suitable for application in the 100 ns range) and the wide family of iron nickel alloys (too expensive in comparison with the amorphous and nano-crystalline materials).

2.1.1 Measuring of the core parameters

In the data sheets of core suppliers all data are normally provided for small signals in the linear range of the core. In pulsed power application the core is normally driven in saturation at very high speed. These data are normally not available.

The mathematic description of the losses in a hysteresis loop is normally given by:

$$W = \int BdH$$

W: energy (J)
B: magnetic flux density (T)
H: Magnetic field (A/m)

For measurements it is more practical to use this definition:

$$W = \int HdB$$

The reason is that it is not possible to measure the absolute magnetic flux. The change in magnetic flux could be measured directly with an induction loop.

$$W = \int HdB \qquad H_{(t)} = \frac{I_{(t)}}{l} \qquad B = \frac{1}{A}\int Udt$$

$$W = \frac{1}{Al}\int I_{(t)}U_{(t)}dt$$

A: magnetic core diameter (m^2)
l: Magnetic path length (m)
U: induction voltage (V)
I: magnetization current (A)
W: energy (J)

This equation provides the core losses in the case that magnetization is in a complete loop.
It is very difficult to measure this fast magnetization. It is necessary to use a fast and powerful voltage generator.
It is possible to overcome this problem by magnetizing the core in one direction by using a simple switch and then to reconstruct the entire loop.
The result of these calculations is:

$$W = \frac{2}{Al}\int_0^{t_1} I_{(t)}U_{(t)}dt - \frac{I_{(t_1)}}{Al}\int_0^{t_1} U_{(t)}dt$$

A: magnetic core diameter (m^2)
l: Magnetic path length (m)
U: induction voltage (V)
I: magnetization current (A)
W: energy (J)

The first term represent the total energy stored in the core including the energy which is in the magnetic field. The energy of the magnetic field is not lost and causes no heating. So it has to be subtracted from the total energy. This is the second term.

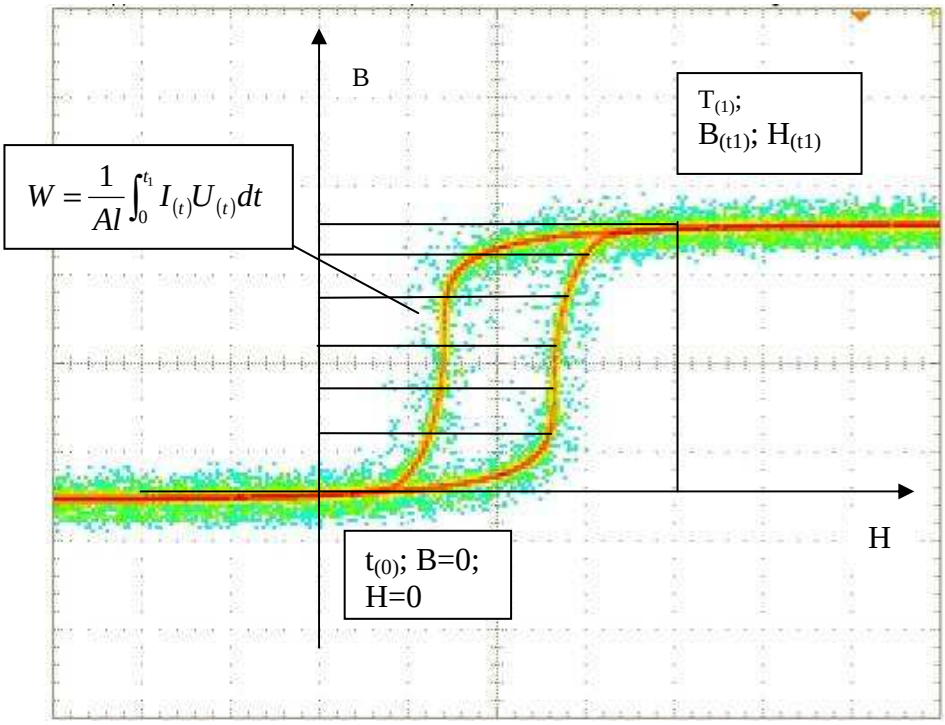

Fig. 5: Magnetization curve and calculations

In the upper equitation T_1 marks the point where the magnetization is complete, the core is saturated.
The first term describes the real losses in the core (the same equation as for a resistor) while the second term describes the energy stored in the magnetic field. The value of the term is normally almost negligible. The calculation could be seen in Fig. 5.
The test circuit is very simple due to the fact that only one branch of the magnetization loop is needed:

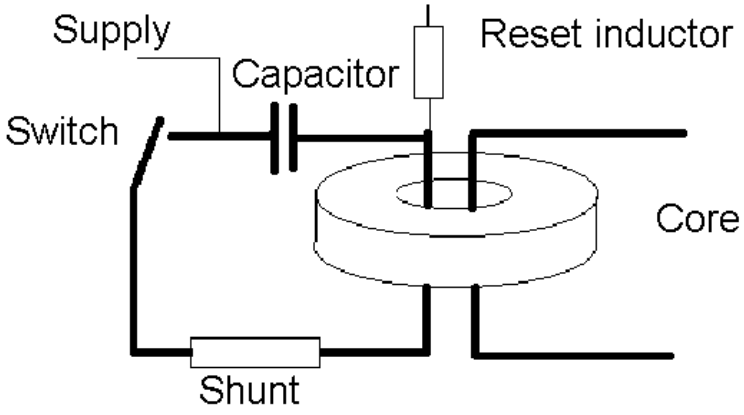

Fig. 6: Schematic of the test circuit

The capacitor is charged by a high voltage power supply. The value of the voltage depends on the magnetization speed and the cross section of the core. In the real test voltages up to 4kV are needed. The switch itself is a very simple manually triggered hand-made part (see Fig.7). The advantage of such a switch is the huge trigger range, the simple construction, toughness and the very fast switching speed.
For the current measurement a low inductivity shunt resistor is used. The induction voltage is measured with an 1:100 probe (Fig. 7).
The waveforms are acquired by a digitizing oscilloscope. The integrals terms are calculated by the oscilloscope (Fig. 8). The dimensions of the cores are available by the manufacturer or could be measured.

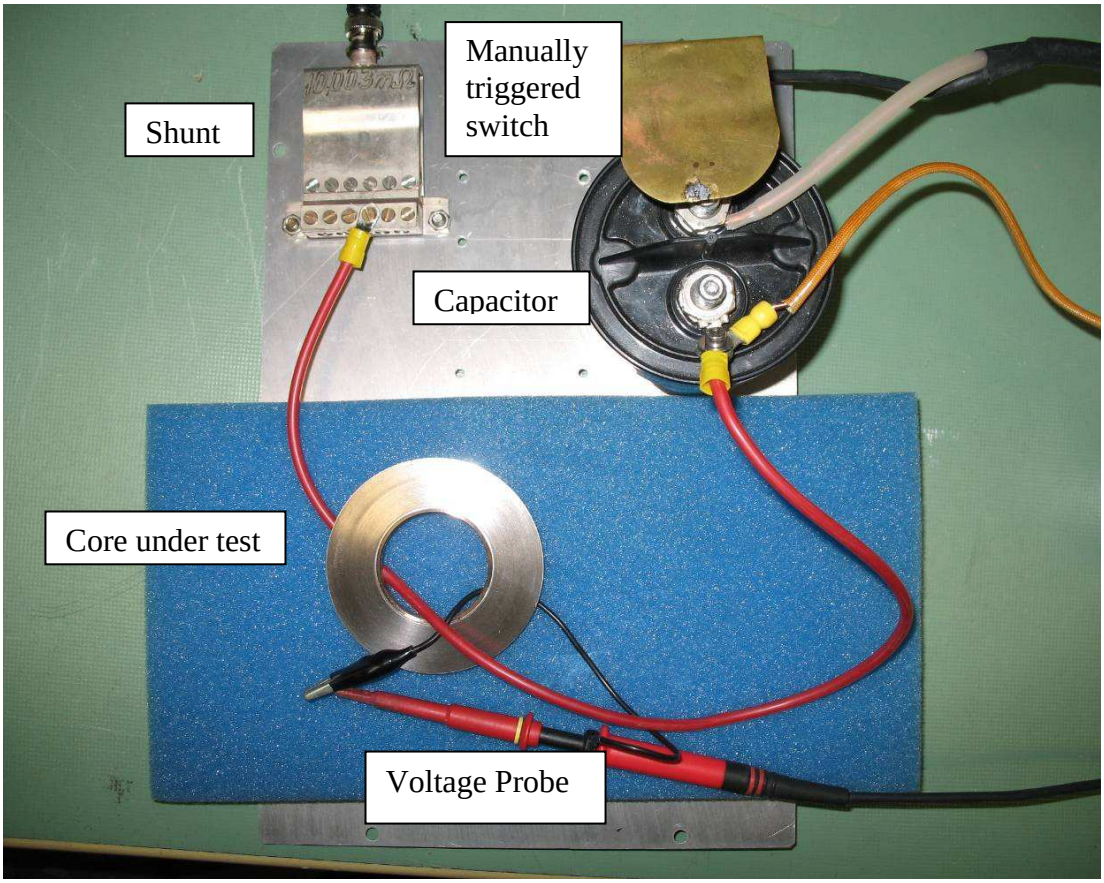

Fig. 7: Test circuit

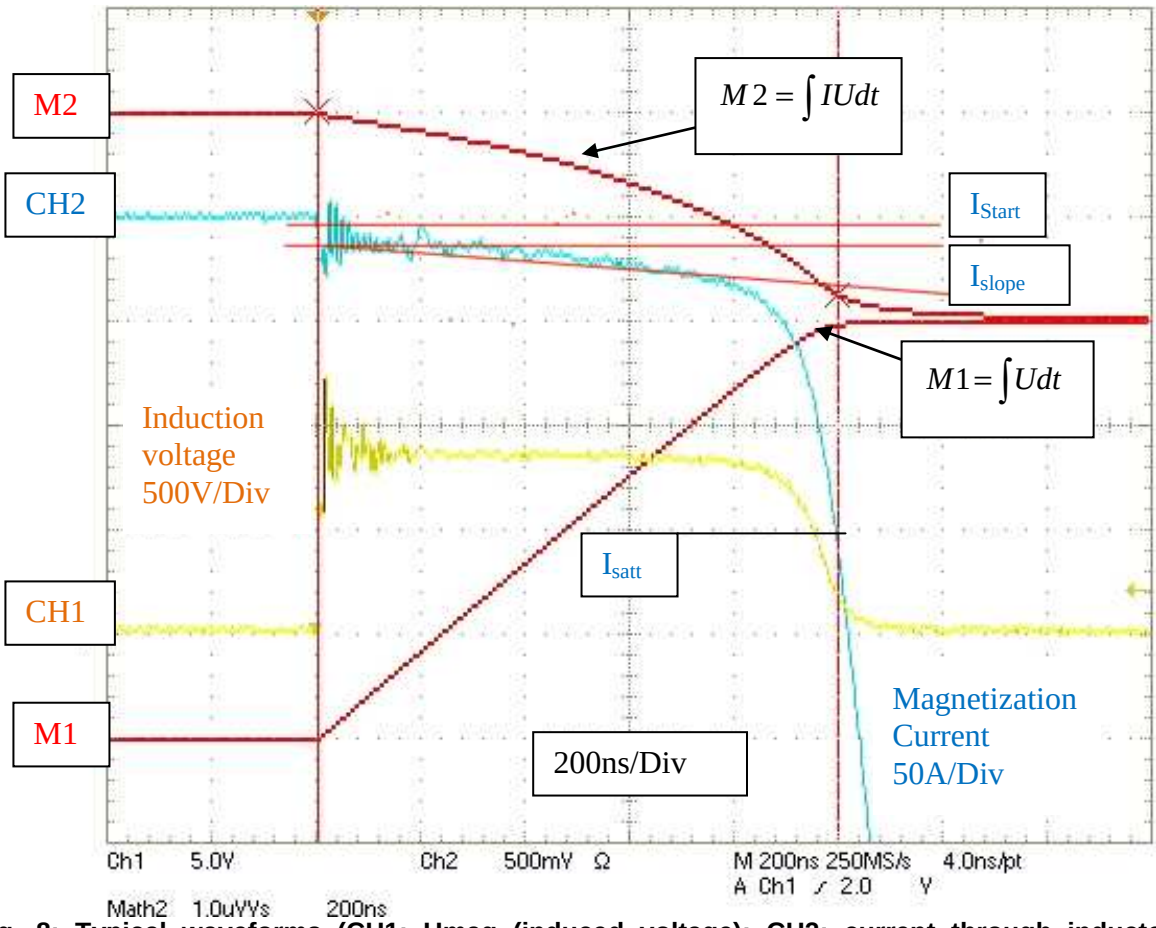

Fig. 8: Typical waveforms (CH1: Umag (induced voltage); CH2: current through inductor; M1: calculation of the voltage time integral; M2: total energy in core)

The equivalent electrical circuit is normally described by a parallel resistor representing the core losses and a series resistor representing the winding losses (Fig. 9).

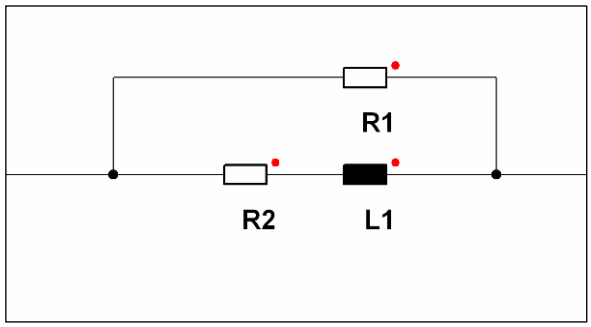

Fig. 9: Equivalent electrical circuit for an inductor with core (R1 equivalent resistor for core losses; R2 Equivalent resistor for copper losses)

R1 (equivalent for the core losses) can be calculated:

$$R_1 = U_{mag} / I_{start}$$ (see Fig. 8)

U_{mag} : induced voltage (V)
I_{Start}: current step (A)

It is normally in the range of 20 to 100 Ohms.
Another way to calculate the R_1 is to start from the calculated losses.

$$R_1 = \frac{\left(\int Udt\right)^2 * n^2}{e * dt * V}$$

$\int Udt$: Voltage time integral (Vs)

n: turns of winding
e: loss per core volume (J/m^3)
dt: magnetization time (s)
V: core volume (m^3)

The calculation based on this equitation is more precise because the losses are calculated from the whole magnetization time, not only from the starting point.

From the slope of the magnetization current it is possible to calculate the inductivity of the coil with an unsaturated core.

$$L_1 = U_{mag} / \frac{dI_{slope}}{dt}$$ (see Fig. 7)

U_{mag} : Induced voltage (V)
dI_{slope}: rise of the current (A)

From the inductivity of the coil and the geometry of the core it is possible to calculate the permeability of the material.

$$L_1 = \mu_0 \mu_r A / l$$

$$\mu_r = \frac{lL_1}{A\mu_0}$$

μ_r : relative permeability

μ_0 : vacuum permeability

A: magnetic core diameter (m^2)
l: Magnetic path length (m)

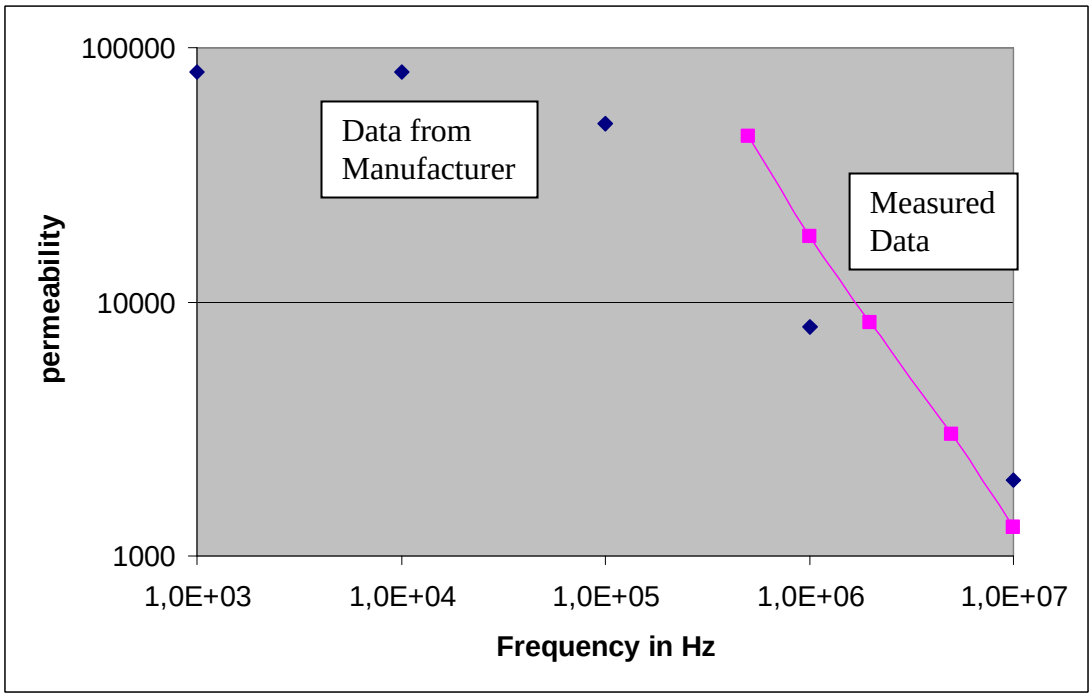

Fig. 10: Permeability at different magnetization speeds[7]

The reason for the reduction of the permeability is the eddy current in the ribbons of the core (Fig. 10). Due to the eddy current the magnetic flux is squeezed out. In the model the hysteresis of the material is not included because the eddy current is dominant. This means that the main losses are produced by eddy current, the hysteresis is negligible. This reduces further the complexity of the model.
The inductivity of the inductor with a saturated core could be calculated simply by the geometry of the winding or measured with the air core model. This approximation is only possible if the material goes hard into saturation like metal cores, this means $\mu_r = 1$. Ferrites are normally harder to saturate and even with very high current it is never fully saturated. Normally it is enough to calculate with $\mu_r = 2$.
For simulation of the nonlinear inductor all needed data are known (Fig. 11).

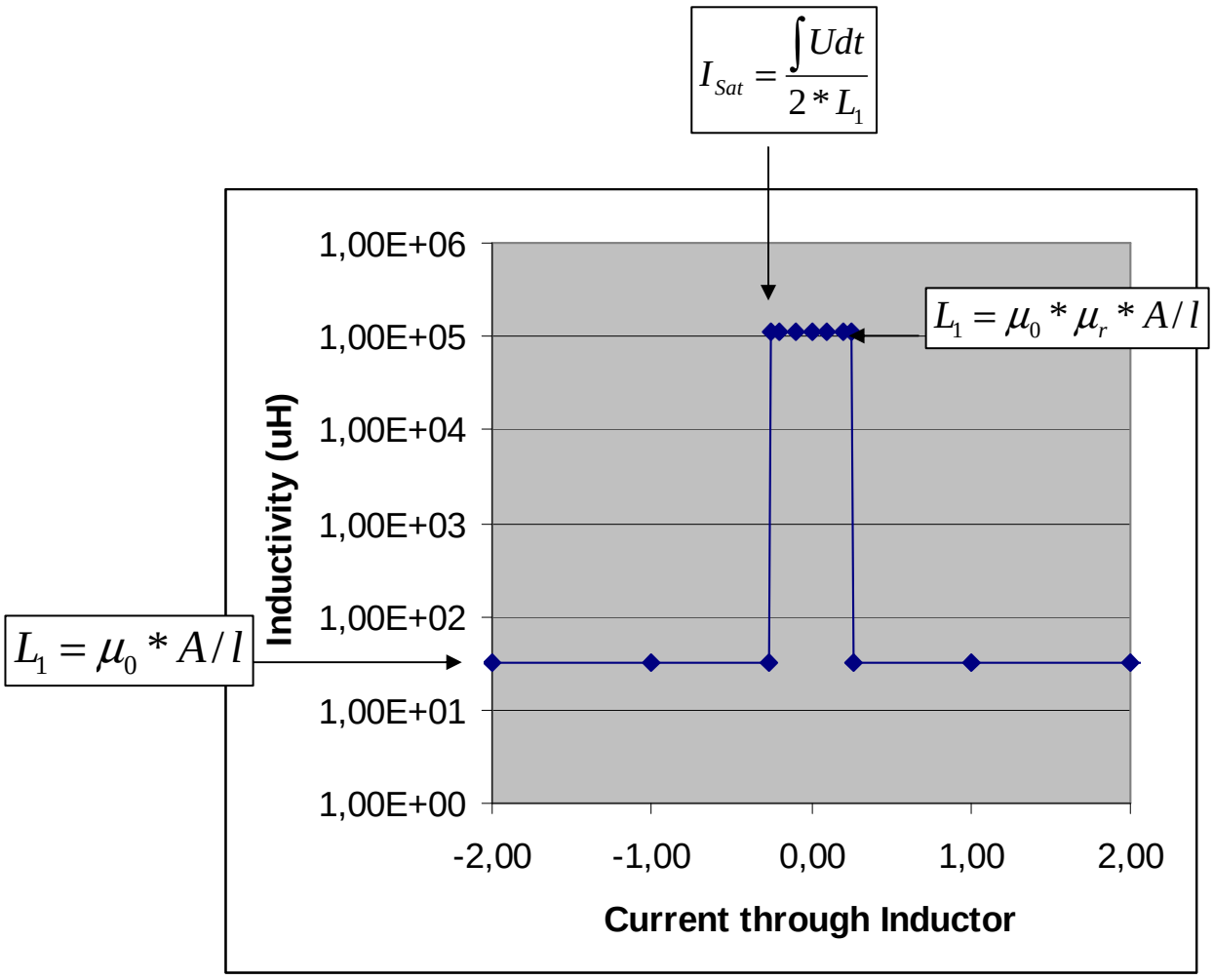

Fig. 11: Typical inductivity of a nonlinear inductor (single turn device)

With the nano-crystalline material and the nickel zinc ferrite the value of the core loss equivalent resistor is nearly constant in this time frame (100ns to 2us).
The inductivity of the unsaturated core reduces with frequency. These models are based on a Z-magnetization loop as it is normally used in magnetic pulse compression. But in principle a Z-magnetization curve is not necessary for pulse compression. The main benefit of a Z-material is that it is easy to reset. It is also possible to implement in the model any magnetization curve.
The current vs. inductivity curve could be put in the simulation one by one. The weakest point of the model is that the inductivity of the unsaturated core is constant independently of the magnetization speed. In applications where the frequency span is wide this may lead to unacceptable deviation. In this case it is acceptable.
It is also clear that the equation for the “hold off” time of an inductor is also valid.

$\hat{B} * A * N = \int Udt$

$\hat{B}$: Magnetic flux swing (T)

A: magnetic cross section (m^2)
N: number of turns

$\int Udt$: Integral of voltage time

The model calculates the current through a linear inductor. If the current reaches a certain value the inductivity of the inductor is changed. Depending of the inductivity and critical current, a very close simulation to a real nonlinear inductor is achieved.
The parallel resistor represents the core losses and is stable for the metallic cores and the nickel zinc ferrite.
It is not constant for the popular manganese zinc ferrite. The reason is that the conductivity of the manganese zinc ferrite changes with frequency and the location of the eddy current changes with magnetization speed. The values given by the supplier are not valid for typical pulsed power application.

2.1.2 Comparison of different materials

In this chapter only a sort over view should be given, on the huge variety of materials, only a few can be considered. A material should have a high magnetic flux density (B) because the volume of a core is:

$$V \approx 1/\hat{B}^2$$

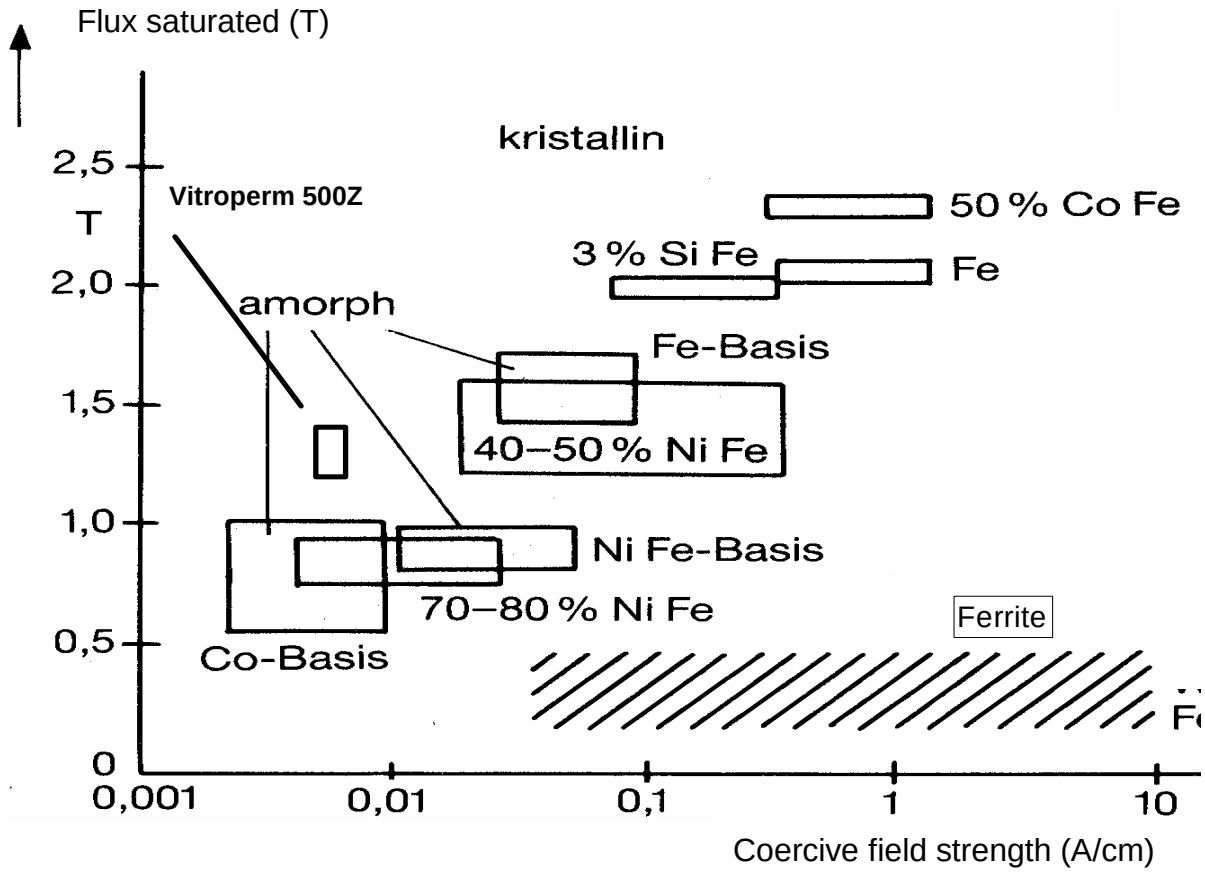

Fig. 12: Comparison of different available magnetic materials[8]

So for a compact pulse power always material with a high flux density should be used. Unfortunately materials with high saturation flux density have also the highest losses. The nano-crystalline material is an exception (Fig. 12).

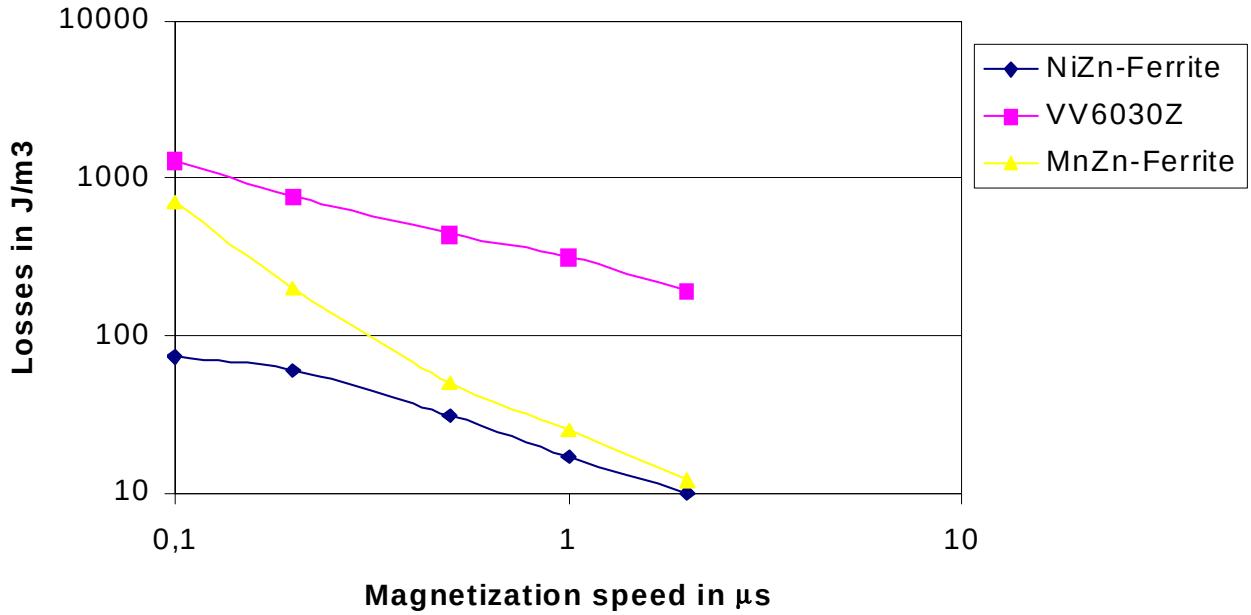

Fig. 13: Losses of different Materials[9]

Nickel zinc ferrite shows very low losses (Fig. 13). The trade-off is that the saturation flux density is small (0.5 T) compared to the nano-crystalline materials (1.2 T).
This material is very useful for magnetic assists. In this application the core size is small and other materials have too high losses at the fast magnetization speed. This material normally is used for EMI suppression. Therefore, a wide variety of (small) core shapes are available. Bigger cores are also available but very expensive. It is the best material for magnetization times lower than 100 ns.
For bigger cores the nano-crystalline material is since 4 years the standard material for power cores. All other metallic materials have mainly historical meaning.
For pulsed power application the insulation and the band thickness of a tape wound core is very important. If the insulation layer is not strong enough especially by higher magnetization speeds, the losses of the core rise dramatically, because of short circuits between the layers. Also the tape thickness is a very important parameter. Due to the eddy current in the layer the magnetic field is compensated in the layer. The active cross section of the tape is reduces, leading to reduced inductivity.
A reduced tape thickness is very helpful for high speed applications (> 2µs) because the losses reduces with losses~$1/d^3$ and the high permeability of the material is also stable for higher frequencies. Unfortunately, the production of tapes with a thickness of less than 15µm is actual not possible, but this material may be available in future.
One critical point with magnetic pulse compression is the leakage current through an unsaturated current. This current has two sources: One is the limited inductivity; the other is the losses of the core. For pulsed power application cores with thinner ribbons would be a great step ahead.
Ferrites are available with different properties (see Fig. 14).

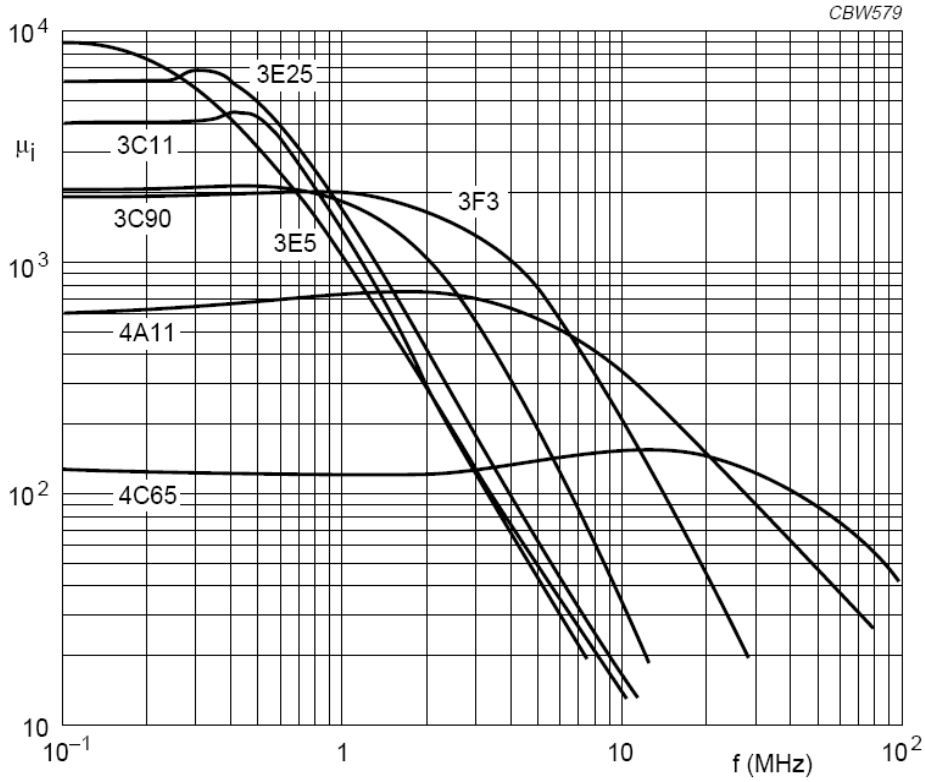

Fig. 14: Frequency behavior of different ferrite materials[10]

Depending of the dominate frequencies different materials show better performance. Normally the best high frequency material shows poor performance at low frequencies. In a pulsed power application the frequency range is huge (from DC up to typical 5 MHz) so to find the best suited material is sometimes quite difficult.

2.1.3 Measuring of the copper losses

The third important loss factor is the copper loss. 30% of the losses in a typical pulse compression application are copper losses.
The resistance of a winding at high frequency is much higher than at DC. The reasons are skin effect and especially proximity effect.
These effects are mainly driven by the magnetic field (H). Depending of the particular design the copper losses can change to some orders of magnitude.
Due to the fact that during the main current flows through a pulse compression inductor the core is saturated, it is possible to measure the losses with an air core model (this is of course not possible with a transformer or linear inductors).
The frequency dependent resistance of the air core model could be measured with a net-work analyzer.

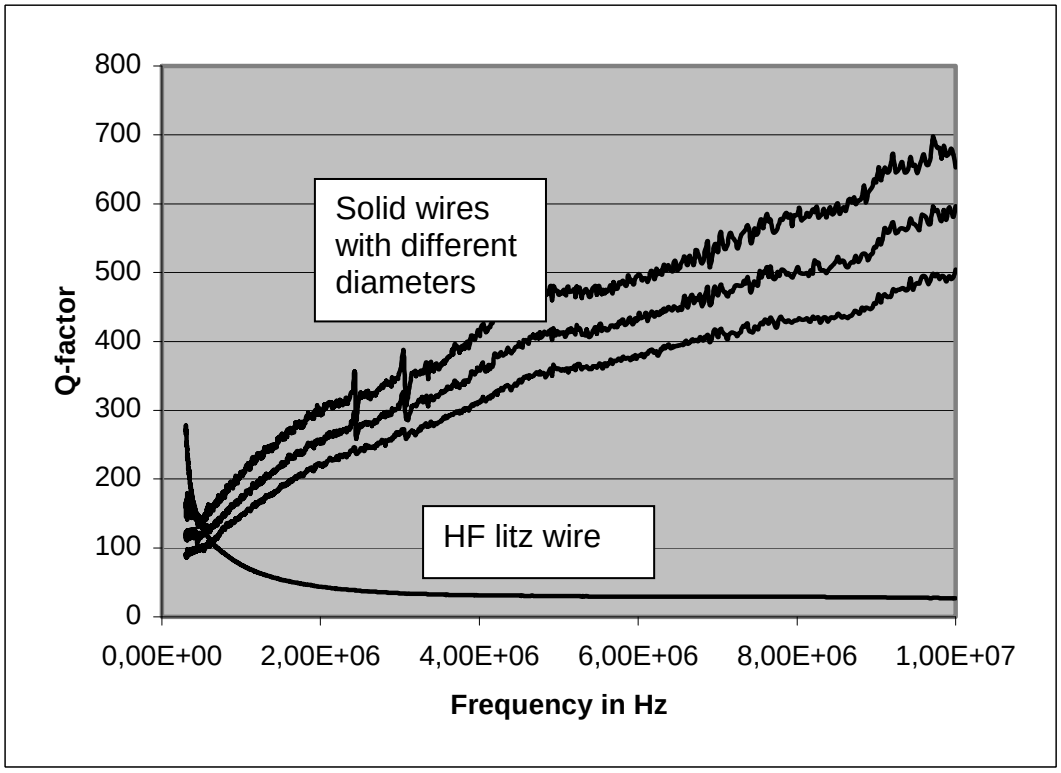

Fig. 15: Typical behavior of different windings of the loss of an inductor[11]

The copper losses are influenced by the geometry of the winding and the wire diameter. The influence of design of the copper losses are amazing complex, and very difficult to calculate. There are special computer programs to calculate copper losses in different applications.
There is some rule of thumb for copper windings. Best performance shows single layer turns, in a toroid coil.
The use of high frequency litz wire is very difficult for frequencies of more than some 100 kHz. Is the frequency higher than optimal the losses rise dramatically.
For a single layer litz wire in an air core for 5 MHz 50 μm wire diameter is necessary. This means for a cable with a total cross section of 10 mm^2, more than 5000 single wires has to braid to a single cable! The use of litz wire is limited to slower pulsed power applications in the frequency range lower than 1 MHz (corresponding to some μs pulse length).

2.1.4 Application and purpose of nonlinear inductors

Nonlinear inductors could be used for different applications in a pulsed power application. The basic design is very similar, but depending on the circuit around different functions was fulfilled.

Pulse compression:

A very typical configuration shows Fig. 16.

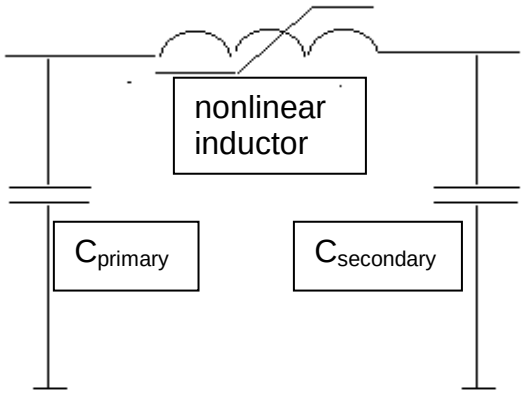

Fig. 16: schematic of a pulse compression circuit

The first capacitor is charged up, during the charging time the inductor is unsaturated, so only small leakage current flows. The capacitor is charged the inductor saturates and the energy is transferred faster to the second capacitor. After the energy transfer the core has to be reset to normally due to a constant current with a single turn winding.
The following relations have to be considered for designing a pulse compression stage:

M_{core} ~ energy
M_{core} ~ compression ratio^2 (relation form charging time of the primary to the secondary capacitor)
$M_{core} \sim B^2_{satt}$
(M_{core} means the mass of a core)

If the compression ratio is more than factor 4 to 8 it is normally better to split the task to two or more compression stages.

Magnetic Assist:
The purpose of a magnetic assist is to reduce the current during turn on of a switch. During the fall time of the voltage of the switch the loss is normally very high in a switch.
The hold-off time of a magnetic assist should be at least in the range of the fall time. It is possible to reduce the turn-on loss at factor 5 with a well designed magnetic assist. The loss of the magnetic assist is normally small compared to the loss in the

switch. At high repetition rates (more than several kHz), for example in converter application, overheating limits the use of a magnetic assist.
Like the pulse compression it is normally necessary to reset the core with a pulsed or DC current. In some application it is possible to use reverse current to reset the core, but it is hard to ensure proper resetting under all operation conditions.
The disadvantage of the magnetic assist is that the inductivity of the switch is increased.

Magnetic Diode:
A magnetic diode is an application of a non linear inductor which is not well known. It is in cases useful where current flows for a long time in one direction and a current reversal only for a short time has to be prevented.
The main advantage of a magnetic diode is that there is no reverse recovery. In some application it is put in series to a standard diode, so helping the diode to open during reverse recovery.
It is important to know that the reverse recovery time of a bipolar diode depends on the reverse current. In cases where a magnetic diode reduce the reverse current the reverse recovery time rise remarkable, because the minority charge carriers are not depleted by the current.
The disadvantage of a magnetic diode is that the voltage drop depends of the prior hold-off time. This limits the benefits of such a device.
The use of a magnetic diode is limited to applications were only short blocking time is necessary.

2.1.5 Design of the non-linear inductor

The practical design of a nonlinear inductor is quite challenging. One key issue is the electric field. Pulsed power means normally high voltage. So electric field strength could reach very high values.
To reduce the electric field strength between the cables it is useful to wind the coil in such a way which is called solenoid toroid (Fig. 17).

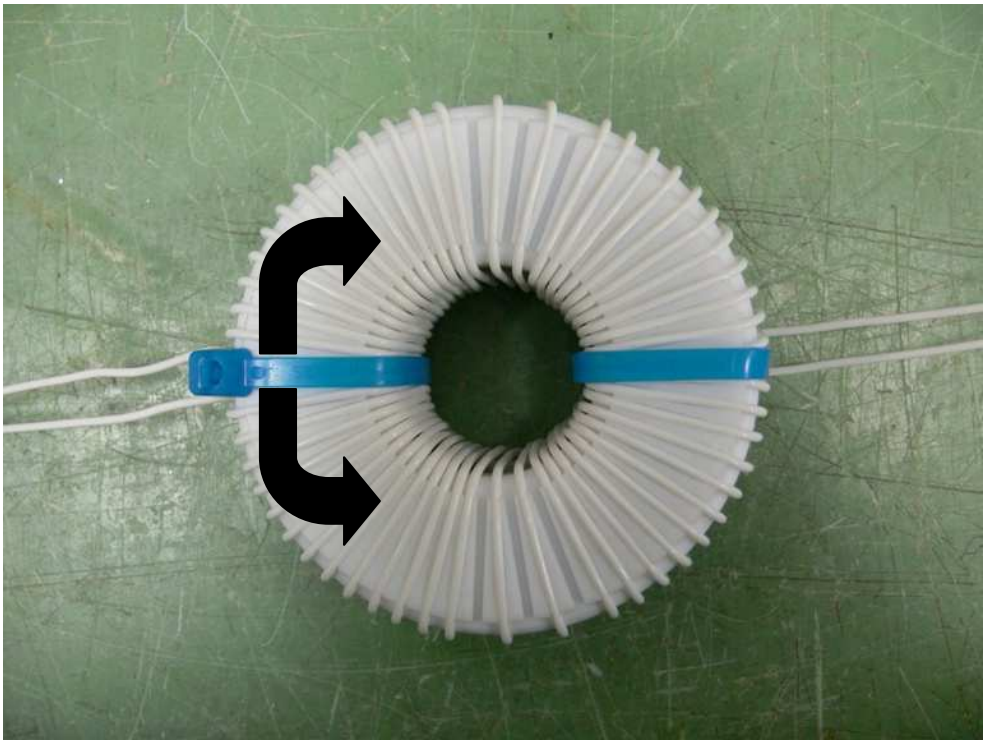

Fig. 17: Picture of a magnetic pulse compression core (the arrows indicate the winding direction)

This kind of winding reduces also the parasitic capacity of the coil. The highest electric field is the field between the conductive core and the ends of the winding (Fig. 18). The average electric field should be less than 3 kV/mm in air. In oil it can be 3 times higher.
The insulation material also influences the parasitic capacity. Teflon is in such case the best material because the dielectric constant (ε_r = 2.2) is remarkably low. (The main disadvantage of Teflon in high voltage application is that it is very sensitive to partial discharges).
Silicon rubber is an alternative, but is very sensitive to mechanical stress.
The electric field could be calculated with special programs. The result of such calculation helps to improve the design, but replaces no long term test. Partial discharges are the enemy of a stable long term operation. For quick tests it is enough to run the coil in a dark room with relaxed eyes. Only bigger partial discharges could be detected in such a way.

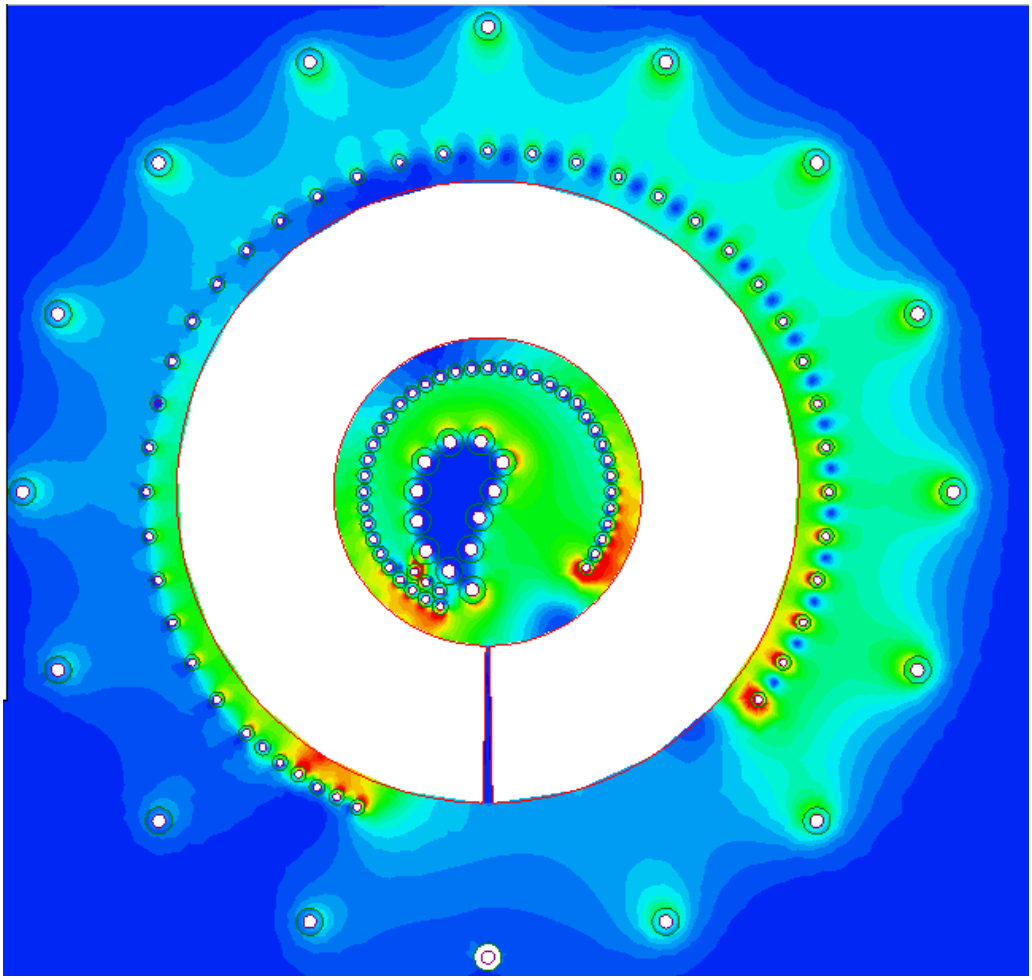

Fig. 18: Typical result of an electric field calculation for a (not properly designed) transformer

Nickel zinc ferrites have due to their non conducting properties less problems with the electric field. In application in the range of 30kV there is no additional insulation necessary between winding and core. This reduces the size of the coil which is much bigger than with wound tape cores due to the low saturation flux density.

2.2 Capacitors

There is an enormous range of different capacitors on the market. This work is only focused on high voltage capacitors for pulsed power application.
For this application ceramic disk capacitors are used. The ceramic material is normally a Class II para-electric (Strontium titanate) material which is doped (for example lead oxide) to adapt the material to different application.
Also possible are Class I ceramic (titanium oxide) capacitors which shows excellent temperature and high frequency properties, but tend to be very bulky.
The losses could be described by a combination of a series resistor of an ideal capacitor.

$$Q = \frac{1}{2 \cdot \pi \cdot f \cdot C \cdot R}$$

C: capacity (F)

f: frequency (Hz)
R: serial equivalent resistor
Q: Quality factor

The 1/Q is the amount of energy (of the total energy) which is dissipated in the capacitor during on charge and discharge. A Q=100 means that 1 % of the total energy is dissipated.
Foil and NP0 Ceramics shows losses in the range of 0.1% (Q=1000) Class II ceramic shows normally 10 time more losses.

2.2.1 Measuring of the losses

The small signal losses of a capacitor could be measured with a network analyzer or L- C- R bridge. The losses are normally temperature- and frequency-depended (Fig. 19).

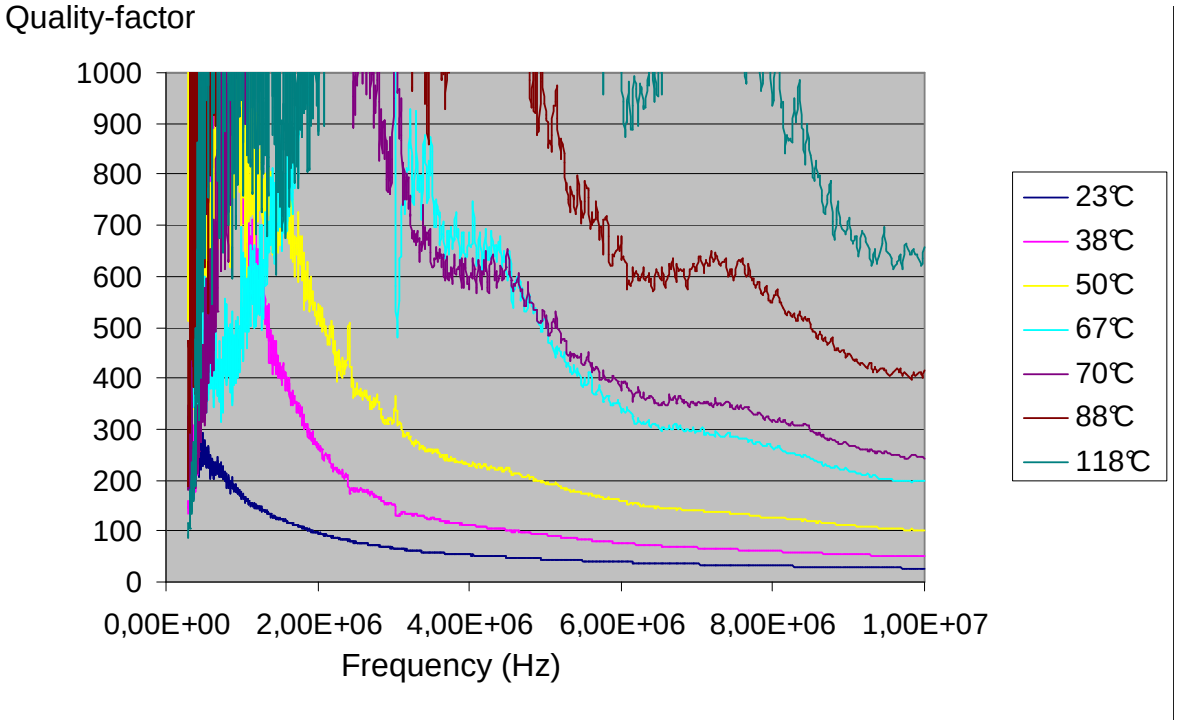

Fig. 19: Quality-factors of a Class II capacitor with different temperatures[12]

The noises are a result of very low losses. The used network analyzer could only measure quality factors up to Q = 1000.
It is clear that in such cases were the losses are temperature depended a simulation is very difficult, because the temperature influences the losses and the losses influence the temperature.
The losses of class II ceramic are not only frequency- and temperature-depended it shows also a voltage-dependency.
There are no standard processes to measure the losses of a capacitor at high frequency and high voltage.
A small test circuit (very similar to Fig. 36) is developed to measure the losses under real conditions.
A high voltage (1kV) MOSFET switch starts an oscillation in a LC circuit. To get the value of the total losses a capacitor with almost no loss (vacuum capacitor) and the same capacity as the test capacitor is installed in the circuit. From the decay of the ringing the total losses of the circuit could be calculated. This value is the losses of the test circuit itself and is the offset for the measurements with the test capacitor.

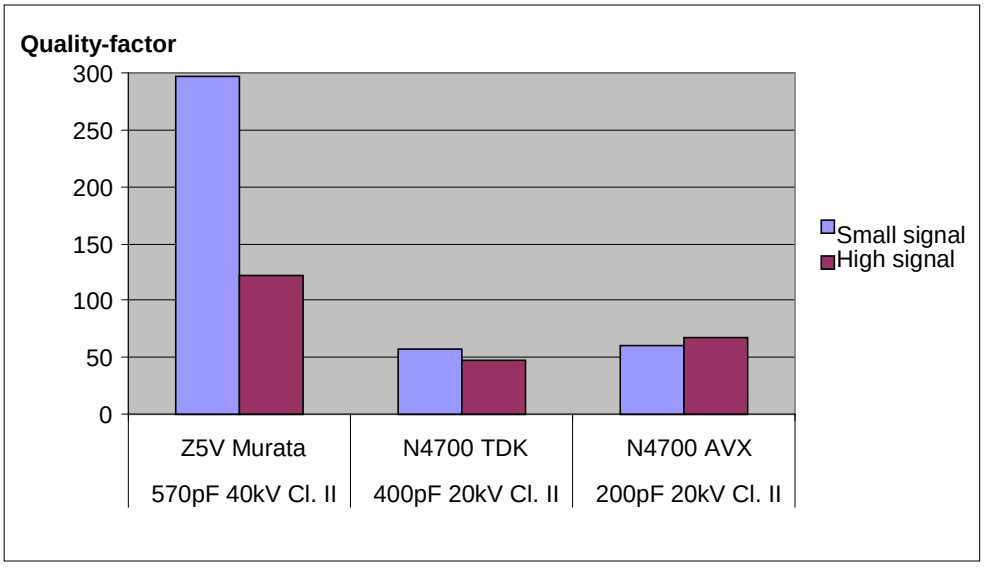

Fig. 20: Losses of different ceramic materials (at 5 MHz) for small signal and high signal.[13]

This high signal behavior is also temperature- and frequency-dependent (Fig. 20).

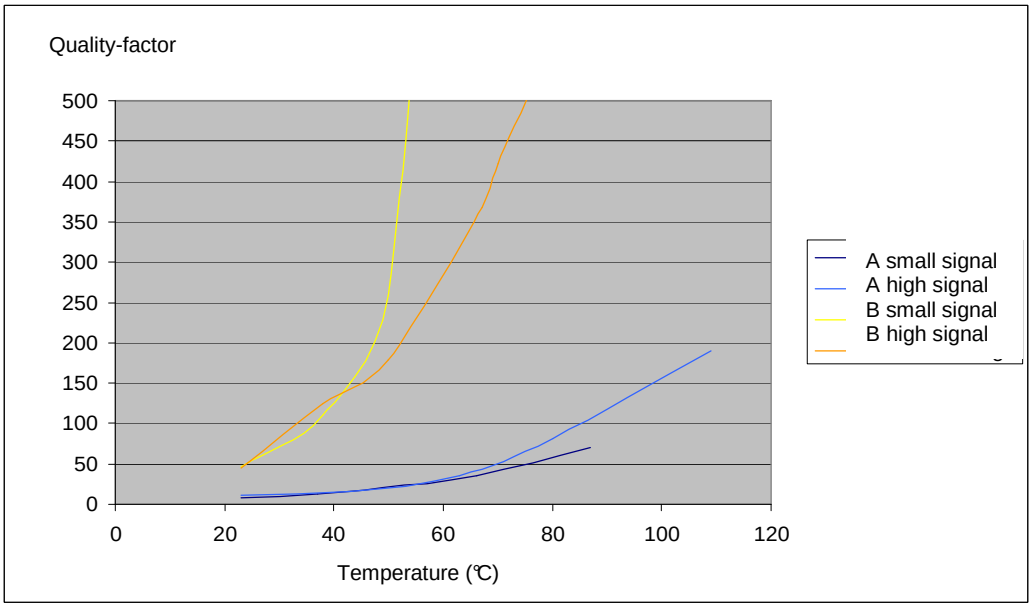

Fig. 21: Quality-factor of small signal and high signal at different temperatures and different ceramic materials (material A and material B at 5MHz)[14]

Class II Ceramic shows also a capacity dependence of the frequency and operation voltage (Fig. 22 and Fig. 23).

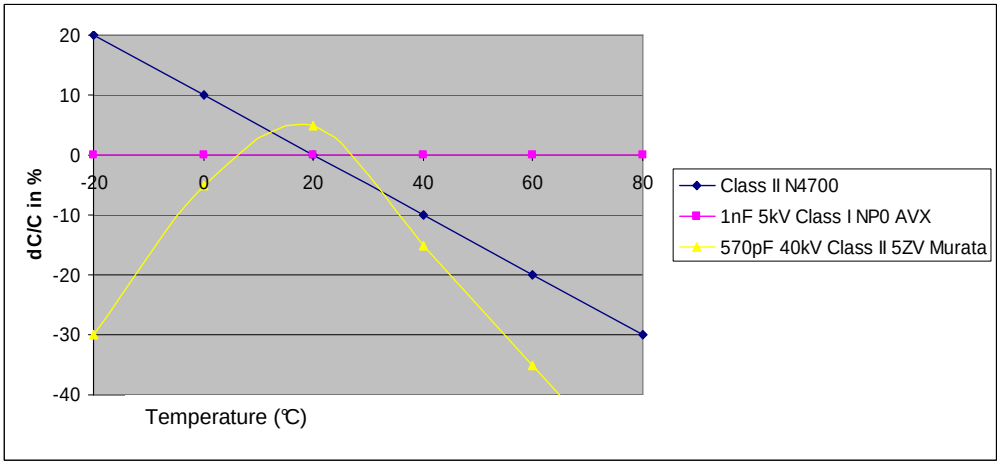

Fig. 22: Capacity changing with temperature[15]

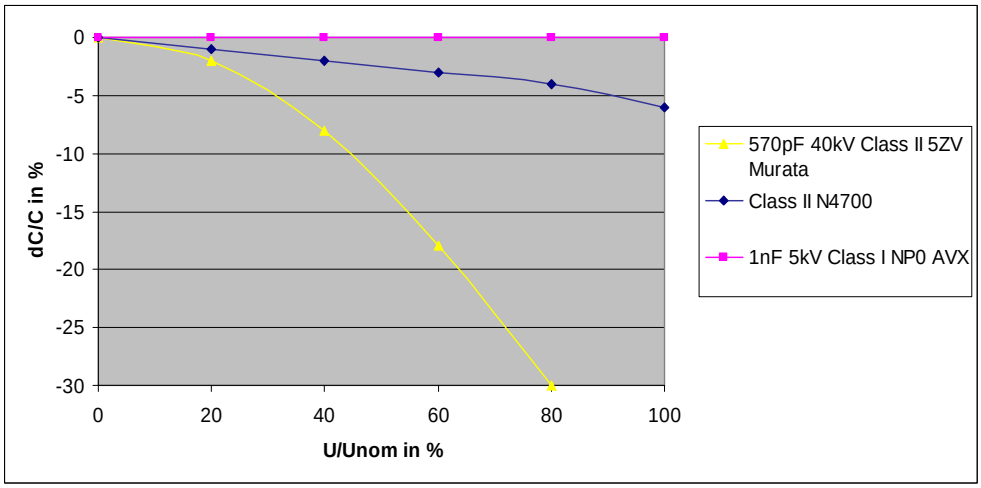

Fig. 23: Capacity changing with voltage[16]

The very complex behavior of the class II materials is a severe problem in pulse power. Practically all parameters are more or less changing with temperature, voltage, and frequency.

2.2.2 The simulation model of capacitors

The realistic simulation of the class II ceramic capacitors is very difficult. In this work it is tried to reduce the complexity of the problem.

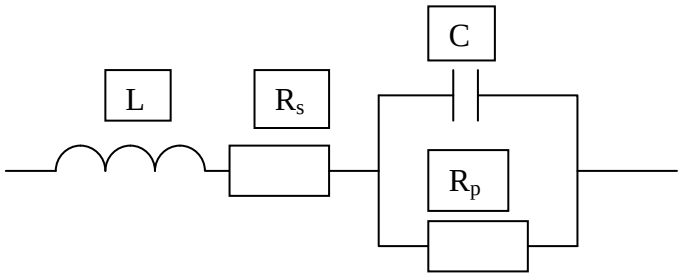

Fig. 24: typical equivalent circuit schematic for a capacitor with losses

In principle it is possible to calculate the R_P into R_S and vice versa. But there are also physical meanings of the resistors.
The R_P represents the leakage current due to finite insulating of the dielectric, the R_S the conduction losses and the losses in the dielectric.
In a pulse power application the RS is the dominate loss factor. The only parameter which is put into the model is the series resistor.
Also, it is sometimes useful to implement the variation of capacity with voltage.

2.2.3 Final considerations about class II capacitors

The very complex behavior of Class II capacitors leads to difficulties, not only in the simulation but also in the real circuit.
The change of capacity with temperature changes the tuning of the circuit and the losses depend on the temperature, too.
Better capacitors would help to get a more stable operation of pulsed power circuits. Candidates for small pulsed power are NP0 multilayer capacitors which are available up to 1 nF and 10 kV (E= 50 mJ). The disadvantage is the small component size and the very high price. Also long term stability under pulsed power conditions is not yet proven.

2.3 Transformer

Transformers are necessary to match impedances between two stages. In modern pulse power modules pulse transformer are becoming more important because the voltage of a semiconductor switch is normally smaller than the typical voltage of the loads.
The loss factors are the same like in an inductor, core losses and copper losses. In most cases the capacitive components of a transformer has an important role, especially if the system is not resonant and the output voltage is high.
The energy which is stored in the capacities causes ringing and slow rising times and additional losses.
The science behind a transformer is amazing complex and knowledge about is not very common
Also the different designs possibilities are enormous and it couldn't be fully discussed in this work. For more detailed information see in references[17] [18].

2.3.1 Core losses

The core losses could be calculated as given in 2.1. The result is the parallel resistor and the value of the main inductivity. This resistor can be also used in the transformer model.

2.3.2 Copper losses

The copper losses are much more difficult to measure and calculate than in a nonlinear inductor. The approximation which is used for the non-linear inductor is not still valid because the core is not saturated.
The situation became worse in cases where gaped cores are used. Due to the fringing field around the gap the losses in the conductors are rising in this area. Even the core losses are rising around the gap because the fringing field induces additional eddy currents in the tapes (with tape wound cores).
In most cases an un-gaped core is the best solution for a transformer, because the energy storage in the core is very low, and the fringing field, too.
The copper losses are in well designed transformer are in the range of 2 %-5 %.

2.3.3 The simulation model of transformers

The complete T-model of a transformer is quite complicated. The model is already a simplification because it is reduced to a 1 to 1 transformer (Fig. 25).

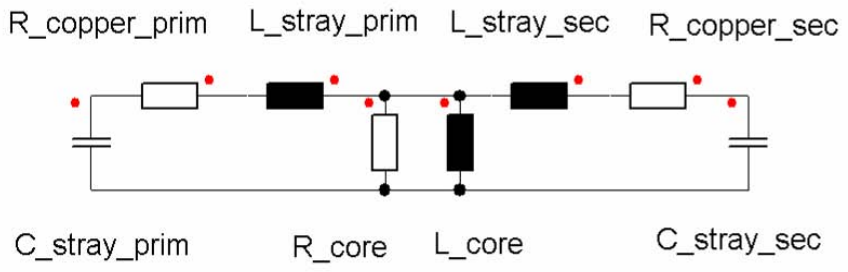

Fig. 25: T-model of a transformer (1:1)

It is very difficult to measure or calculate all sub-components of a transformer.
From the measurements of chapter 2.1 the values of 2.1 R_core and L_core are known. The total losses could be measured with a network analyzer with a short circuited transformer. From the total losses the sum of the copper losses can be calculated. For the model the resistors can be split on both branches.
The total stray inductivity could be also measured with the network analyzer and the result could be also split on both branches.
The easiest way to determine the stray capacity is to calculate (or better appraise) it from the geometry.
In a real transformer there are also coupling capacities between primary and secondary windings. This could be measured also with the network analyzer by sorting the primary and secondary winding and determine the coupling capacity.
In the simulation the core loss and the core inductivity, the stray inductivity (measured or appraised) and the stray capacity from the high voltage winding (it is normally the dominant capacity) is implemented.
This basic model is enough to compare different topologies of the circuit.

2.3.4 Designs of transformers

There is a huge variety of transformer in use. For transformer used in such fast applications, normally single turn (primary) transformers are suitable.
Even in such a case the stray inductivity may be too high, so a fractional turn transformer is the more appropriate. Such a transformer consists of several transformer cores with one primary and one secondary winding. The primary windings are connected parallel the secondary windings are connected in series.
The main problem of using transformer in the 100 ns range is the poor quality of the magnetic material. Most materials show very high losses in this frequency range and very low permeability. So an efficiency of maximal 90% is expected.
In modern pulsed power designs one seeks to avoid the use of pulse transformer.

2.4 Semiconductor switches

From the huge varieties of semiconductor switches used in power electronics, only IGBT´s or MOSFET´s are suitable for very fast switching. To give a complete picture "super GTOs" were also tested which are produced under the name of Soliton and Plasma-Switches. These exotic switches are described in Chapter 2.5.5.
The main difference between both switches is that the MOSFET only work with the majority charge carriers and therefore show superb high frequency behavior. The IGBT is a bipolar switch which uses minor charge carriers. The benefit is that the chip surface is reduced in comparison with a MOSFET, the disadvantage being that the behavior is slower, in principle.
All other switches are not suited in fast industrial pulse power sytems at the moment.
Both switches could be controlled power less, which does not mean that no power is necessary, but means that for a continuous turn on no continuous power is required. For fast switching application remarkable high control currents are required to switch the devices on.
Power electronics is dominated by these two kinds of switches. This switches are build in high quantities from different suppliers and the availability is very good. This is also a big advantage compared to other more exotic solutions, like SOS diodes which may be an alternative solution.
IGBT switches are available in two different designs PT (Punch trough) and NPT (non punch trough). The NPT design is better suited for modules because due to positive temperature coefficient they are easier to switch in parallel. Fall times are normally longer compared to the PT design.
In this application the PT design may be better suited, but may bring problems in current sharing.
The MOSFETS are also available in two designs. The common MOSFET which is available from different suppliers are showing especially for high voltage high conduction losses (switch on resistance, R_{SDon}). The COOL MOSFET© (trademark Infinion) reduces this resistance by a factor of 5 (compared to same voltage and chip size).
These four different switches are tested under conditions comparable to the application in a test circuit.

2.4.1 Measurement of the switch behaviour

The data sheets are not offering enough information to make a selection. The data sheets are adapted for the main application, traction and offer insufficient information about pulsed power application. To compare the different data sheets is nearly impossible because the test conditions are different.
For such exotic application of semiconductors it is necessary to test the components.
A small test circuit was built to compare the switches under the same condition.
Most of the voltage drop of the switch is inductive. So it is not possible to distinguish voltage drop due to the on resistance and due to the inductivity.
A remarkable part of the energy is stored in the inductivity of the switch. This energy came back during the current decay. It can be seen that the calculated energy loss reduces after the peak current.
After the sine half wave the current is zero and the inductive energy store is also zero. This value represent to real energy drop in the switch.
The test circuit is described in Chapter 3.

2.4.2 Measurement of the switch behaviour of the IGBTs

The fall time of the PT IGBTs is fast enough to fit in this application. Different switches of different suppliers are tested.

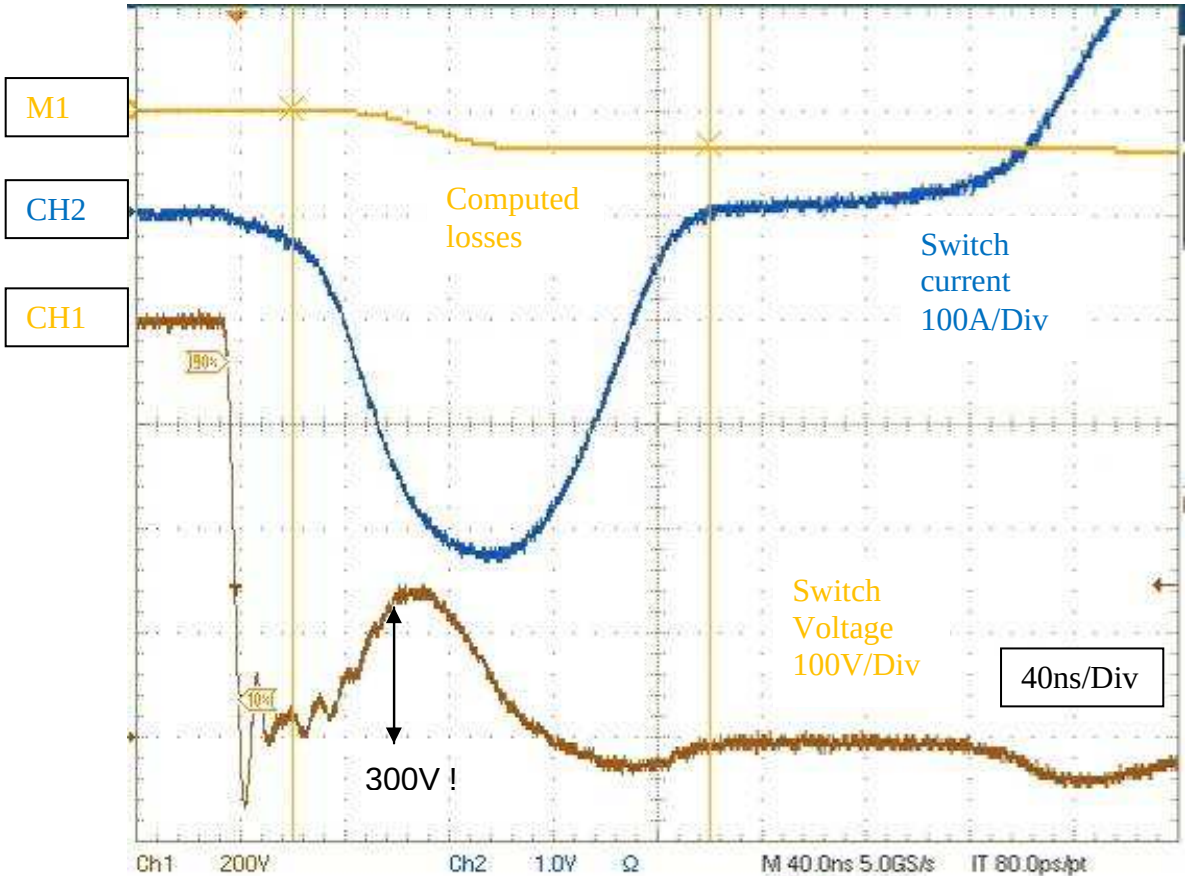

Fig. 26: Switching behavior of a PT IGBT (note the voltage drop during the current rise) (CH1: Switch voltage; CH2: switch current; M1: Loss computation)

The voltage drops as described in the datasheet. But due to the fast rise of the current the switch has an unacceptable voltage raise (Fig. 26) causing very high losses in the switch. 30% to 50% of the energy is lost in the switch.
All tested IGBTs show more or less the same behavior.
It is clear that IGBT´s are not suited for application in the 100 ns range. From this data the application of IGBT´s are in the range of pulse lengths longer than 1 µs.
The reason for the high voltage drop is that the minority charge carriers have to migrate into the drift zone of the semiconductor. During this time the voltage drop is very high. This diffusion time depends of the thickness of the drift zone. This is the reason why high voltage bipolar semiconductor devices are less dynamic than low voltage devices.
The NPT IGBTs shows a very similar voltage drop, with a much slower fall time (ca 50ns).

2.4.3 Overview of the differences of the tested MOSFETs

MOSFETs are known to have excellent high frequency behavior. On the other hand the conduction losses of especially high voltage MOSFETs are known to have very high conduction losses (compared to IGBTs).
In power electronic the MOSFET is the preferred switch up to 200 V and for more than 200 V the IGBT dominate the market.
First measurements shows that MOSFETs have 1.2 to 1.8 more losses than calculated with the $RSD_{(on)}$ from the data sheet.
A better understanding is needed what is going on. To understand the differences of the components 3 different MOSFETs are tested which seem to be best suited for this application (Tab 5).

Part	Voltage	Current (25℃)	RSD(on)
A	800V	50A	0,150Ω
B	800V	52A	0,140Ω
C	800V	17A	0,290Ω

Tab. 5: Overview of the tested semiconductors

One reason for the differences of calculation and measurements could be the dependence of the $RSD_{(on)}$ on the current.

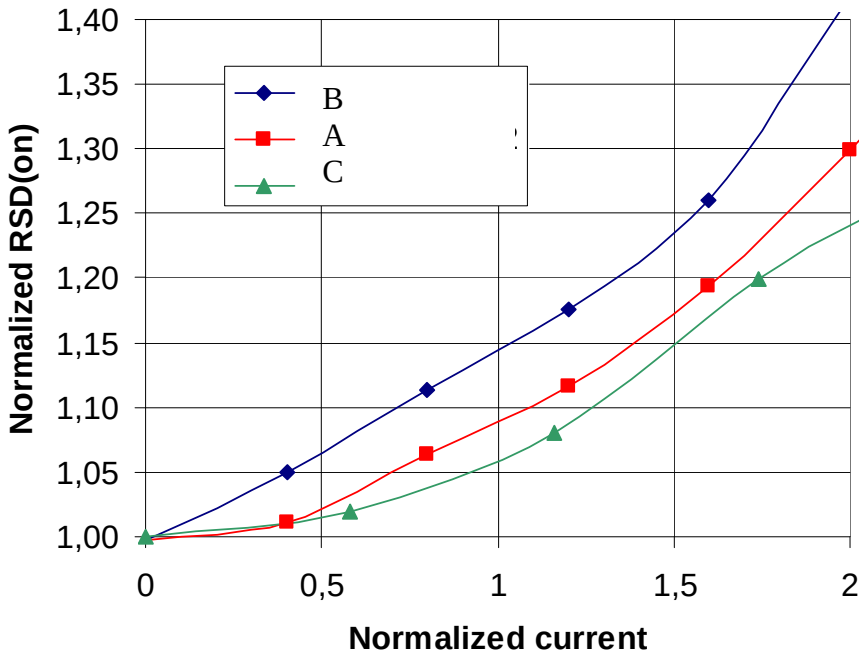

Fig. 27: Comparison of different MOSFETs from different suppliers[19]

It is very difficult to get an objective comparison between the different suppliers. All data were taken from the data sheets (Temperature 25℃). The data from the transistor C has to be calculated from the output characteristic. The transistor C shows the lowest dependence of the RSD(on) from the current.
During operation the temperature of the switches rises. This may lead to a runaway effect. On the other hand a small positive temperature coefficient helps to ensure good current distribution in paralleled devices. Generally all MOSFETs have a positive temperature coefficient.

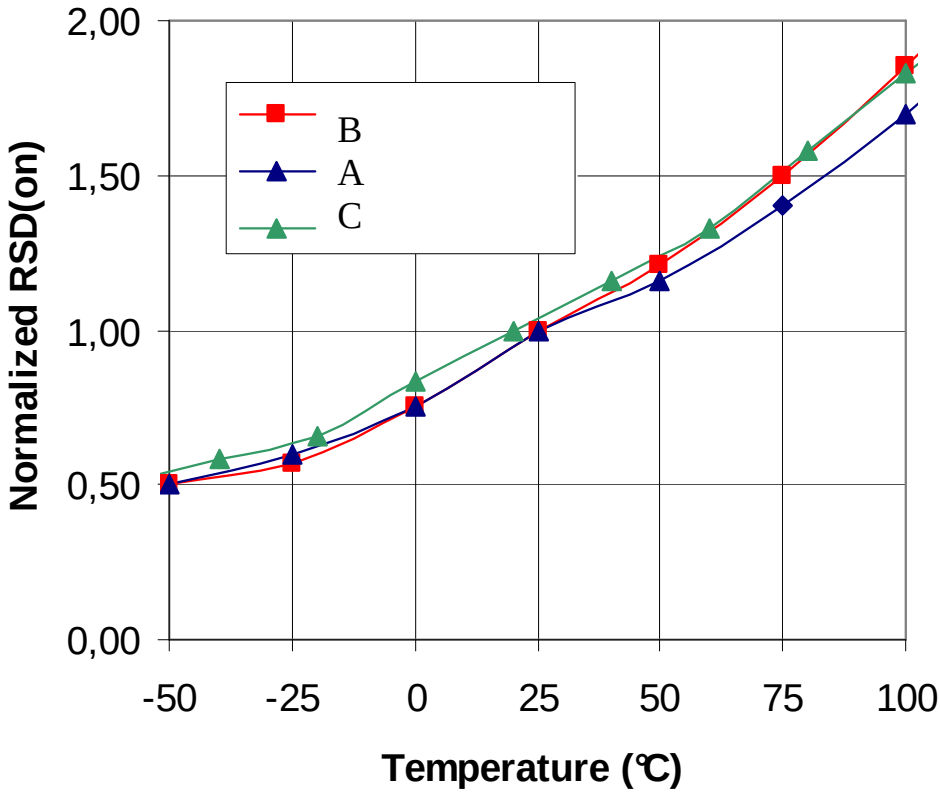

Fig. 28: Comparison of the normalized RSD(on) (25℃) from different suppliers[20]

There are nearly no differences of the data of the MOSFETs from the different suppliers.
All other data like the fall time shows very little differences and shouldn't have any influence on the switching losses.

2.4.4 Measurement of the switch behaviour of the MOSFETs

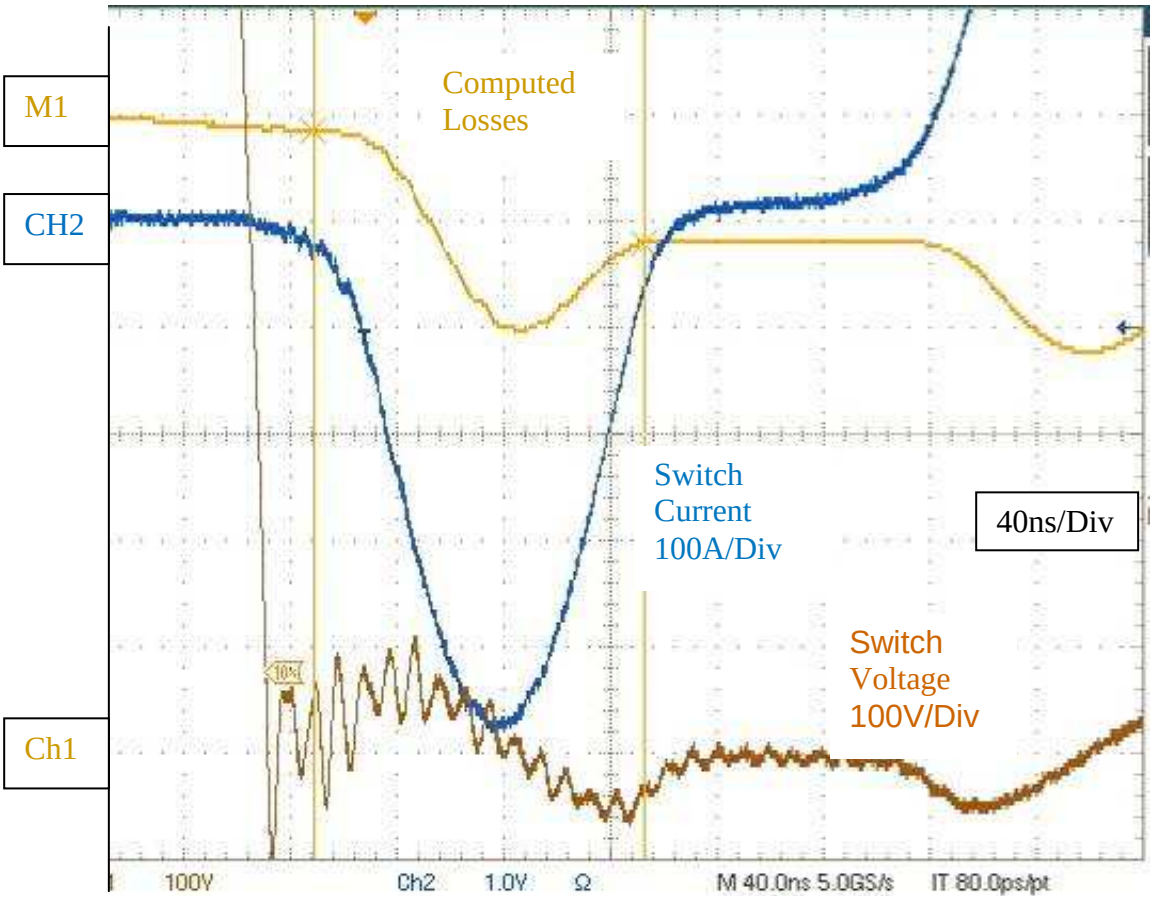

Fig. 29: Typical switching waveforms of the MOSFETs (CH1: Voltage drop switch; CH2: Current of switch; M1: Computed losses)

The dynamic behavior of the MOSFET is much better compared to the IGBTs. The most important difference is that there is no forward depletion. A typical waveform could be seen in Figure. 29.
MOSFETs are in principle, suitable switches for the planned application.

2.4.5 Simulation of the preferred switch

The model of the MOSFET switch could be kept simple. It is represented by an ideal switch with a resistor. This resistor is current-dependent. At the peak current the RSDon is ca 1.4 times higher than at zero current.

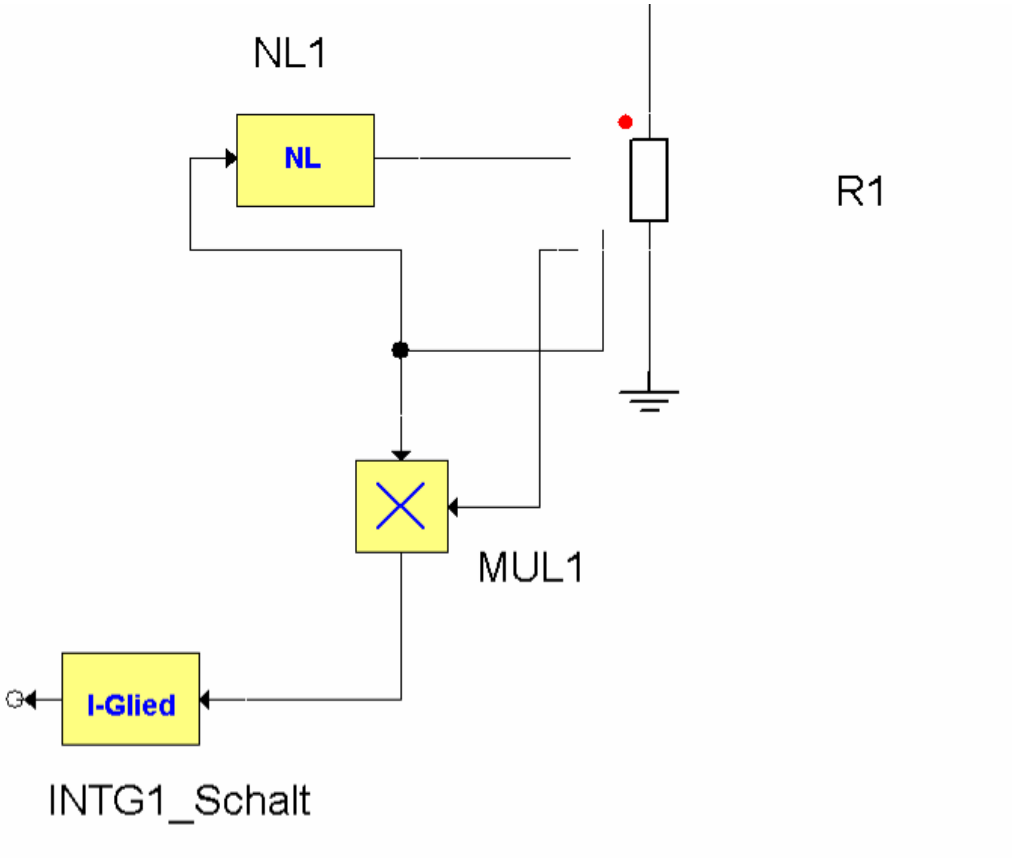

Fig. 30: Implementation of the current depending of the RSDon

In the module NL1 (Fig. 30) the current – resistance function is implemented. With this kind of simulation every odd behavior of a resistor could be simulated.
With the integrator the losses are calculated of the resistor. This value has to be compared with the real circuit.

2.4.6 Comparision of measurements and simulation

In the test 3 different die designs in two different housings are used. The main differences of the housings are if they have 3 or 4 legs. The 4-legs housing (Isotop SOT-227) have a Kelvin design to control the gates without interaction of the main current due to Voltage drop of the source leg.

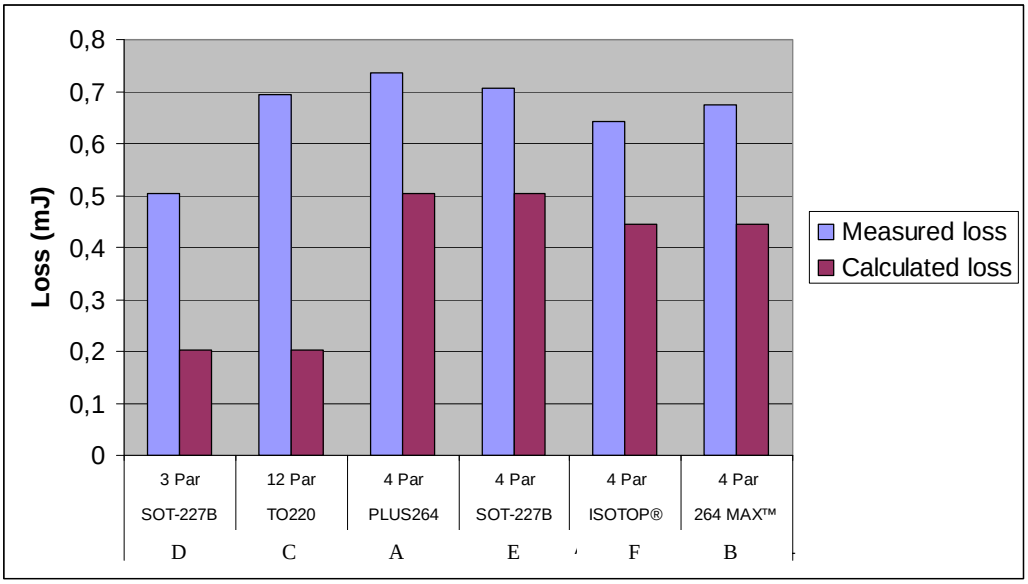

Fig. 31: Comparison of the measured and calculated switch losses of the investigated MOSFETS

With the standard MOSFETs it is ca 1.4 time difference in losses compared to the measurements and simulation. (It is the same factor with the diode, which may indicate a systematic error, but there was no evidence for that).
The main deviation in loss was found with the COOLMOS FETs (in the SOT housing 4 Chips of the transistor C were built in so the total amount of Silicon is the same). The losses with the COOL FET are still smaller (30%) compared to the standard MOSFET (same amount of components) with a 4-leg housing. This advantage nearly vanished with the 3 –leg housing.
One reason for the higher switching losses with the COOL FET should be found in the thermal equivalent circuit. The thermal capacitance scaled on the same on-resistance is with COOL FET ca 20 times higher than with standard FET.
This leads to a remarkable higher junction temperature, which may explain the higher losses. Long term stability considerations suggest standard FETs for pulsed power application.
For further tests, with the transistor A is proceeded because it is the cost effective solution.

2.4.7 Exotic switches

One of the exotic switches is a so-called super GTO or plasma switch. This switch is a GTO with very fine gate structures to enable fast switching. The switching capabilities of such a small device are impressive.
Losses are very high in the 100ns range, due to the fact that it is also a bipolar component.
For longer pulses it is a very attractive switch.
The name plasma switch is misleading because normally the term plasma is used for ionized gases. The reason for the name is that a conductor has some similarities with gaseous plasma.

2.5 Diode

The diode is the most critical part in the circuit. It is necessary to have a diode in series with the switch to control the reflected energy from the laser head.
The reflected energy charges the bank capacitor positive (the bank is charged negative, to have negative output voltage, which is preferred for the laser head).
This energy would ring in the circuit till it is damped out. This ringing would lead to severe electrode erosion and less efficiency because the laser couldn't emit over such a long time.
Because the circuit is very fast the diode has to be very fast, too. The magnetic assist helps to turn off the diode but this pause is only 40 ns long. During this time the diode has to fully reverse recover.

2.5.1 Different kind of semiconductor diodes

In principle there are two different kinds of diodes, the very popular bipolar diodes and the Schottky diodes.
The bipolar diodes are not suited for this application because of the reverse recovery. There are no diodes on the markets which have a faster reverse recovery than 250 ns, under realistic conditions. As usual with data sheet, it is hard to extract the important information. Very often, data were given under unrealistic conditions to produce nice results. A typical example is the reverse recovery time. This really important value is measured with a forward current of 1A, by a diode with maximal average current of 50A. Due to the low concentration of minority charge carriers the value is remarkably good, but has nothing to do with the behavior of the diode in a real circuit.
The Schottky diode has the best dynamic behavior. Schottky diodes are available in silicon for 30 years. Typical application is always in the low voltage range together with a low voltage MOSFET.
It was not possible to expand the operation voltage because of the low band gap of silicon, as the leakage current becomes too high.
This has changed some years ago with the availability of Silicon carbide. Silicon carbide is the perfect material for power electronics and especially for Schottky diodes.
Due to doping problems switches are very difficult to produce and not available on the market.
The availability of these diodes makes this kind of circuits possible and is the key component.
This work is focused on Schottky diodes.

2.5.2 Measurement of the different diodes

The market for high voltage Schottky diodes is clear. Only 2 suppliers are producing such devices worldwide. This is remarkable because these diodes show in a lot of applications dramatic raise in performance, sometimes just by a one-to-one replacement.
The main reason is that the quality of silicon carbide wafers is poor compared to silicon wafers, so that only small components could be economically produced.

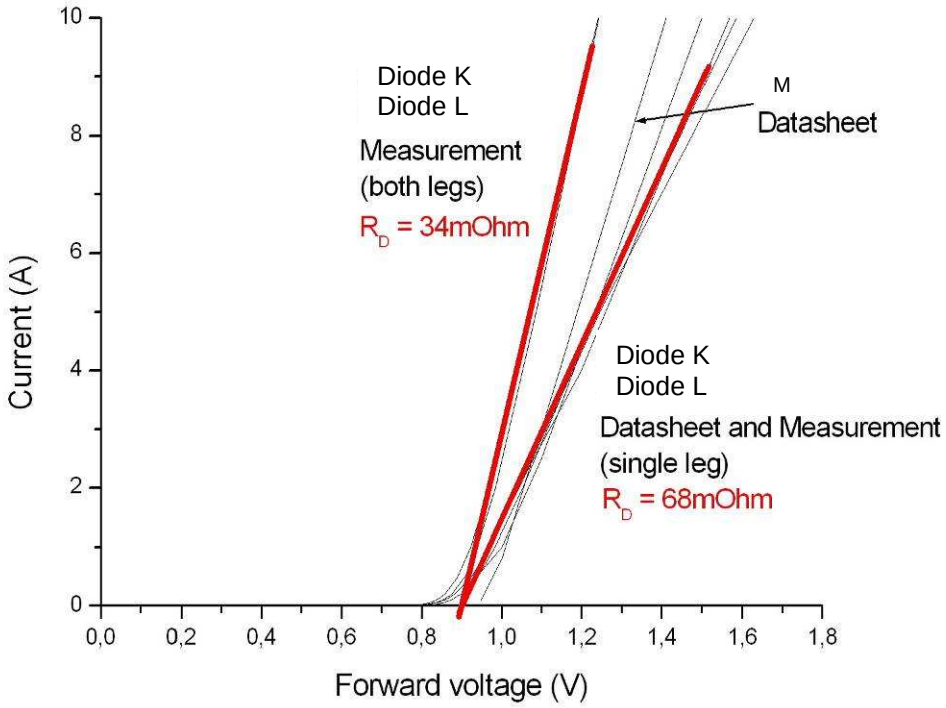

Fig. 32: Comparison of forward voltage and current of different diodes (T=25℃) [21]

The datasheets and the measurements match remarkable well. The diode K and diode L consist of two chips in one housing. Diode M is a smaller device.
Remarkable is that the 1200 V device (diode L) and the 600 V device (diode K) has exact the same forward characteristic.
It might be supposed that there is a selection in production, but according to the supplier the design of the chips is matched to have the same forward characteristics.

Typ	$I_{averarge}$	V_{RRM}	Threshold V	$R_{Dynamic}$	price
Diode K	20A	600V	0,90V	34mΩ	11,95€
Diode L	20A	1200V	0,90V	34mΩ	24,00€
Diode M	10A	600V	0,96V	44mΩ	7,54€

Tab. 6: Overview of available SiC Diodes

(The current prices are put into the overview, to show how well performance and prices match.)
The 1200 V device has outstanding performance regarding the blocking voltage to the forward voltage drop. Actually it is the most advanced device on the market.
The threshold voltage is nearly independent from temperature, but the dynamic resistance is highly temperature-dependent.
Like MOSFETs the dynamic resistance has a positive temperature coefficient. All calculations are made for 25℃ because due to the low thermal load, only a very small temperature rise is expected.
The dynamic resistance should be stable over a wide current range (Information from the supplier).

For the simulation only the threshold voltage and the dynamic resistance needs to taken into account. The barrier capacitance is small (Fig. 33) and very voltage-dependent. The typical energy which is stored in one device is ca 10 µJ. In the whole circuit it is 2 % of the total stored energy and could be neglected.

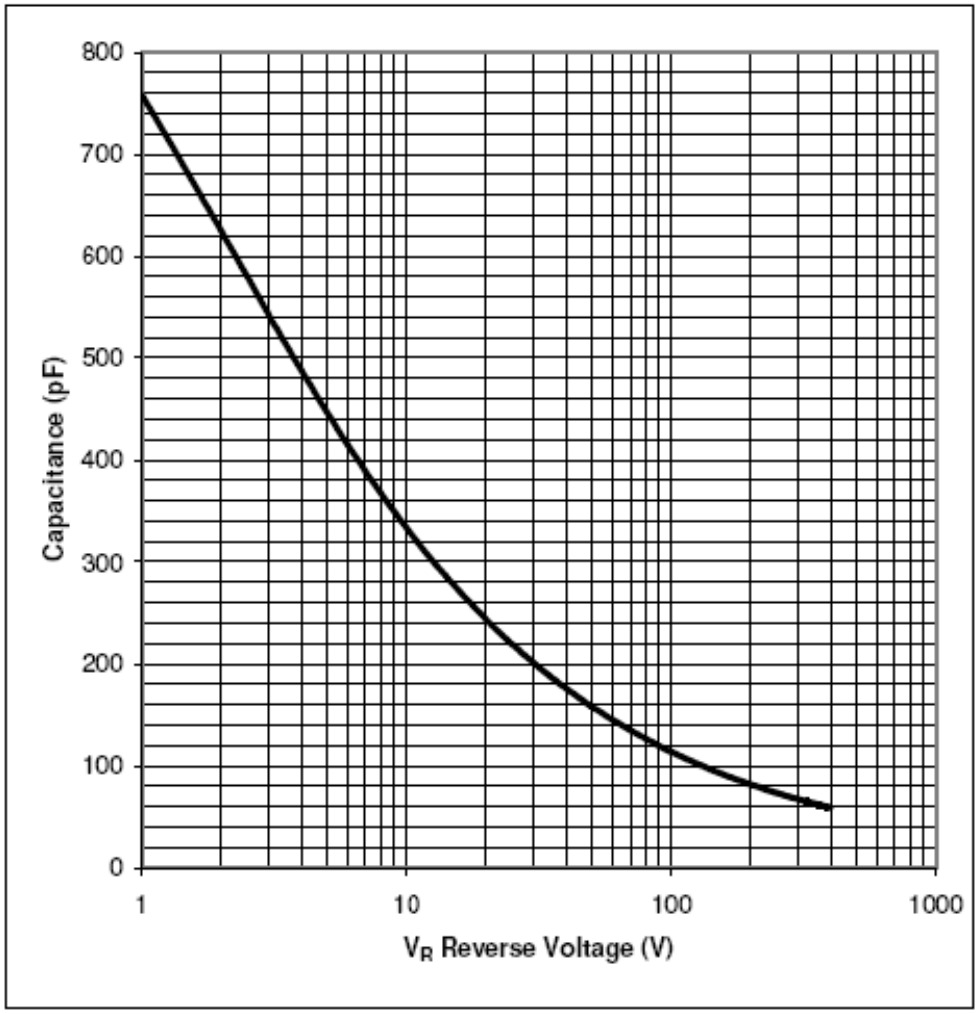

Fig. 33: Typical barrier capacitance versus blocking voltage[22]

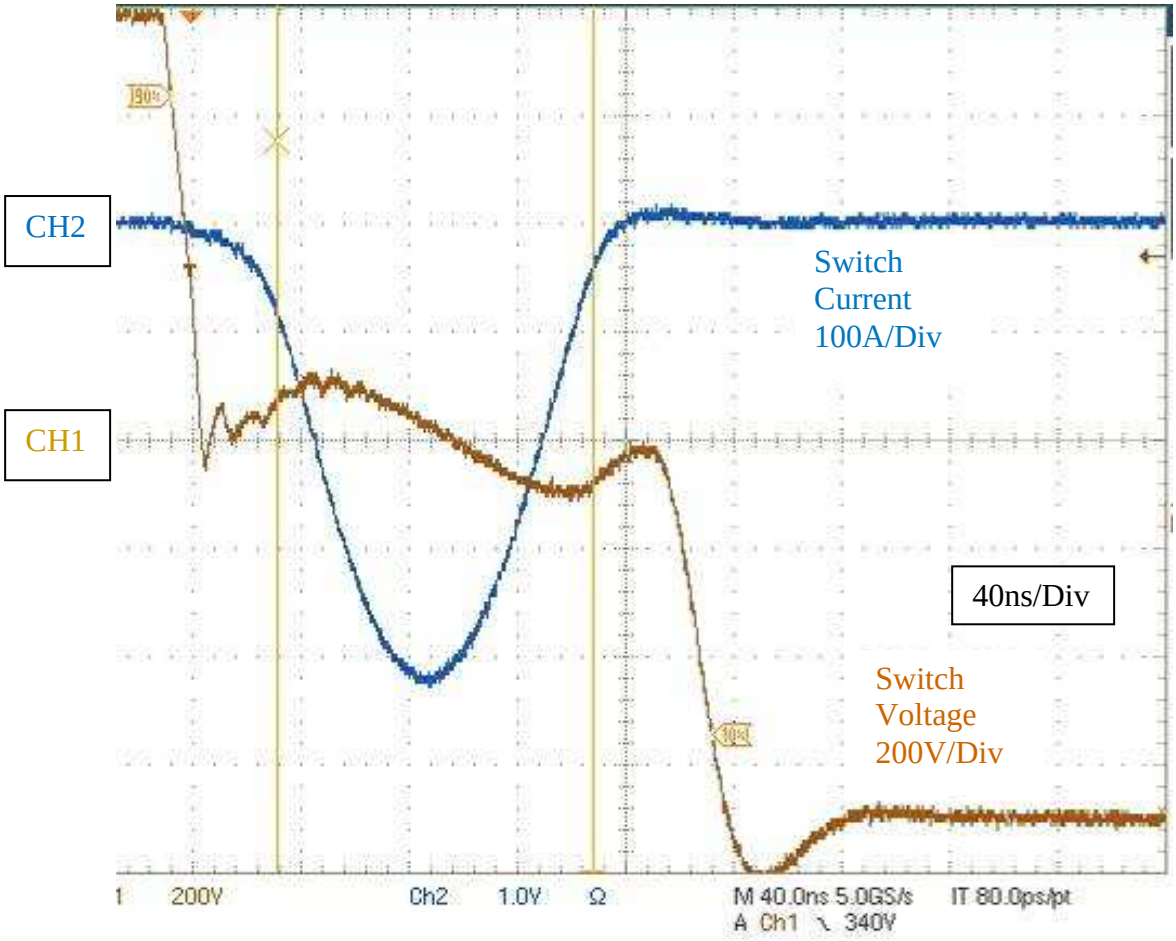

Fig. 34: Typical voltage of diode and MOSFET (CH1: Voltage of switch and diode; CH2: Current of Switch and diode)

After the first half wave the diode blocks the current. The waveforms indicate the nearly perfect behavior of the Schottky diode. Due to the very low capacity and the lack of storage time there is nearly no overshoot of the reverse voltage.

2.5.3 Simulation of the preferred diode

The model is based on an ideal diode with a threshold voltage and a dynamic resistance.
This could be directly implemented in the diode module of the simulation program.

2.5.4 Comparison of measurements and simulation

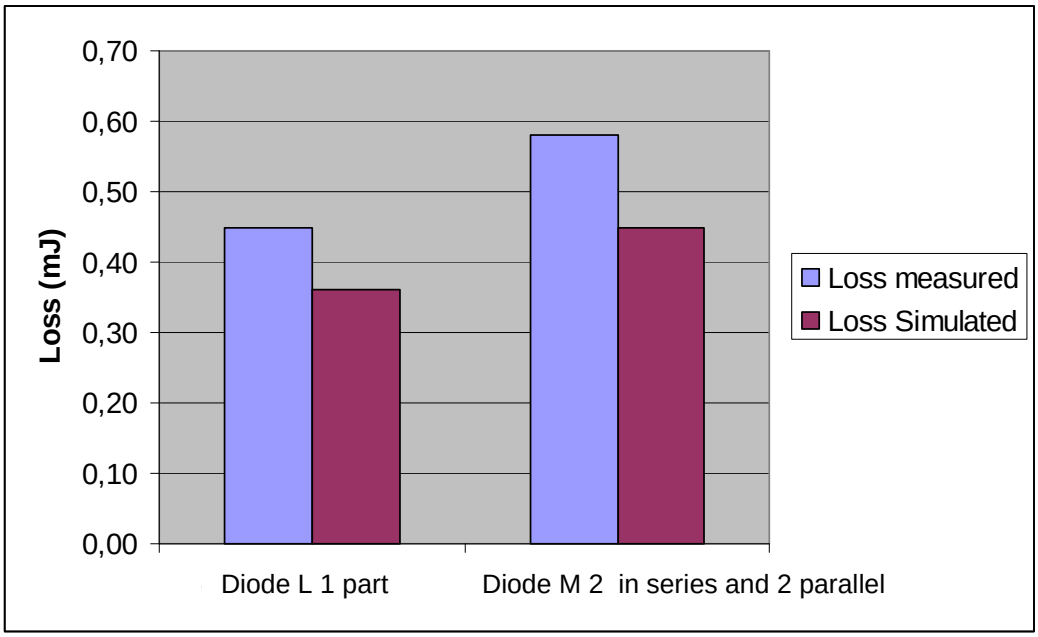

Fig. 35: Comparison of the measured and calculated losses of the two different diodes

The value of the diode conduction losses are acquired by measuring the loss of the switch and measuring the losses of the switch and the diode, the difference is the loss in the diode. The result is pretty close to the simulated values.
The dynamic behavior of the diodes of each supplier is very good.

2.5.5 Considerations about schottky diodes

The dynamic behavior of the Schottky diodes is nearly the same like the static behavior. There are no drawbacks like forward recovery or reverse recovery. It is amazing to what extent the availability of materials has influence the technologies.
Silicon carbide semiconductors will change power electronics dramatically in coming years.
The next key question is if switches can be produced in series production. However even the diodes available today have a strong effect on power electronics.

3 Verifying of the Models

3.1 Design of the test circuit

Irrespective of the circuit topology semiconductors have more or less subject to the same stress. This stress would be only reduced by introducing a pulse compression with all its consequences.
To test the components under real condition a very low inductive circuit has been developed.

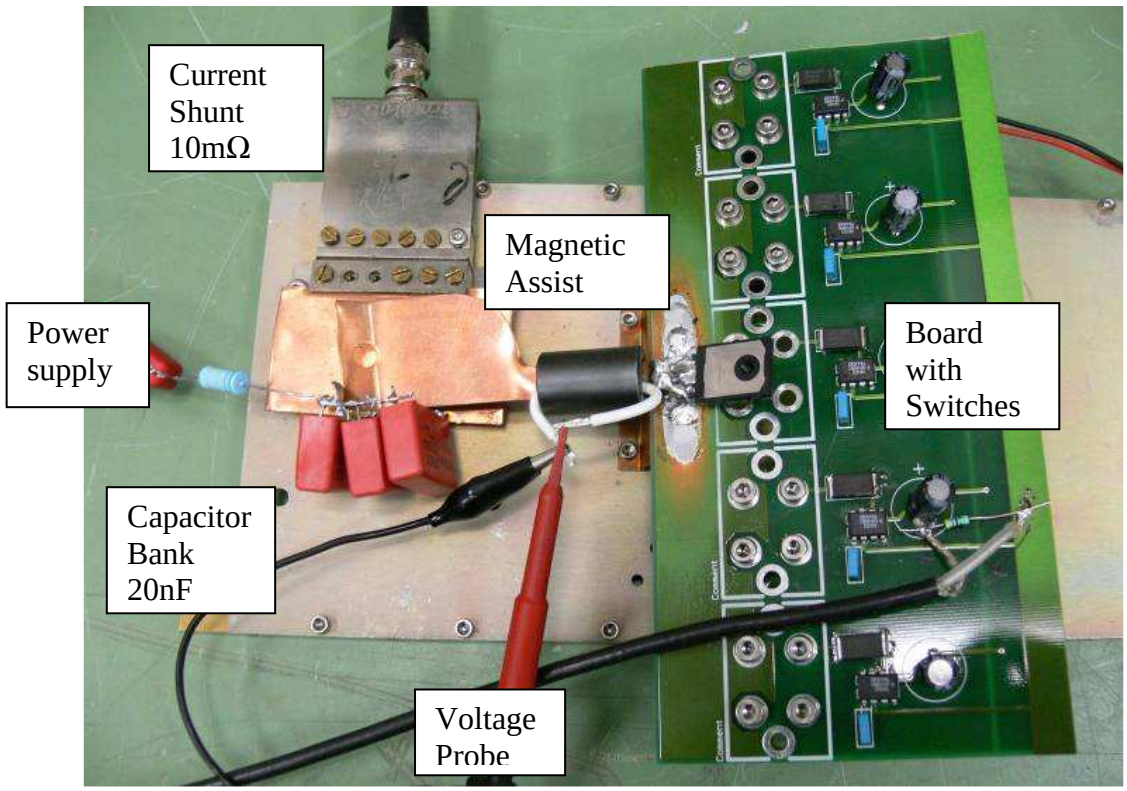

Fig. 36: Test circuit (the magnetic assist is measured) Peak current is 500A at 1000V supply voltage

The semiconductors are built on a low inductivity PCB board, for good current charring.
The current is measured with a low inductivity shunt resistor, the voltage with a 1:100- probe (Figure 36).
The critical point is the perfect tuning of the voltage probe. It is imperative to ensure an exact tuning of the probe. It is possible to tune the probe in the circuit; because due to the magnetic assist there are points where the current and rise of the current is nearly zero. At these points the measured voltages have to be also zero. Even with these adjustments the errors in the loss measurements are quite high and in the range of +/- 20 %.
The reason is that the voltage drop of an on-switch is small (in the range of 30 V) compared to the operation voltage (in the range of 1000 V), so very small measurements deviation causes a remarkable change in loss calculation.
For the calculation of the real circuit, the measurements in test circuits are valid.
The losses of the components are calculated with the integral of the multiplication of current and voltage. This works with the switch, the diode and the magnetic assist.

3.2 Comparison of the model and measurements

The single components are already simulated and compared with the measurements. In this chapter all components are put together in a test circuit and the results are checked for plausibility.

3.2.1 Comparison of the models and measurements switch

The results are already discussed in chapter 2.4.5. The measurements show a factor of 1.4 more losses than calculated in the simulation.
A reason couldn't found whether the measurements are the reason for the deviation or the switch has more losses than calculated.

3.2.2 Comparison of the models and measurements diode

The results are already done in Chapter 2.5.4. Both diodes were suitable in this application. The measurements show a factor of 1.3 more losses than calculated in the simulation.
A reason couldn't found whether the deviation is caused by the measurements or whether the switch has higher losses than calculated.

3.2.3 Comparison of the models and measurements magnetic assist

The development of the model for the magnetic assist was made in a circuit which is very similar with the test condition.
So the loss measurements and the models go very well together.

Materials of cores	NiZn Ferrite	
Core outer dimensions		
Core height	17,00	mm
Core inner diameter	10,00	mm
Core outer diameter	17,00	mm
Magnet flux swing	0,80	T
Filling factor	1,00	
Magnetic Cross section	59,50	mm^2
Magnetic path length	42,39	mm
integral of voltage time Core	0,05	mVs
Magnetic Volume	2522,21	mm^3

Insulation Thickness of core	2,00	mm
Wire diameter ink. Insulation	2,00	mm
Cross section of magnetic	218,50	mmxmm
windings	1,00	Wdg
Inductivity saturated µr=1	0,0067	µH
integral of voltage time	0,05	mVs
Cross section of all parallel wires	4,00	mm^2
Wire length	0,06	m
Resistance of wire (without skin effect)	0,0003	Ohm
Loss (volume)	11	J/m3
at magnetisation time	2	us
R parallel	40,83	Ohm
H-Saturated	300	A/m
Saturation Current	12,717	A
Inductivity unsaturated	1,87	µH

Table for Z-loop

X (current in A)	Y (inductivity in H)	
-10000,000	0,01	µ
-12,717	0,01	µ
-12,081	1,87	µ
12,081	1,87	µ
12,717	0,01	µ
10000,000	0,01	µ

Tab. 7: Calculation sheet for the magnetic assist

Magnetic assist:
Loss calculated: 0,56 mJ
Loss measured: 0,55 mJ

The losses are remarkable high. The total energy in the capacitors is 10 mJ (at 1000 V). The cause is that the magnetic assist is oversized for this application.
Also the leakage current in the model fits very well to the real measurements.
The model was originally developed for taped wound cores, but fits also very well for nickel zinc ferrites.
The model has one constraint. The permeability is constant irrespective of the magnetization speed. This leads in the model to a higher reset current than needed in reality.
In practice the resetting of the core is no big issue so this constrain is acceptable.

3.2.4 Plausibility check of the measurements

Due to the difficult measurements of the losses a plausibility check has been made. In this measurement the voltage in the capacitor bank is measured before and after the switch. This measurement is less sensitive because the voltage measurements are on a longer time scale. The disadvantage is that only the total loss of the circuit could be measured.

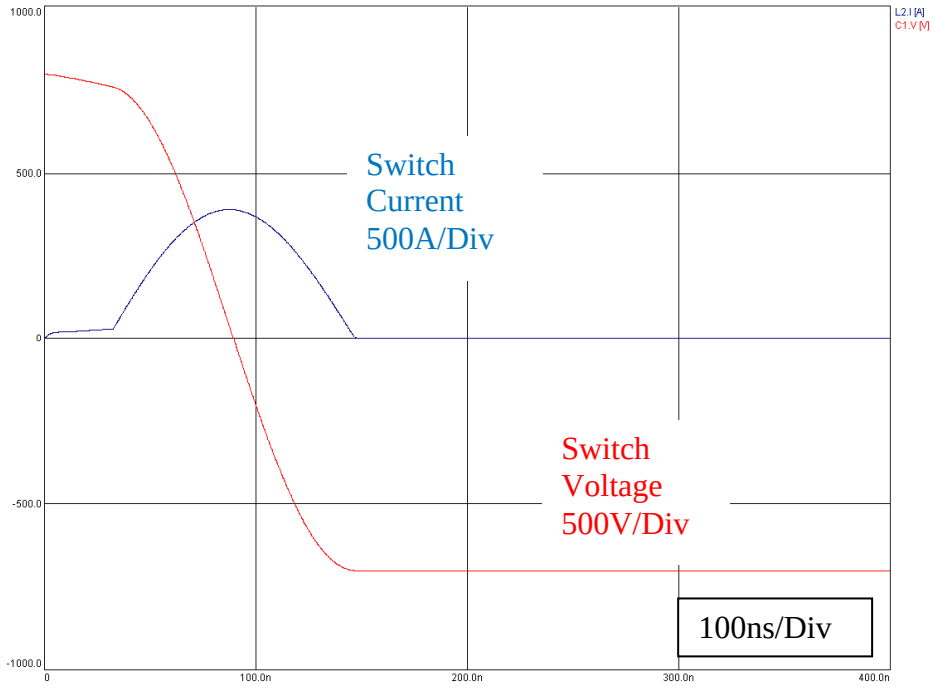

Fig. 37: Simulated test circuit (Red: Voltage of switch and diode; Blue: Current of Switch and diode)

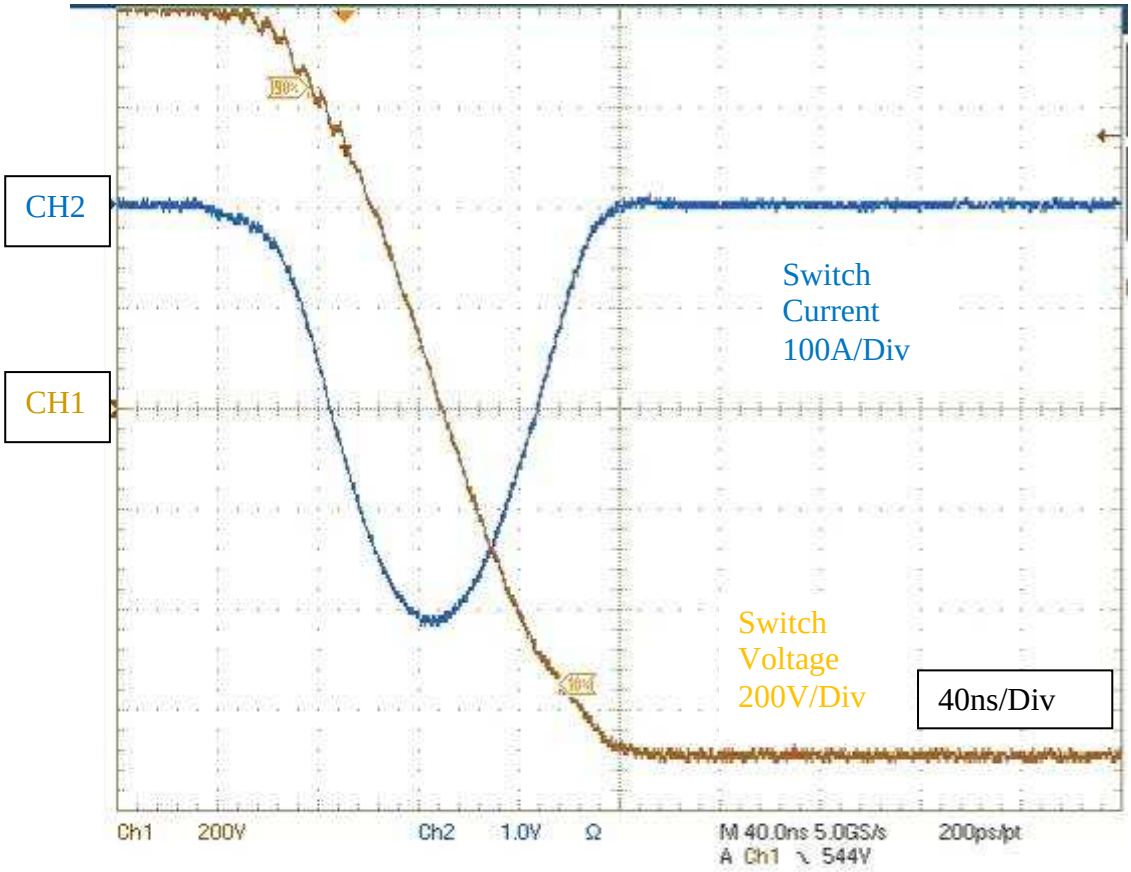

Fig. 38: Measured test circuit (CH1: Voltage of switch and diode; CH2: Current of Switch and diode)

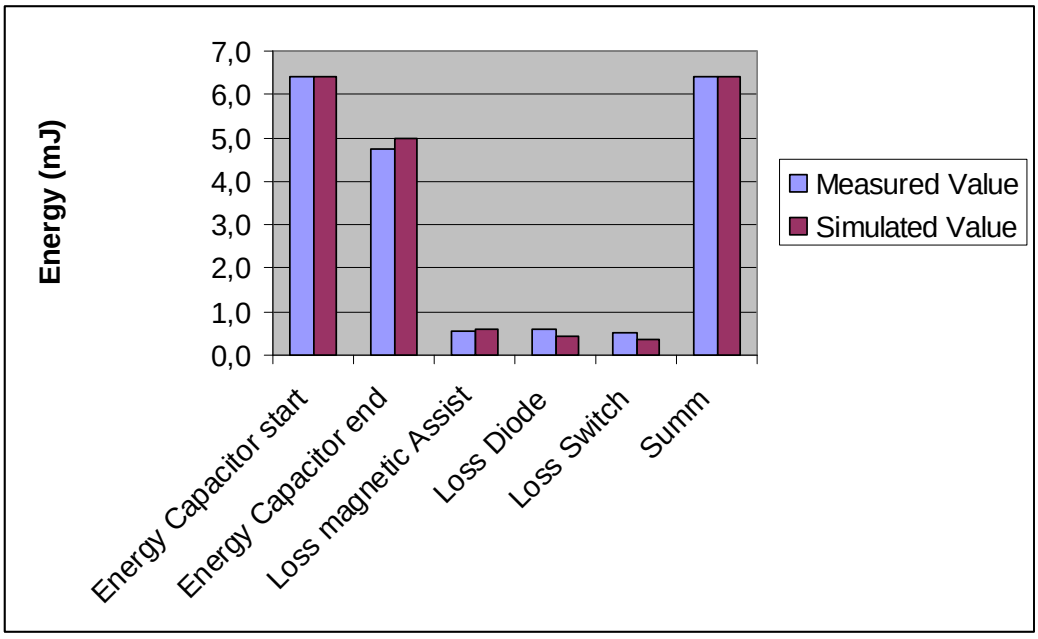

Fig. 39: Overview of measured and calculated losses (the data of the diode, switch and magnetic assist were measured with the method described in chapter2)

The comparison of the measured (Figure 38) and calculated (Figure 39) values shows that the measurements are better than expected. This result gives us a strong indication that the losses on the switches and diodes are 20 % to 30 % bigger than calculated (Figure 39). All in all the results are very good and show that such a fast circuit is possible with the parts suggested.

4 Topologies for the circuit

The topology of a circuit is normally the first consideration, because the needs for the parts depend of the topology. Here, the stress of the components (exception is the capacitor) is independent of the design as long as there is no pulse compression. Depending of the design the semiconductors are stacked or paralleled, but the peak current and peak voltages for each component keep within the same range.
In the next chapters some possible concepts are presented.

4.1 Marx design

The Marx design has some very useful features which make it very attractive for pulsed power application.
The main benefit is that the voltage is pushed up without a pulse transformer. This is the reason why it is used for high energy pulse generation, especially for lighting simulation, cable testing, EMP pulses and many other applications.
The exact and fast charging of the paralleled capacitors is not possible, because of the coupling inductors or resistors.

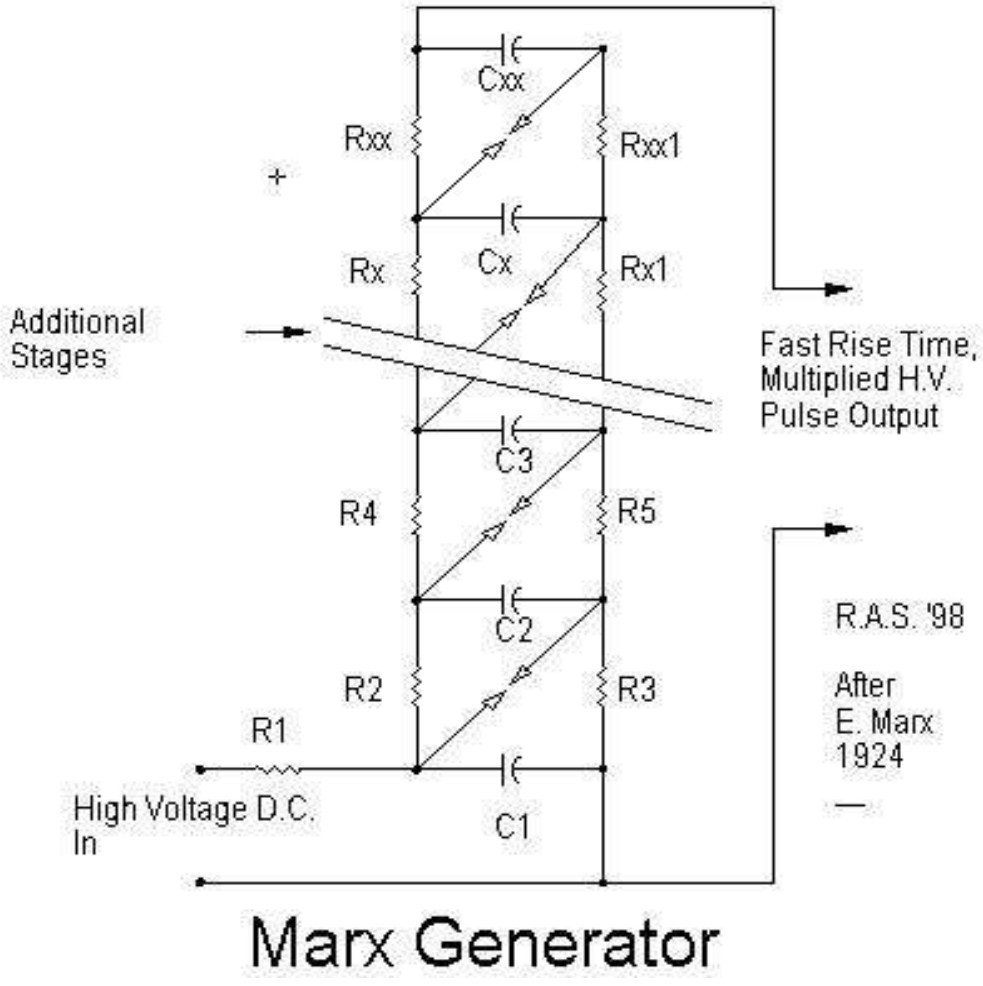

Fig. 40: schematic of a Marx generator (Hendrik Hoelscher Web site)

This limitation is nearly impossible to overcome. The only chance is to charge all capacitors with floating current sources.
So Marx generators are very versatile high-energy low-repetition rate pulse generators, but not suitable in this application.

4.2 Design with step-up transformer

The main advantage of a design with step-up transformer is that the semiconductors have only to be paralleled. The challenges for the power supply are also lower because the charging voltage is low (800 V).
On the other hand the efficiency of the circuit is reduced (10 %) because of the transformer.
The primary side has to be very low inductive (2.4nH) and such a low inductive design is quite challenging. In this loop the inductivity of the semiconductors, the magnetic assist and the stray inductivity of the pulse transformer has to be included.
For proper operation it is also necessary to ensure a good current sharing.
In this case only a fractional turn transformer could do the job.

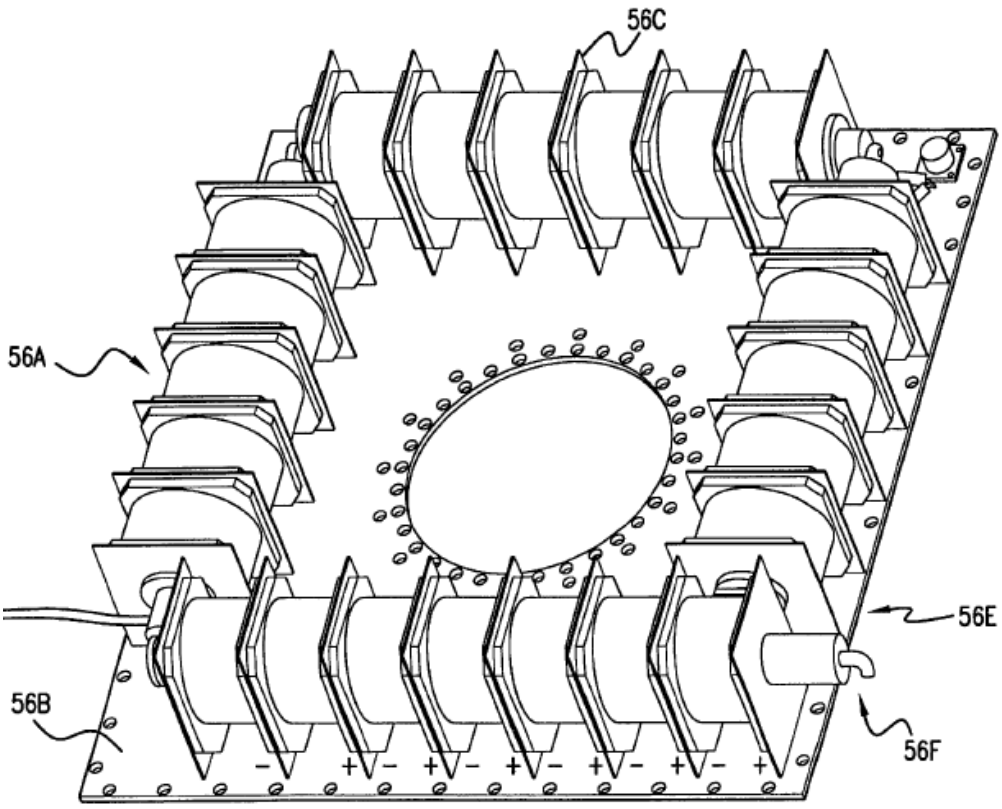

Fig. 41: Fractional turn transformer[23]

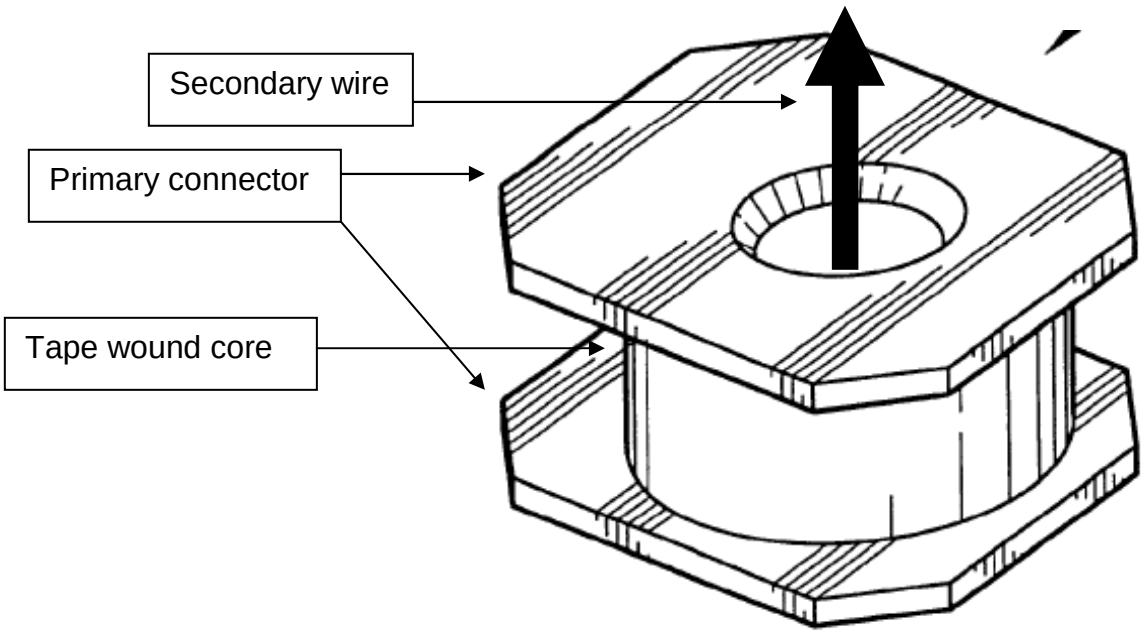

Fig. 42: Fractional turn element[23]

The design of such a transformer is very laborious. Also the amount of core materials is quite big. Due to the huge amount of core material the losses in the material are quite high. Approximate calculations show that at least 10 % of the transferred energy is dissipating in the core.
So, such a fast pulse transformer is very challenging and is not suited for this application.

4.3 C-C Transfer circuit basic concept

The C-C transfer circuit is well known from the Thyratron design. The schematic can be seen in Fig. 43.

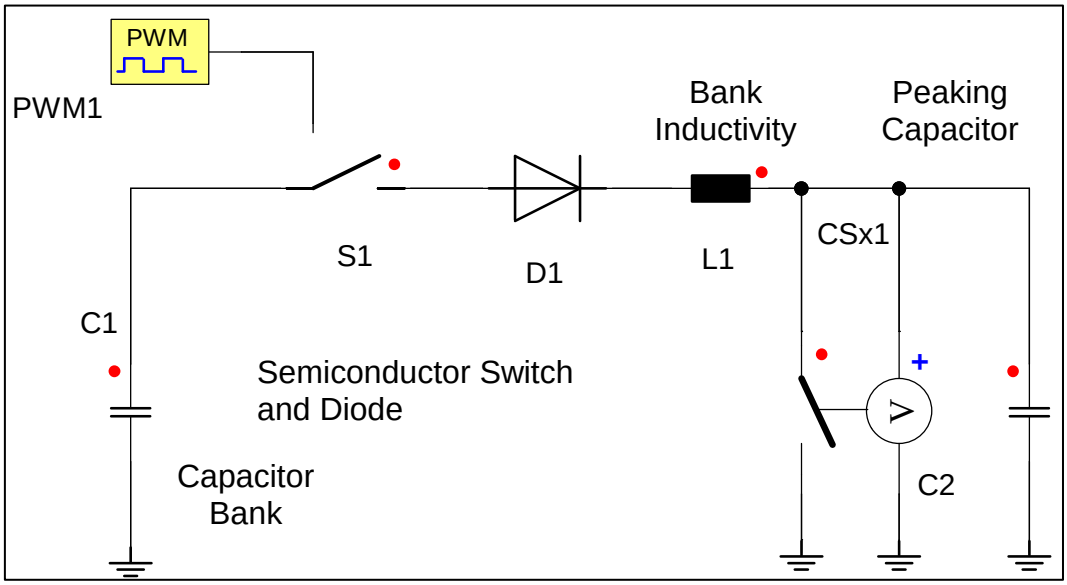

Fig. 43: Schematic of the C-C transfer circuit

The energy is stored in the primary capacitor (bank). The voltage is already in the required range of the load. If the switch closes the energy is transferred to the peaking capacitors. The duration of the energy transfer is determined by the inductivity of the bank (and the magnetic assist which is located in series to the bank).
The discharge is simulated by a switch which discharges the energy of the peaking capacitor. The discharge represents more or less a short circuit for the bank circuit. The energy which is left in the bank circuit has to be controlled. The diode prevents the ringing of the circuit and is so very important for the operation of the laser (Figure 44).

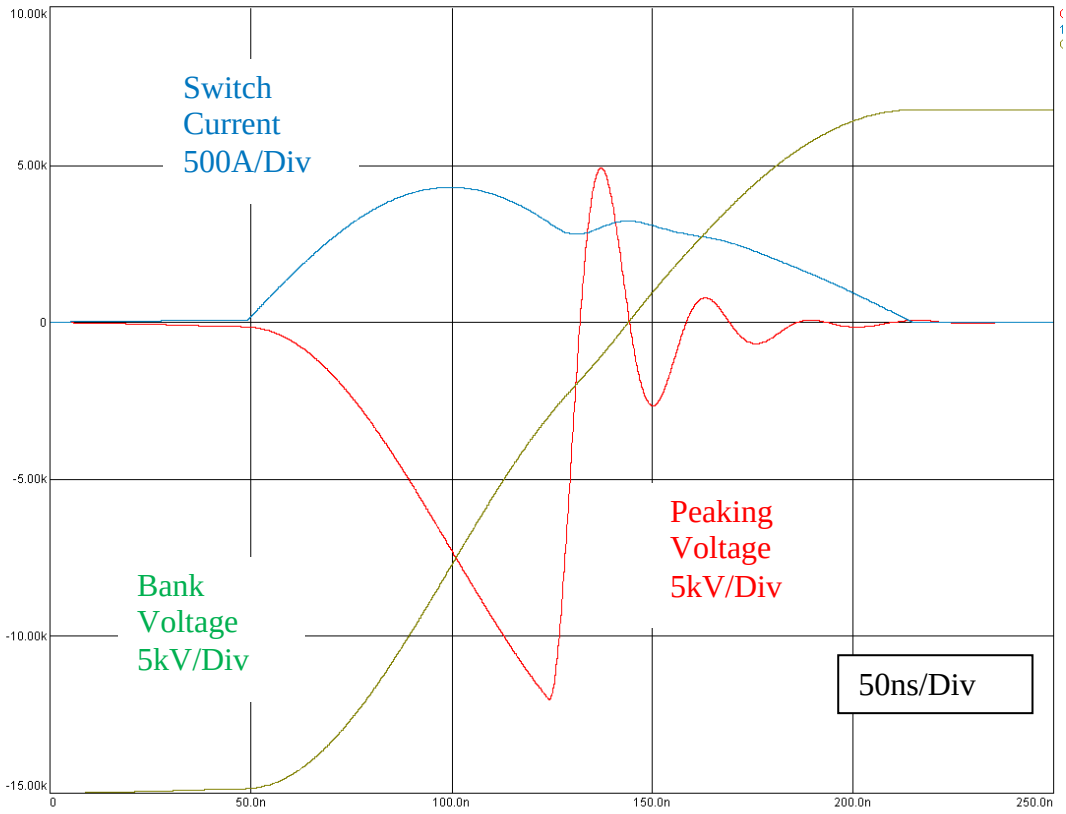

Fig. 44: Simulation results of the C-C transfer circuit (Red: peaking voltage; Blue: Switch current; Green: Bank voltage)

In principle, the design is very simple and straight forward. The challenging part is to stack and control the semiconductors.

Parameter	Calculation result
Peak current:	0,5kA
Peak voltage:	15kV
Reverse Voltage:	8kV
$I_{average}$ =	0,5A (@10kHz)
I_{RMS} =	13A (@10kHz)

Tab. 8: Calculation results of the proposed design

From our point of view a C-C transfer circuit seems to be the smartest solution and will be realized.

5 Design of the circuit

5.1 Selection of the components

The selection of the components has some non-objective aspects. Performance price sizes and availability are important, but also experiences and preferences.
System constrains, production equipment and relations to the supplier could play also a role. For industrial production it is very helpful to have a second source for the crucial parts.

Primary Capacitor:
For this application the standard is normally a Class II high voltage disk capacitor. The losses are in the range of 2% of the stored energy. Due to the high repetition rate big changes in temperature are expected. This would results in changes in capacity.
Due to the low energy it is possible to implement multilayer high voltage NP0 capacitors. The losses are very low (in the range on 0,1% and negligible).
All properties are very stable even with very long operation time.
In this case four 10kV 2nF capacitors put in series. The result is a nominal Voltage of 40kV. This overrating is necessary because of the voltage reversal of 50% (peak to peak voltage of 23kV).
To get a total capacity of 2nF, 4 rows have to put in parallel. This results a total quantity of 16 components.

Switch:
The most cost effective switch is the MOSFET A in Plus246 housing.
For low losses and safe operation 4 parallel and 24 in series are taken.

	Stack	calculated
Peak current	800A	500A
Peak voltage	19,2kV	15,0kV

Tab. 9: showing the requirements for the switches

Diode:
Due to the smaller reflected voltage the peak voltage for the diode is reduced. For low loss and safe operation 4 parallel and 24 in series (diode K or diode M) are taken.
The reason why the obviously optimal component the 1200 V diode is not taken, is that with the 600V diode with the Infinion type a “drop in replacement” is possible, whereas an uncomfortable single-source supply with the 1200 V are taken place.

	Stack	calculated
Peak current	1000A*	500A
Peak voltage	14,4kV	8,0kV

Tab. 10: Show the requirements for the diodes. *The value is for non-repetitive 10µs pulses. Due to the shorter pulses no life time problem with the design is expected.

Magnetic assist:
The magnetic assist is made of an EMI suppression core. One critical point is the losses of the core. Even this material has very low losses (in comparison to all other materials) the thermal load is remarkably high.
The exact values are calculated in chapter 5.3.

5.2 The switching cell and PCB board design

To ensure good current and voltage charring 4 parallel switches and two parallel diodes are connected to one switching cell. 24 switching cells make one complete stack.
The layout is quite challenging. The design has to be as low inductive as possible, to reduce the inductivity of the complete stack. The gate control has to ensure that every switch carries the same current. The design provides that every transistor has its own gate transformer wire loop. Hence drop of voltage in the bottom plane ("ground") did not lead to different gate signals.
The top plane works also as a heat sink for the transistors as well as for the diodes. Fortunately the cases are connected in the right way that no insulation is necessary.

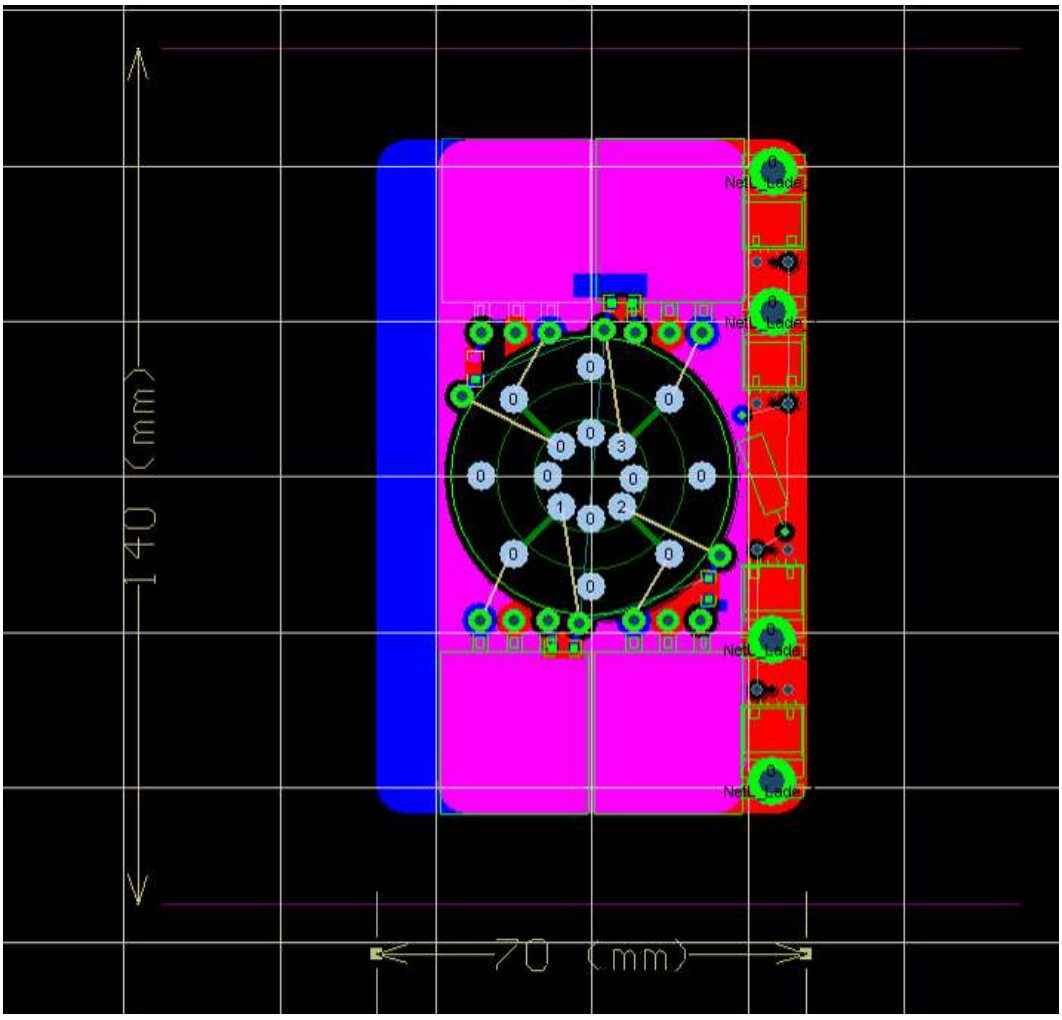

Fig. 45: Showing the Layout of the switching cell (red top layer); blue Bottom Layer). (The width of 140mm is the width of the total PCB with insulation distances).

The layout is arranged in such a way to ensure that the switching cells could line up. The design is very symmetrical so the boards could be stacked up and the transformers are in a line. The calculated inductivity of one board is approximately 100nH. For the complete stack the stray inductivity is ca 600nH. The arrangement can be seen in Fig. 46.

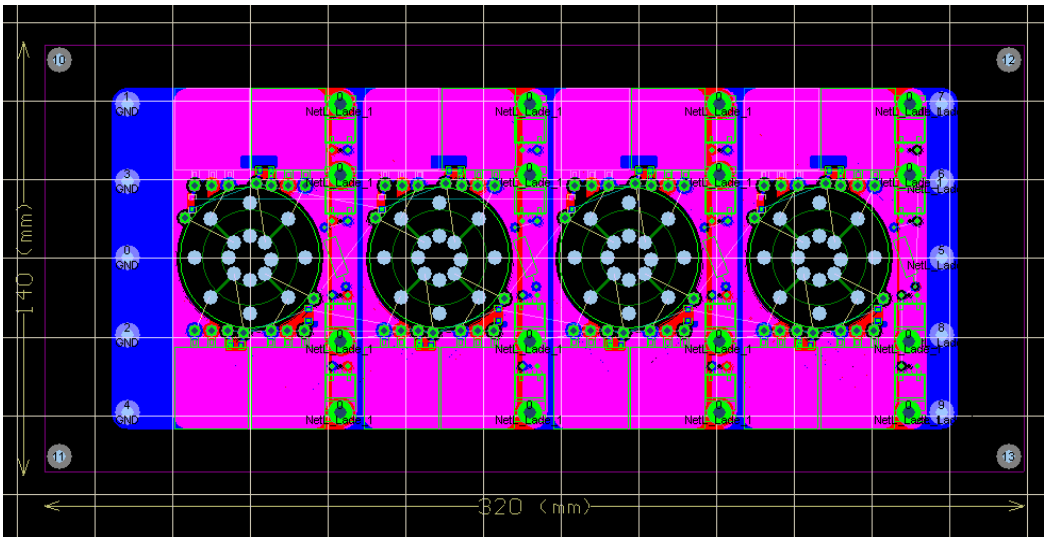

Fig. 46: PCB board with four switching cells (red top layer); blue Bottom Layer

5.3 Simulation of the final laser circuit

The information from the test circuits is summarized in Tab. 11.

Part	Type	Parallel	Series	Sum
Primary C 2nF	NP0 1nF 10kV	8	4	32
Switch	Transistor A	4	24	96
Diode	Diode M	4	12	48
Magnetic Assist	costume	1	1	1

Tab. 11: Overview of proposed part

Primary capacitors:
The very small losses are neglected in the calculation. The effective capacity is 2nF (0,22J of stored energy in total).

Diode:
Diode M is chosen.
The key data of the diode are:
Voltage drop at very low current: 0,95V
Dynamic resistance: 44mΩ

4 diodes Parallel and 24 stages in series resulting:
Voltage drop at very low current: 22,8V
Dynamic resistance: 264mΩ

MOSFET:
From the values from the single device the stack could be calculated.

current (A)	RSD on (Ohm) (single Device)	Current (A) (stack)	RSD on Ohm (stack)
0	0,14	0	0,86
20	0,15	80	0,90
40	0,16	160	0,95
60	0,17	240	1,01
80	0,18	320	1,08
100	0,20	400	1,22
120	0,23	480	1,35
140	0,27	560	1,62

Tab. 12 Overview of the RSDon of the stack

These values are put into the simulation. The RSD on of such a high voltage stack is quite high.

Magnetic assist:
Due to the higher operation voltage the magnetic assist has to be adapted to the stack. Higher stray inductivity is acceptable. The overall inductivity is ca 1µH. 400nH is acceptable in the magnetic assist. The other 600nH we need for the stack. The stray inductivity of the magnetic assist might be a little tuned during the first tests.

Materials of cores	NiZn Ferrite	
Core outer dimensions		
Core height	17,00	mm
Core inner diameter	27,00	mm
Core outer diameter	41,00	mm
Magnet flux swing	0,80	T
Filling factor	1,00	
Magnetic Cross section	119,00	mm^2
Magnetic path length	106,76	mm
integral of voltage time Core	0,10	mVs
Magnetic Volume	12704,44	mm^3

Insulation Thickness of core	0,00	mm
Wire diameter ink. Insulation	5,00	mm
Cross section of magnetic	264,00	mmxmm
windings	6,00	Wdg
Inductivity saturated µr=1	0,1157	µH
integral of voltage time	0,57	mVs
Cross section of all parallel wires	4,00	mm^2
Wire length	0,35	m
Resistance of wire (without skin effect)	0,0015	Ohm
Loss (volume)	11	J/m3
at magnetization time	2	us
R parallel	1167,34	Ohm
H-Saturated	300	A/m
Saturation Current	5,338	A
Inductivity unsaturated	53,50	µH

Table for Z-loop

X (current in A)	Y (inductivity in H)	
-10000,000	0,12	µ
-5,338	0,12	µ
-5,071	53,50	µ
5,071	53,50	µ
5,338	0,12	µ
10000,000	0,12	µ

Tab. 13: Magnetic assist for the stack

The stray inductivity of the magnetic assist is in reality ca 1.3 to 2.0 times higher than in the calculation (ferrite μ_r~1.3 to 2.0). In the simulation this is put in the stray inductivity of the stack.
To reduce the power losses in the magnetic assist a gaped core is used. In this case a reduction of the heat production to ¼ of the original value is achieved. The reduction of the hold of time to the half is compensated by a second magnetic assist in series. The resulted doubling of the saturated inductivity is compensated by paralleling two rows of magnetic assists.
The other advantage is that the core resets itself and no additional reset loop is necessary.

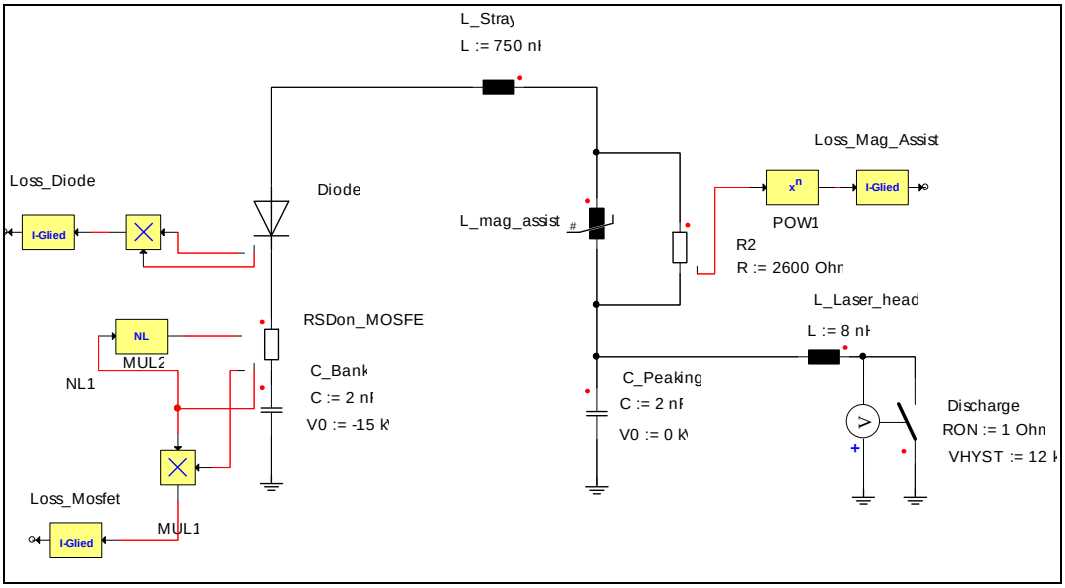

Fig. 47: Simulation model of the stack

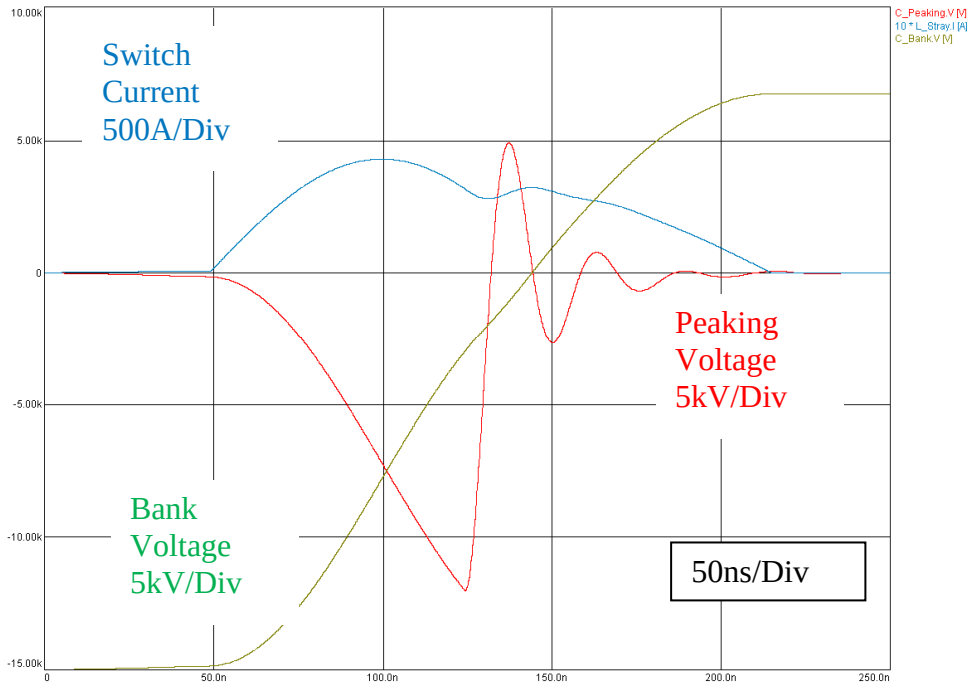

Fig. 48: Shows the result of the simulation of the final circuit (Red: peaking voltage; Blue: Switch current; Green: Bank voltage)

From this simulation (Figure 47 and Figure 48) the losses could be extracted (Tab. 14).

C_Bank start	225,00	mJ
C_Bank end	47,00	mJ
Energy difference	178,00	mJ
Magnetic assist	4,99	mJ
Loss Diode	2,27	mJ
Loss MOSFET	15,54	mJ
Loss sum	22,80	mJ
Energy Peaking	151,29	mJ

Tab. 14 Overview of the energy in the circuit

According to the calculations the efficiency of the total stack is 90% which is remarkable high. The original values from the data sheet were taken in the calculation. So in reality in the semiconductors ca 1.3 times higher losses are expected. The efficiency of the circuit would be in this case 87%. Also the losses of the switches and diodes rise with higher temperatures the overall efficiency still remains superb compared to other solutions.

5.4 Thermal considerations

The thermal load for each component could now be calculated easily.

Each MOSFET:	1,6W average
Each Diode:	0,5W average
Each magnetic assist core:	12,5W average

Tab. 15 Thermal load of the main components of the stack

The main energy is dissipated in the component within the 100ns of current pulse length. During this short time no heat conduction takes place.

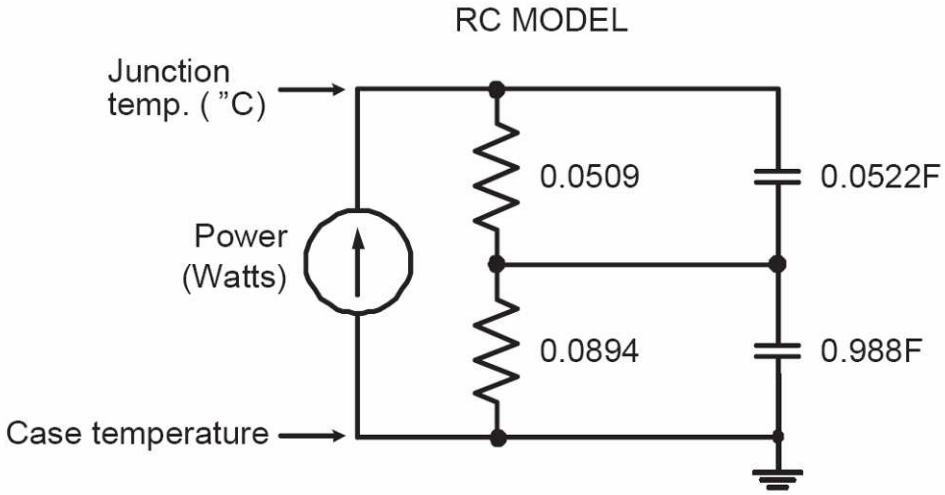

Fig. 49: Thermal Model of the transistor B[24]

The thermal capacity is represented by the capacitors. The thermal resistance is represented by the resistors. Due to the very short current pulse the calculation could be spitted in two steps. One step calculates the thermal rise due to energy deposition during the short pulse; the other step is to calculate the average temperature rise due to the heat flow.
To calculate the peak thermal power flow only the current and conduction resistance is necessary.
The peak current for each switch is 120 A. The nominal resistance of each switch is 0.15Ω. Due to high current and thermal effects 0.3 Ω are assumed.
The peak power loss is calculated 4320 W.
The thermal capacity is in total 0.05F. The temperature rise of the crystal is only

ΔT=0,01K for each pulse.

The average thermal flow is 2W for each switch. A heat sink temperature of 40℃ is expected. The total thermal resistance is 0,14W/K. The temperature rise is

ΔT=0,28K in average.

The average power is also quite small and should be no issue with forced air cooling. So only a small raise of crystal temperature of the semiconductor is expected.

The main issue is the loss in the magnetic assist. The calculation is made under the condition that the core is reset. If the core isn't reset the losses are reduced due to smaller flux swing. Under this condition the hold of time is only half (app. 30ns) of the reset core and the losses are only a quarter of the reset core.

5.5 Voltage sharing static

The voltage sharing is a critical part when stacked semiconductors are used. The main problem is that the leakage current is not well defined and depends also largely on the temperature.
The current through the resistor chain has to be 5 to 10 times higher than the leakage current through the components.
On the other hand all modern semiconductors are avalanched rated. This helps to ensure a safe operation even when on stage should have more leakage current.
The leakage current of a semiconductor switch depends on temperature and operation voltage. The values in the data sheet are normally much higher than the real conditions. Also the leakage current is smaller if not the full voltage is applied (Fig. 50).

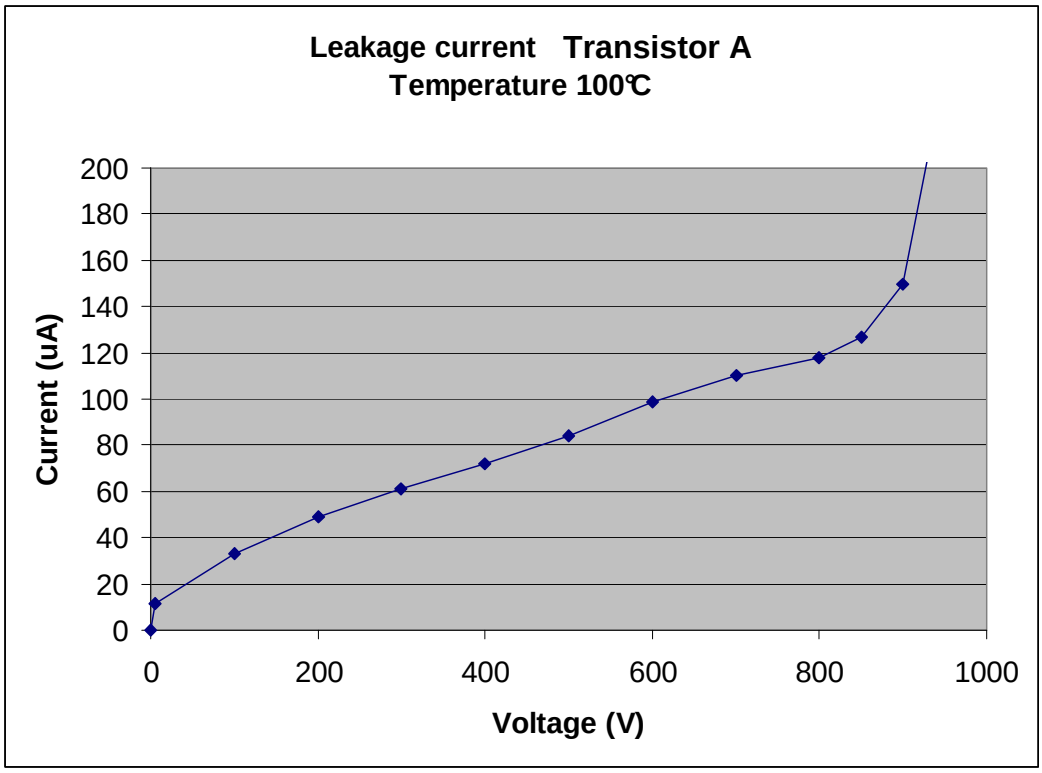

Fig. 50: Leakage current at 100℃ at different volt ages

The Switch is operated at 625V. Hence the leakage current (100µA) is 20% less than at nominal voltage.
The expected operation temperature is 40℃.

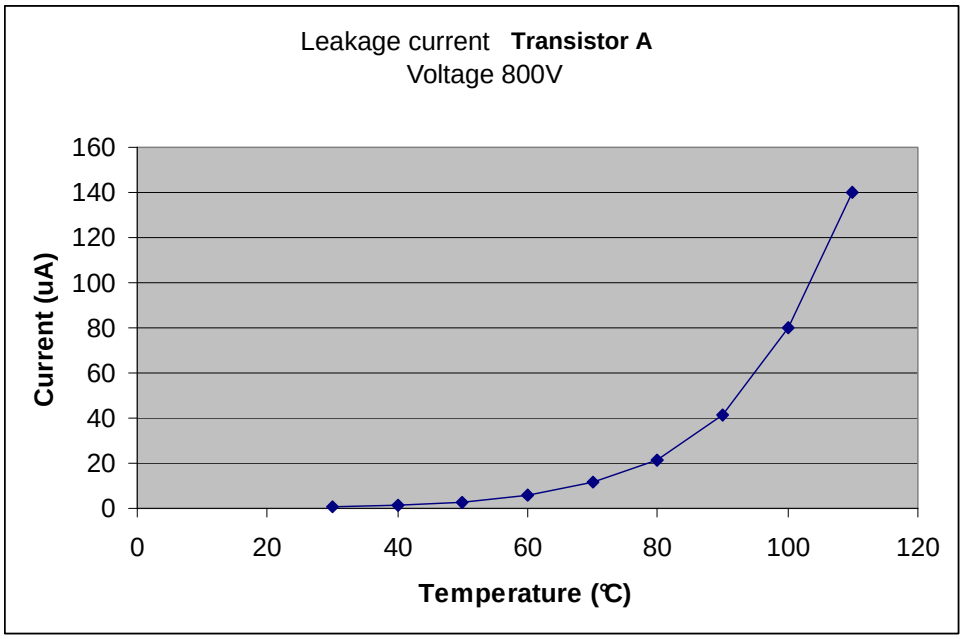

Fig. 51: leakage current at different temperatures at 800V

At 40℃ the leakage current is 1.0 µA for each switch. 4 switches in parallel resulting 4µA at 40℃, 10uA at 50℃ and 24 µA at 60℃ are expected.
In a total leakage current of ca 100µA could be expected. To fulfill the 1:10 rule (current through balance resistor should be 10 times higher than the leakage the temperature of the switches must be lower than 50℃ .
The result is a time constant of ca 0.3 s (discharge time of the bank). The resistor parallel to each stage has to be 10MΩ.
It is also a good practice to use all components from one batch, reducing the variation of all parameters.

5.6 Voltage sharing dynamic

Sometimes a dynamic voltage sharing is necessary. A rule of thumb is that the capacity should be 10 times higher than the junction capacity of the switches.
First test with the stack shows that dynamic shows that especially the diodes have problems with voltage sharing (see chapter 5.8).
In the first tests only with static voltage sharing is used. A first test with the stacks reveals that only static voltage sharing is not enough for save operation and dynamic voltage sharing elements has to be added.
One problem is that the capacity of the depletion layer is voltage-dependent. The factor is remarkable high in the range of 10 (see Fig. 32).Small deviation of the timing or the depletion layer capacity result in much higher differences in the voltage across each device than the deviation.
To improve voltage sharing dynamic balancing element have to be added. Because it seems that the diode is more affected by unbalanced voltage distribution it has to be focused on this component.

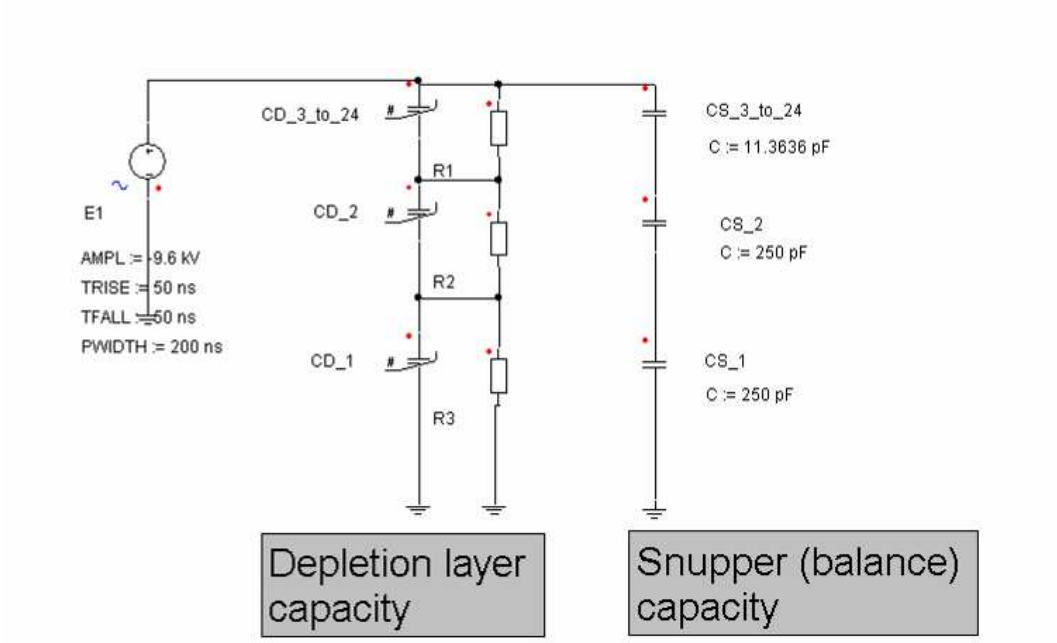

Fig. 52: Simulation circuit to compute the effect of unbalanced diodes

First the effect of one slightly smaller (-10%) depletion layer capacity (CD_1) is checked.

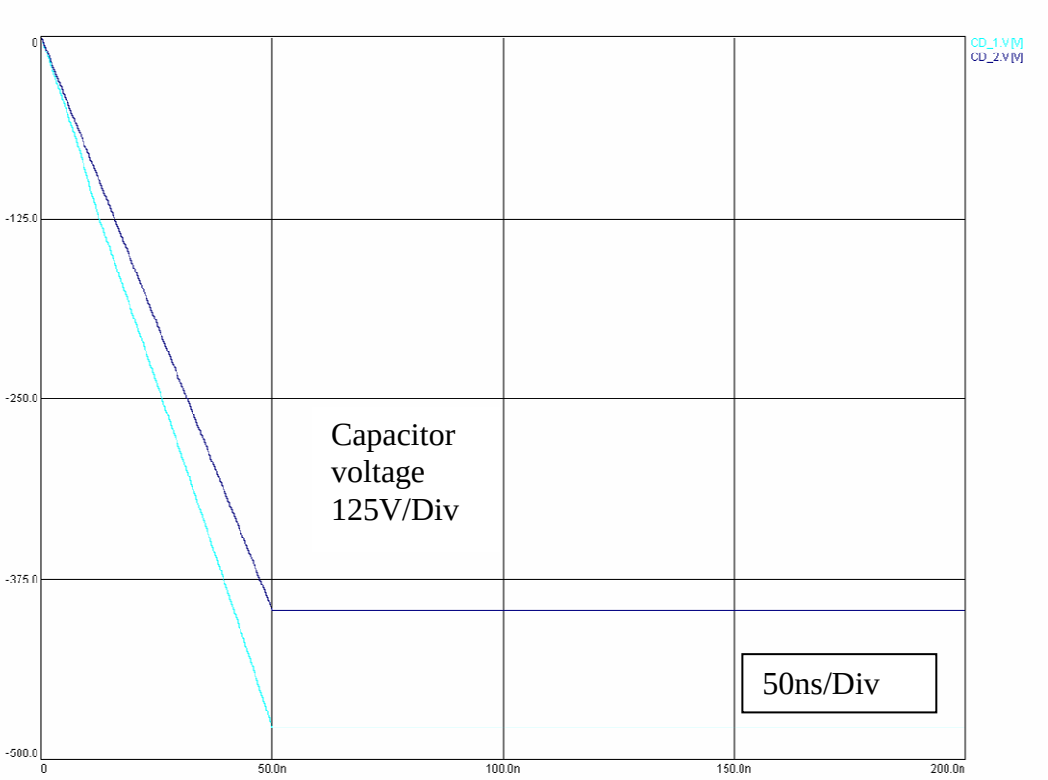

Fig. 53: Voltage sharing of a slightly unbalanced diode line

The effect is amazingly high in this example ca +20% Voltage. This example gives an impression of the fragile voltage distribution (Fig. 53).

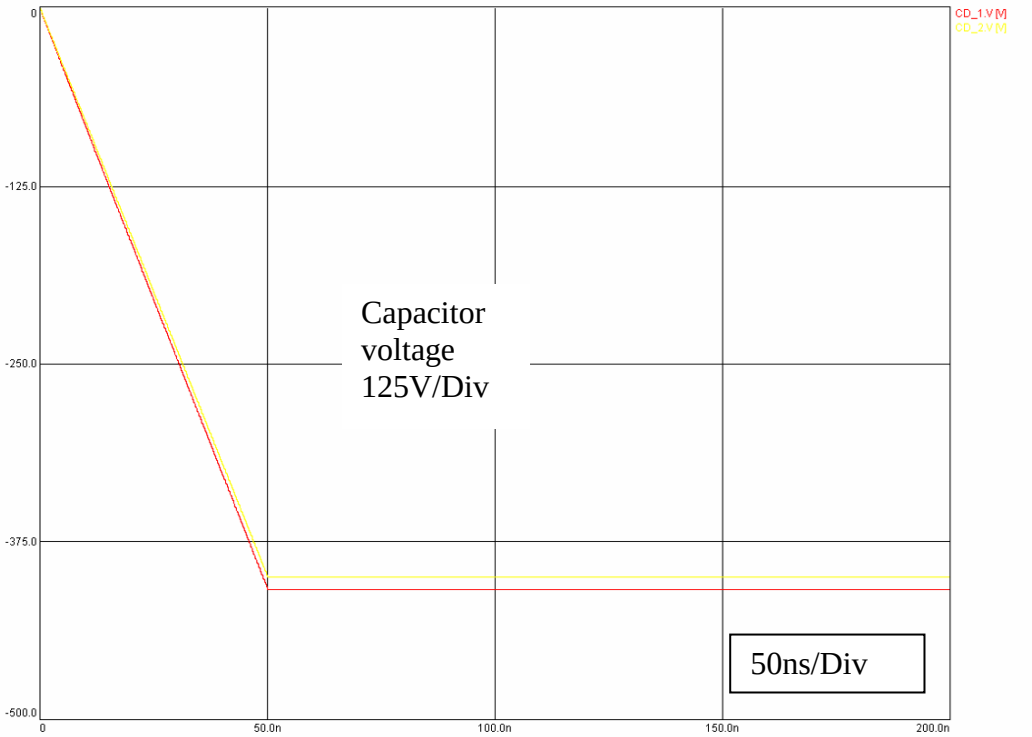

Fig. 54: Voltage sharing of a slightly unbalanced diode line and balancing network

For this example calculation was only one row of diodes. In the real circuit we have 4 Diodes in parallel hence balancing capacitor has to be 1 nF. The calculation shows (Fig. 54) that the dynamic voltage sharing works and voltage differences are reduced. To avoid ringing the balancing resistor needs also a damping resistor.
The overall inductivity of the circuit is ca 1 μH. The capacity of all balancing capacitor is 41pF (1nF divided by 24).
The impedance calculates to 156 Ω. There are 24 stages so each damping resistor should be in the range of 6.5Ω. We start with 5 Ω and 1nF.
The components have to be chosen carefully. One important parameter is the stray inductivity. In this case carbon mass resistors and high voltage disc capacitors are used. It is important that the leads are as short as possible and close to the load.
One other source of unbalance is the coupling capacity of the gate transformer and the coupling capacity to the ground.
The gate transformer has a coupling capacity of 10pF (see chapter 5.6).
The coupling capacity to the ground is in the range of 1 pF (A= 15cm^2; d= 2cm) and is negligible compared to the gate transformer.
On the first point of view it seems that the capacitive coupling of the gate transformer is negligible compared to the dynamic voltage sharing capacitor of 1 nF (factor of 100). The punch through is remarkable higher as the capacity relation indicates.
The voltage drop of the transformer is 24 times higher (at the last stage and hence worst case) than the voltage top of the balancing capacitor. So the effective capacity is ca 240pF. This is one quarter of the balancing capacitor (1 nF). Hence maximum voltage deviation is ca 25% which is less than the safety margin of the components.
The additional loss of the balancing capacitor is ca 2 % of the total energy and hence is acceptable.

5.7 Gate control

The gate control of floating semiconductors is a well known problem in power electronics; especially for motor driving different solutions are used. In this case only two designs are feasible, gate control with optic fiber or gate transformers.
The controlling with optic fiber is very precise versatile and the on-time could be from some ns to continuously.

Fig. 55: Stack of Thyristors with fiber optic control (orange wires) (ABB web site)

The disadvantage is that the gate control electronic need a power supply. This has to be done with transformers (dark red wire with cores) with high insulation between the windings (Fig. 55).
A design with a gate transformer needs no (or nearly no electronic) on the high voltage side and the power for the gate control is transferred with the gate transformer.
The gate transformer has to be of low inductivity to ensure a tight timing and fast turn on and off.
A very important part is that the loss on the core is not too high. The losses in the cores tend to absorb driving energy and could also reduce the dynamic response.

The voltage time integral of the core has to be much higher than the voltage time integral of the signal to prevent saturation of the core even without reset the core.
In this case the signal is ca 20V and 200ns long, resulting an $\int Udt = 4\mu Vs$. The core has an $\int Udt = 40\mu Vs$ which is by far sufficient.

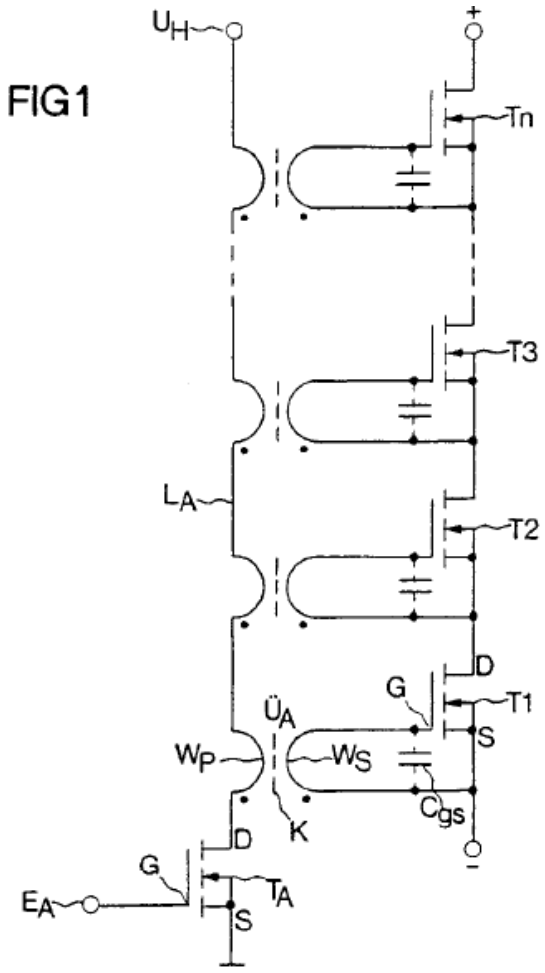

Fig. 56: Principle design of the gate transformer (Patent DE3630775C2)

Our design is not affected by the patent because several parallel wires are used.

Materials of cores	NiZn Ferrite	
Core outer dimensions		
Core height	8,00	mm
Core inner diameter	19,00	mm
Core outer diameter	31,00	mm
Magnet flux swing	0,80	T
Filling factor	1,00	
Magnetic Cross section	48,00	mm^2
Magnetic path length	78,50	mm
integral of voltage time Core	0,04	mVs
Magnetic Volume	3768,00	mm^3

Insulation Thickness of core	0,00	mm
Wire diameter ink. Insulation	5,00	mm
Cross section of magnetic	143,00	mmxmm
windings	1,00	Wdg
Inductivity saturated µr=1	0,0024	µH
integral of voltage time	0,04	mVs

Tab. 16: Data for the gate transformer

In this case the transformer consists of a Ni Zn ferrite and the primary and secondary windings are made of 20kV silicon rubber insulated cable.
Thus the insulation of the transformer is 40 kV nominal, which should be sufficient to ensure safe operation.

A approximate calculation gave us a stray inductivity of ca 2.4nH for the total transformer and 10nH for each tap, which is low enough for tight control of the gates (according to a rule of thumb that the stray inductivity of a transformer is in most cases in the range (or less) of the inductivity of the coil with saturated core).
To verify this remarkably low stray inductivity a gate transformer with the same core and wire but with 4 primary and secondary turns are tested. Also the winding has been done as close as possible to the design of gate transformer.
The inductivity of the original gate transformer is ca 1/16 of the test transformer.

Frequency	Serial resistance	Stray inductivity
300kHz	13mΩ	211nH
1MHz	34mΩ	199nH
5MHz	35mΩ	196nH
10MHz	190mΩ	195nH

Tab. 17: Measurements of frequency behavior of the short circuited test transformer

Frequency resistance	Serial resistance	Parallel inductivity	Main inductivity	coupling
300kHz	0,05Ω	(calculated)	5.02µH	14.9pF
1MHz	3Ω		5.01µH	12.3pF
5MHz	45Ω	550 Ω	6.01µH	11.7pF
10MHz	207Ω		4.05µH	11.5pF

Tab. 18: Measurements of frequency behavior of the open test transformer

In the real transformer has four single turn windings in parallel. The impedances changes to a factor of 1/16. The values are related to one single tab the values have to be multiplied by a factor of 4. Hence the values changes to:

Serial resistance = 10mΩ
Stray inductivity = 50nH
Main Inductivity = 1,25µH
Parallel Resistor = 137Ω
Coupling capacity = 3pF (related to each tab at 5Mhz).

Tab. 19: Calculated parameter of the real gate transformer form Tab. 17 and Tab. 18

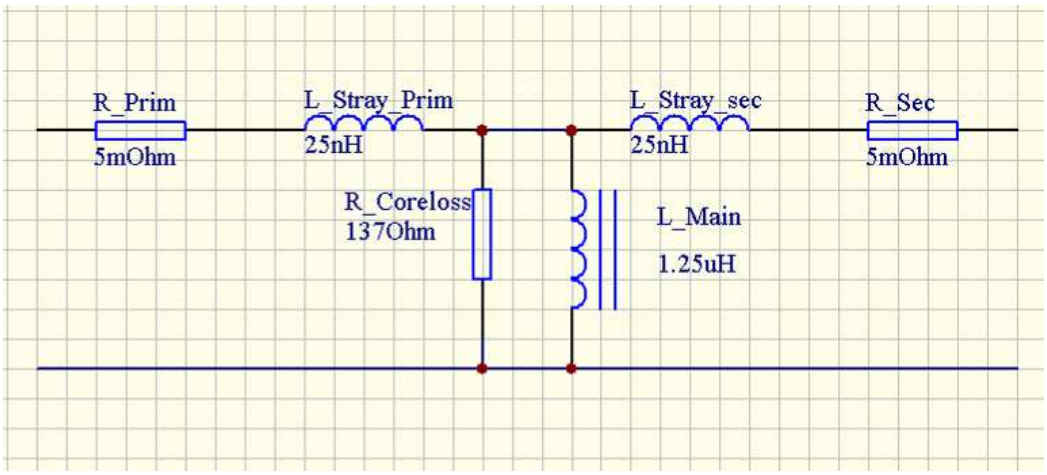

Fig. 57: Equivalent circuit for the gate transformer (related to one tab)

Especially the stray inductivity is remarkable higher than the calculated value. The reasons are that in the calculation the inductivity of the connection wires is neglected reason and that only 4 windings are possible and therefore the magnetic flux is not well confined, hence high fringing fields tend to raise the stray inductivity.

The nominal input capacity of the switch is 10 nF. Together with the stray inductivity the impedance of the LC circuit is 2 Ω.
With a slightly under-damped circuit is used and an 1 Ω gate resistor is chosen.

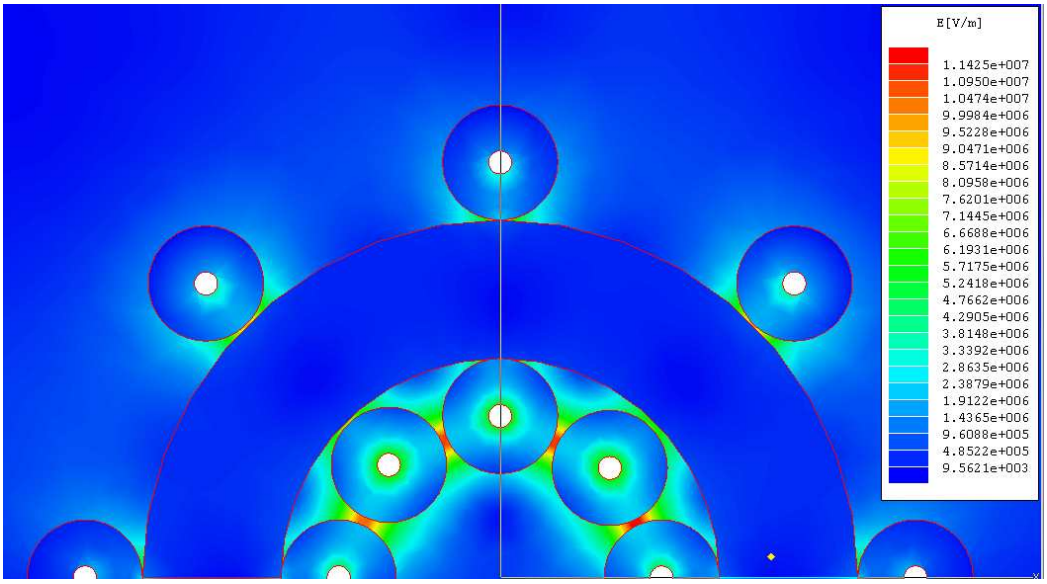

Fig. 58: Electric field of the gate transformer

The calculation of the electric field of the pulse transformer shows an amazingly high electric field. The reason is that the electric field is squeezed out the insulation material. At the small gabs the field rises to very high values in the range of 10kV/mm. This is ca 3 times higher than the breakdown voltage of the air and partial discharges are expected.
The problem could be overcome by molding the transformer.

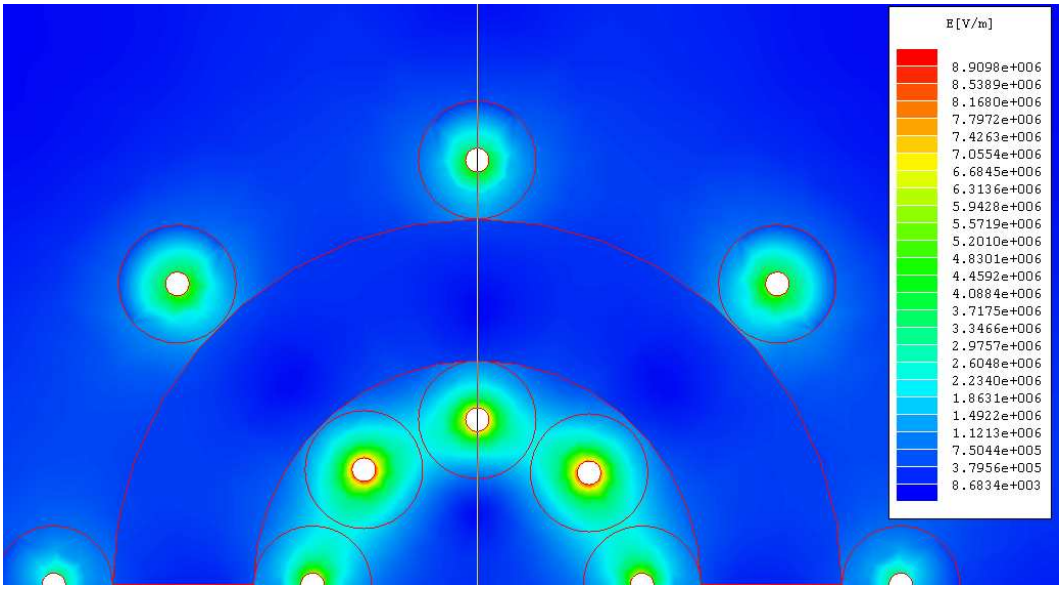

Fig. 59: Molded gate transformer

The electric field is moved around the copper core of the cable due to the 1/r- law (linear cylinder) of the electric field.
For the primary side 500V (24 stages with 15V gate voltage) is needed to control the switches. The peak current is in the range of 50A. These values could be controlled with a power MOSFET which is used already in the stack.
To ensure proper and exact timing a push-pull driver circuit is chosen.

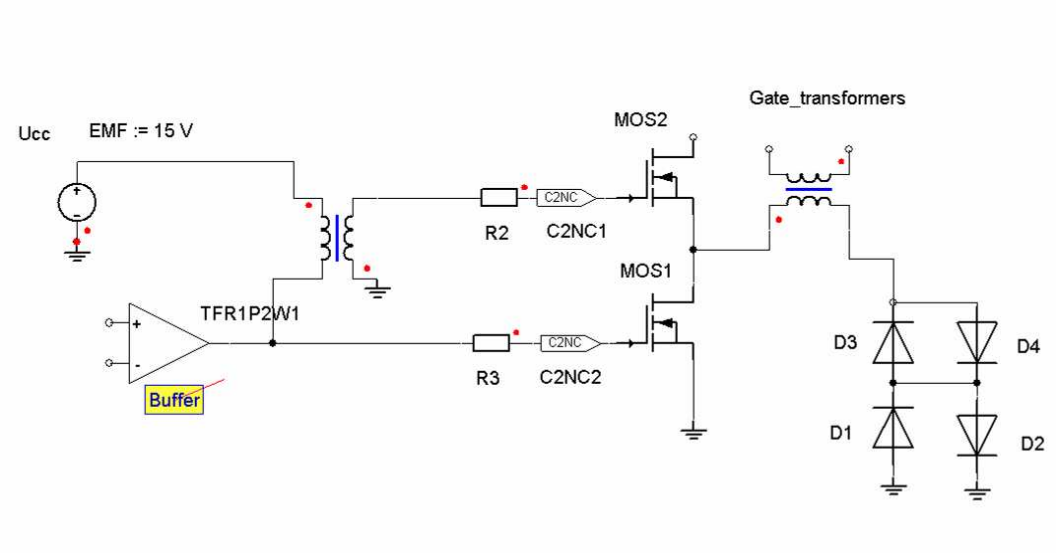

Fig. 60: Schematic of the gate driver

The upper transistor switches the stack on, the lower switches it off. Due to the very short on-time a small gate transformer is sufficient to control the switch. The buffer is a commercial available MOSFET driver.

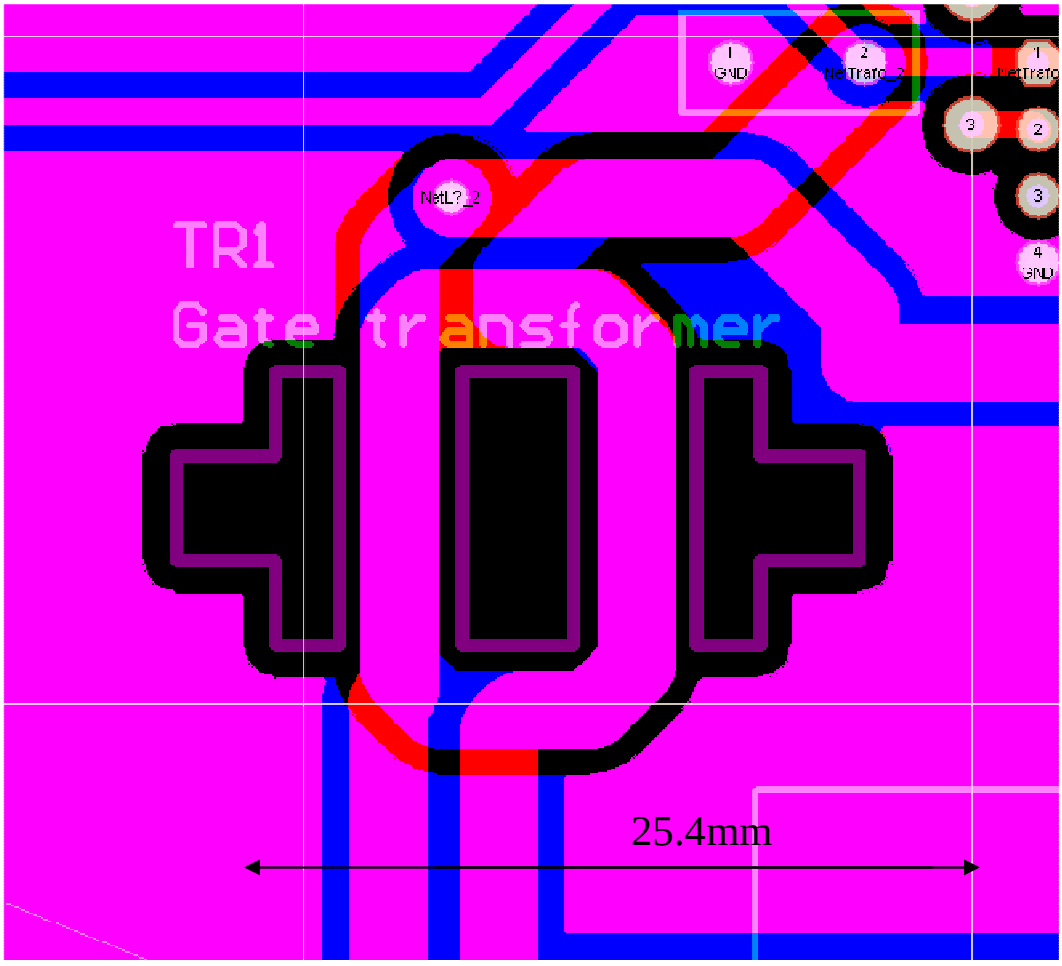

Fig. 61: Design of the gate transformer (red Top layer; blue Bottom layer)

The gate transformer is designed in a planar design. Only a single turn is required because the on-pulse is short. Such an integrated transformer is very simple in manufacturing and is getting more and more common in many applications.

Fig. 62: Output voltage of the gate driver with load (CH1: driver output voltage)

One very important issue is that all transistors are switching simultaneously. Due to the fact that all stages are connected serial each stage gets the same amount of charge and hence same gate voltage. If every transformer and gate capacity is identical a simultaneous switching should happen in each stage.
During the first test of the gate control it showed that voltage shapes of the gate signal is largely differing from one switch to the other.
A closer check of the cores showed that the distributor mixed different materials. So the main inductivity of the pulse transformers shows a difference of a factor 2(!).
A new delivery directly from the manufacturer overcomes this problem. The delivery was very uniform and the AL-Value (inductivity a single turn coil) of the cores differ only a few percent.
The purpose of diode 1 to diode 4 is not obvious. During initial tests it showed that the gate transformer runs into saturation above some 100Hz. The reason was that the average voltage of a transformer has to be always zero. Otherwise the core of the transformer runs into saturation.
With low frequencies there is enough time to reset for the gate transformers. With higher repetition rates it is necessary to have more voltage to reset the cores. The voltage drop on the diode (ca 1V) allows the cores to fall back.
This can be seen in Fig. 63.

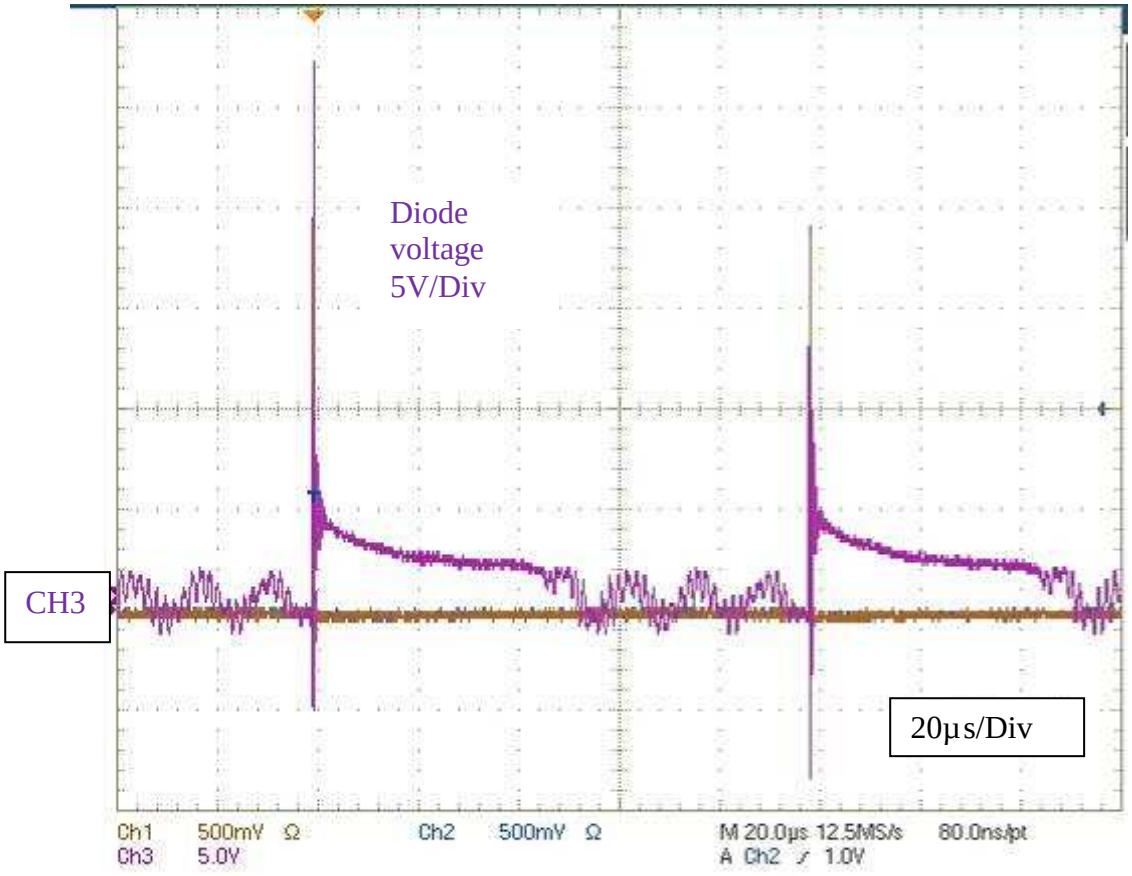

Fig. 63: Voltage drop across the diodes (all) at repetition rate 10 kHz (D1 to D4) (CH3: Diodes voltage)

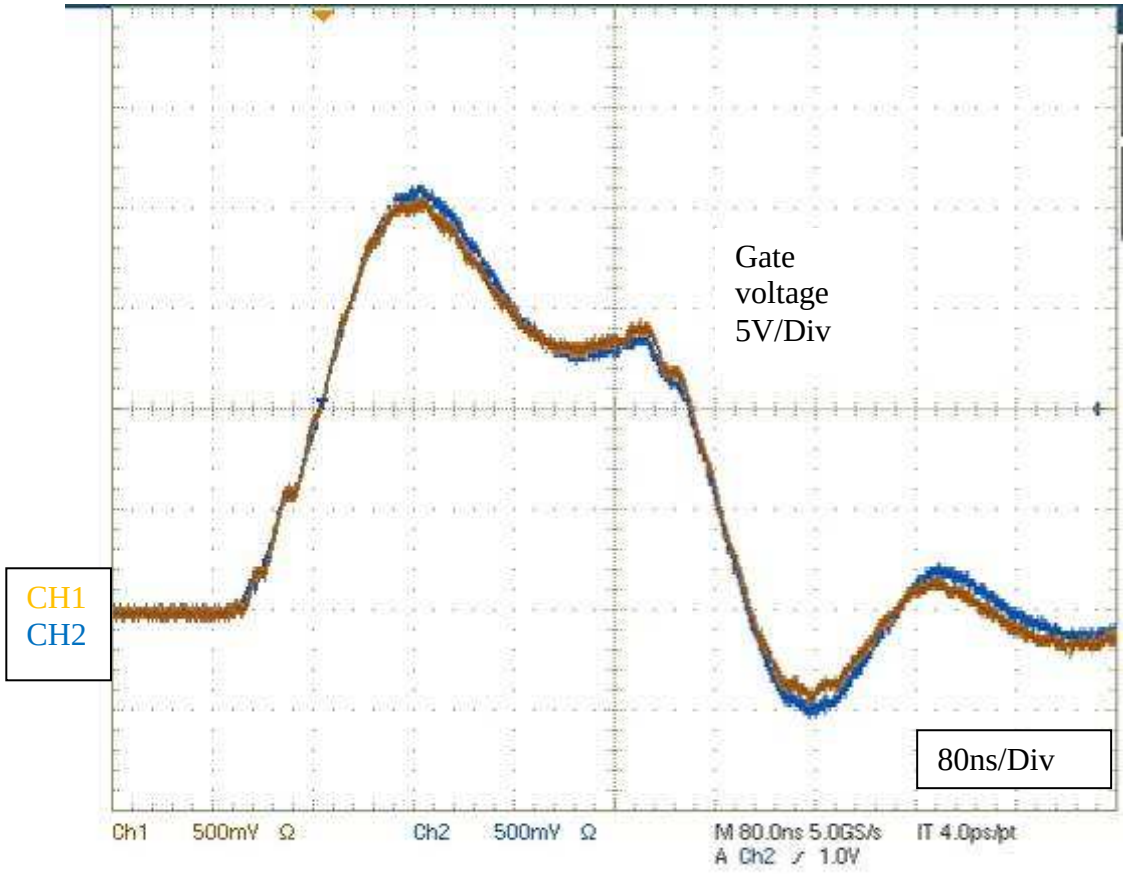

Fig. 64: Gate voltage at 2 stages stage number 6 and 19 (the number indicates the distance to the buffer) (CH1 and CH2: Gate voltage)

The gate signals are nearly the same. Hence the switches are very well synchronized.

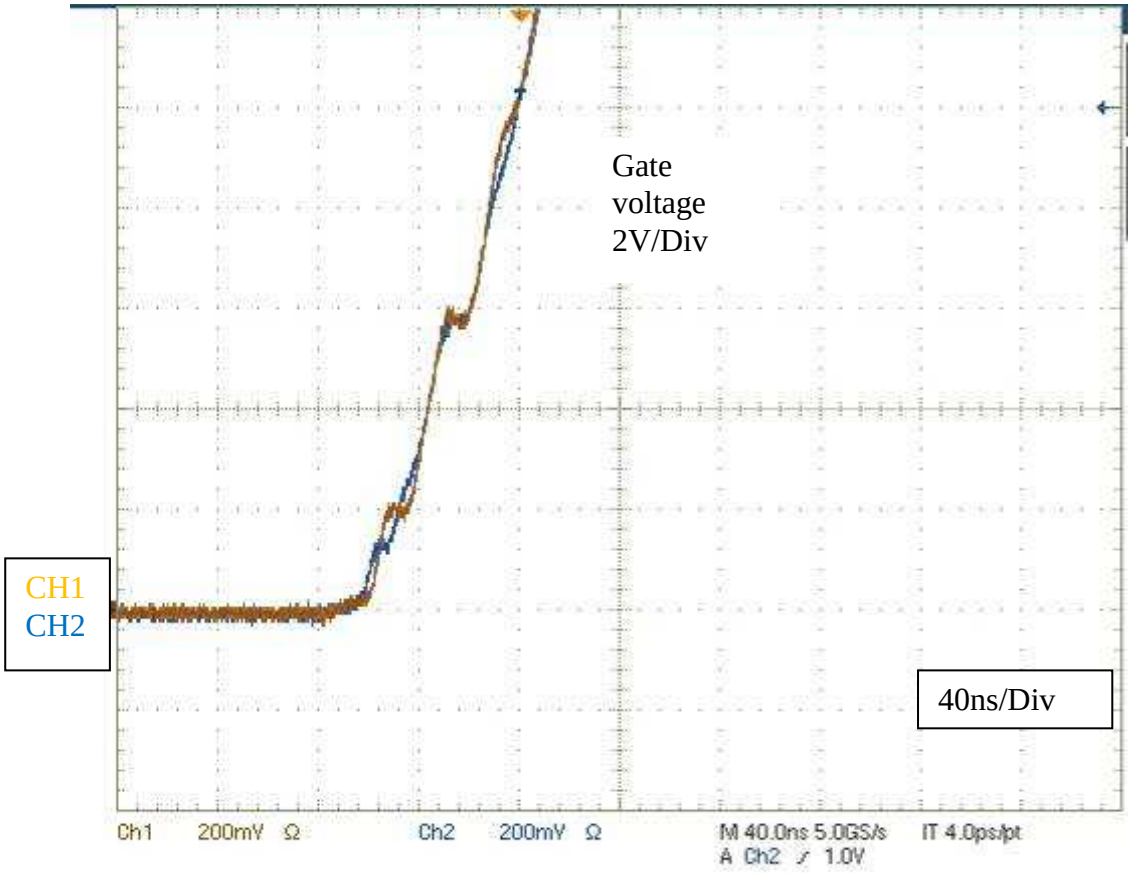

Fig. 65: magnification of Fig. 64 rise time) (CH1 and CH2: Gate voltage)

The differences are very small and could be neglected. This is a key feature of a semiconductor stack. Also all other stages shows deviations in that range.

5.8 Mechanical Design

The mechanical design is a very important part of the design, because the mechanical design influences also the electrical characteristic, like inductivity.
An economic and reproducible production is a very important parameter. It is also important that the design fits in the production flow of the manufacturer.
In this case a stacked PCB design is used. The current flows like a meander through the boards and the inductivity is very low.
The gate transformers are located on top of each other 6 pieces and in 4 rows; hence the trigger wire could be threaded though. The overall height of the PCB board is given by the gate transformer core and its high voltage winding. It is approximately 15 mm to 20 mm, hence a very compact design in possible.

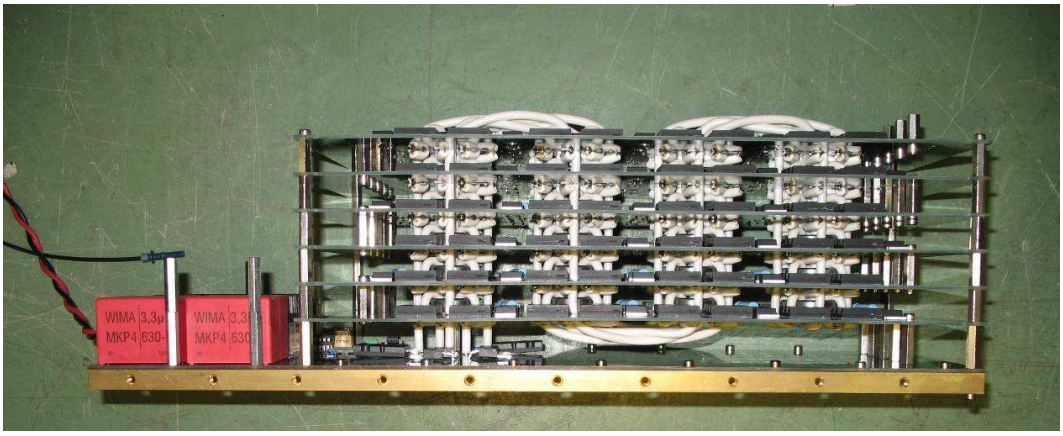

Fig. 66: Side view on the stack.

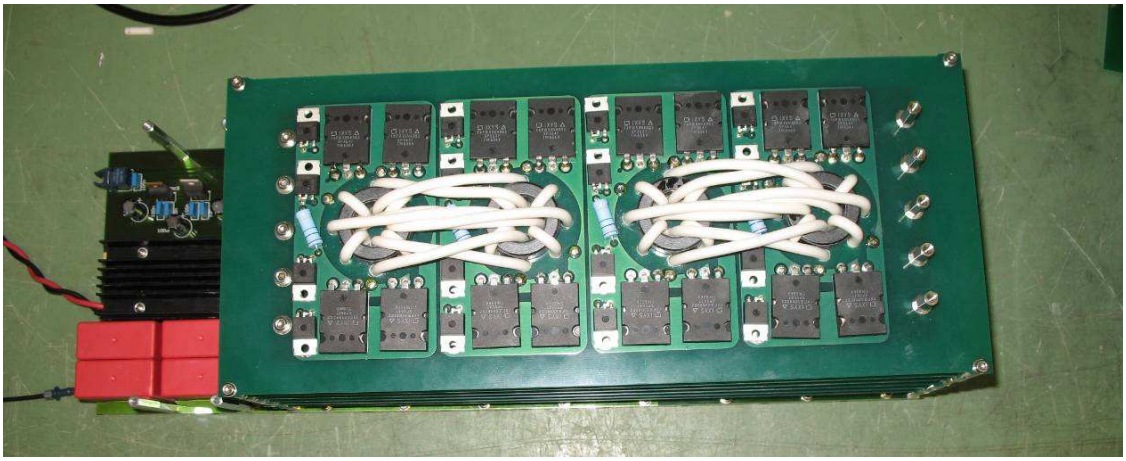

Fig. 67: Top view on the stack

In the later system a forced air cooling removes the heat of the stack.

6 Test of the complete stack

6.1 Medium voltage tests at 3kV and capacitor load (without dynamic voltage sharing)

Given the complexity of the circuit the start of the system should be very slow, starting with a test voltage which ensures safe operation, even under faulty conditions.
In this case a single 2.2nF capacitor is used as a dummy for the real laser head.
For the first tests the voltage drop across the stack the bank capacitor and peaking capacitor voltages are measured.
The measurements of the current through the stack were not possible, because the sensitivity of the current shunt (1mΩ) was too low.

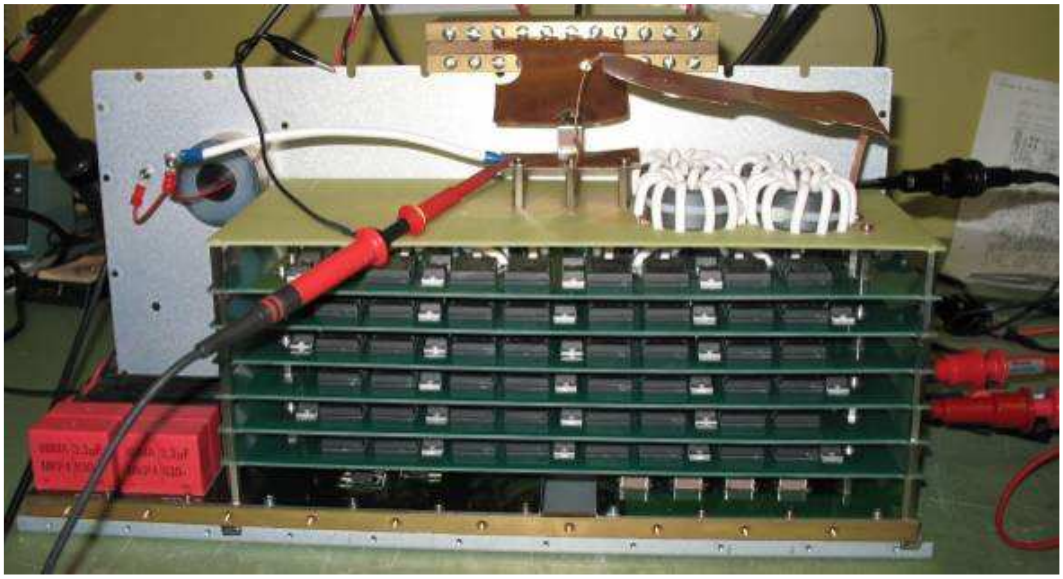

Fig. 68: Arrangement of the medium voltage test (with bypassed magnetic Assist)

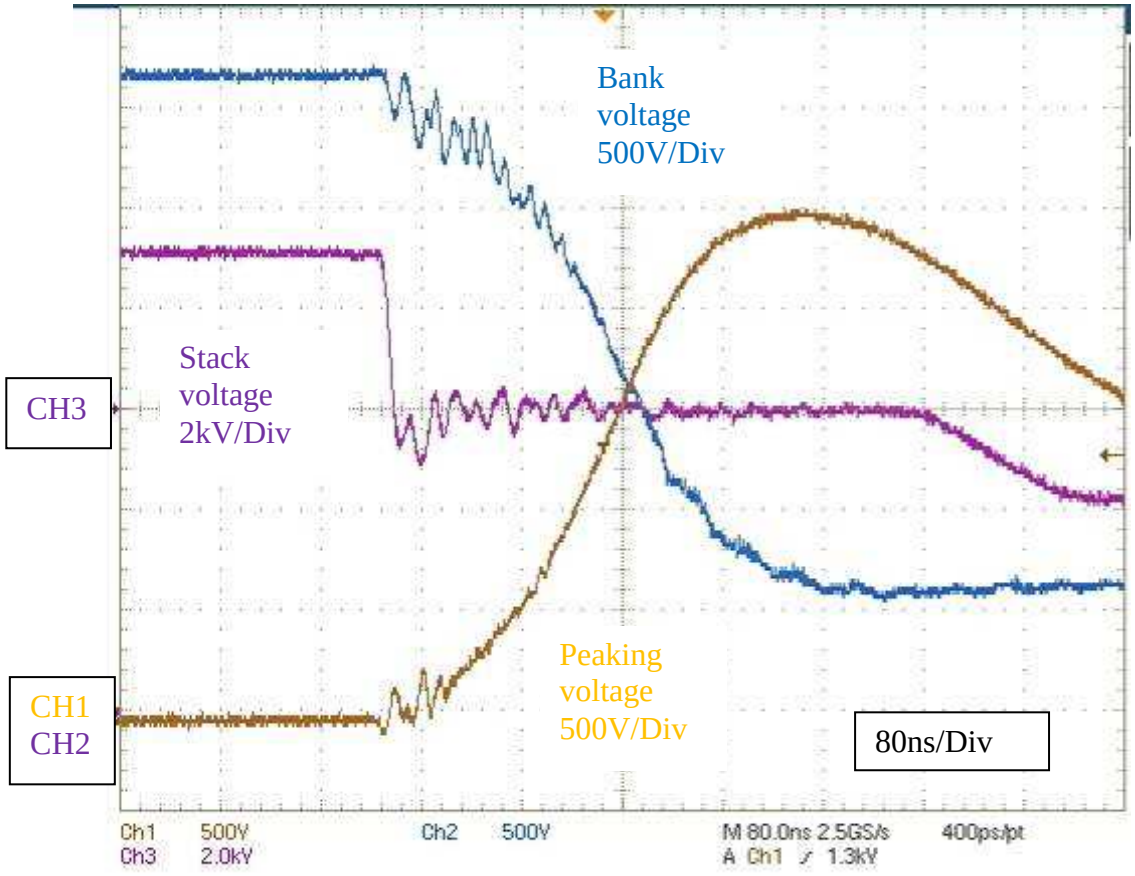

Fig. 69: voltage traces of the medium voltage test (CH1: Voltage peaking capacitor; CH2: Voltage bank capacitor; CH3: voltage across the stack)

The time of the energy transfer is much longer than calculated. The reason is that the magnetic assist is not driven into full saturation, so the remaining inductivity is far too high.

The efficiency of the circuit is disappointingly low in the range of 60%. The reason is the low operation voltage. To energy loss due the threshold voltage of the semiconductor and the oversized magnetic assist is higher (in relation to the stored bank energy) compared to normal operation condition.

To verify this assumption a test with a bypassed magnetic assist is made (Fig. 70).

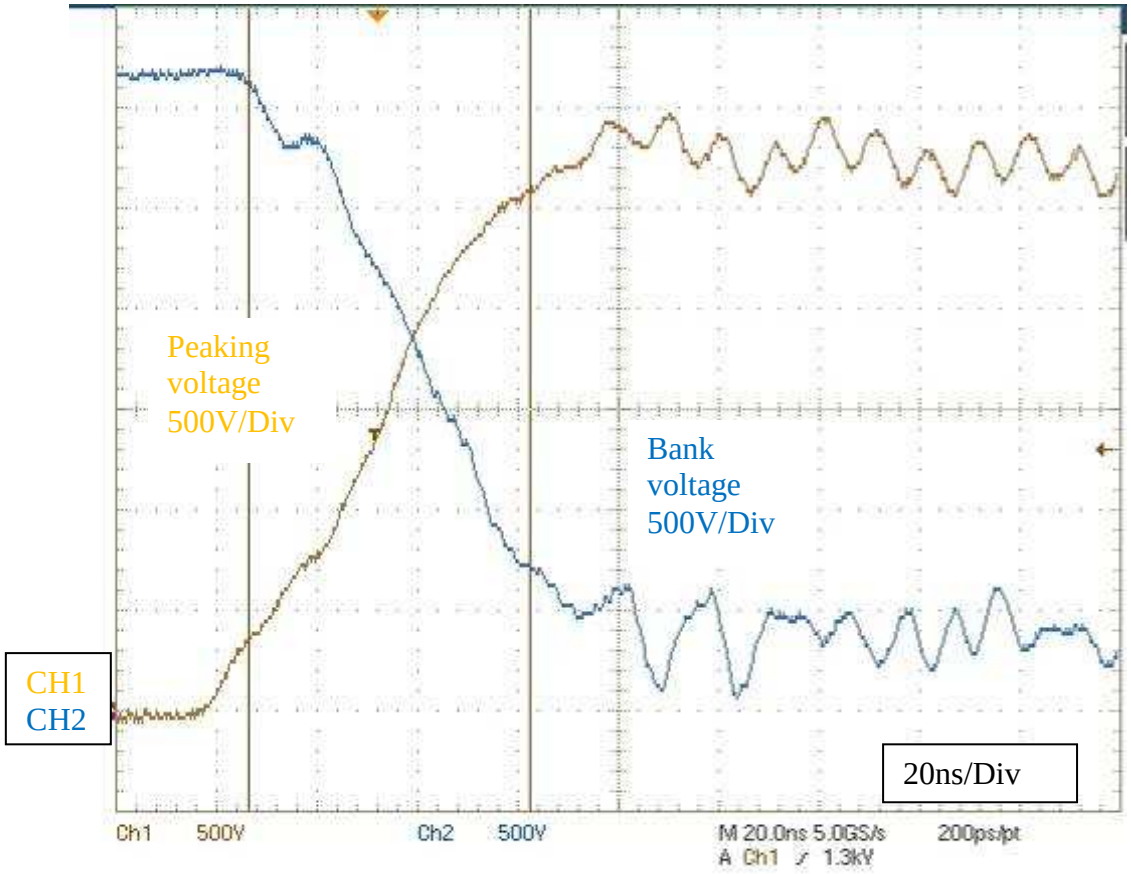

Fig. 70: Voltage traces of the medium voltage test with bypassed magnetic assist (CH1: Voltage peaking capacitor; CH2: Voltage bank capacitor)

The efficiency rises now to 80%. It is expected that with nominal voltage the results will be close to the calculated value.

6.2 *Measurements with higher voltage (8kV; 10kV) and capacitor load (without dynamic voltage sharing)*

For the measurements with higher voltages insulations foil has to be added. The most critical part of the design is the relative short distance from the switch to the housing. The main reason for the foil is that the electric field, due to space charge effects, is homogenized. The insulation properties of the foil itself are mostly insufficient to avoid a flash over.

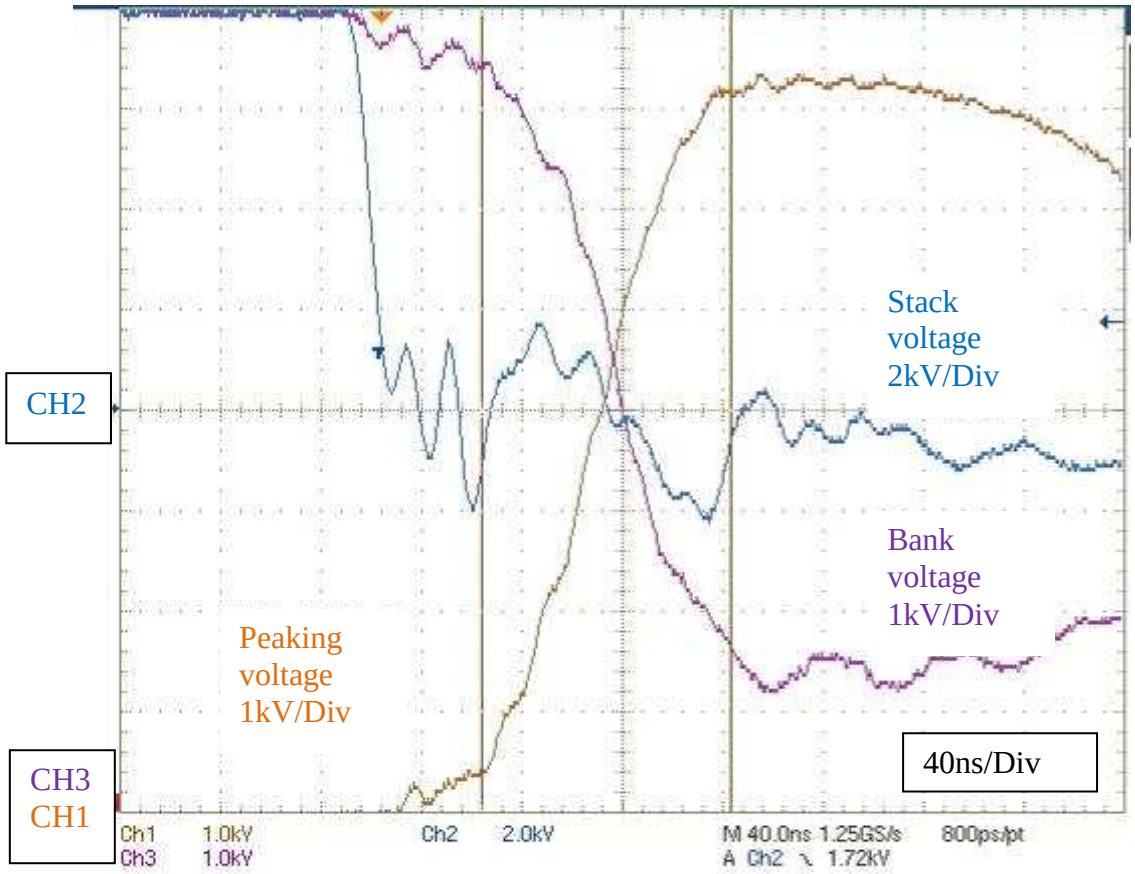

Fig. 71: Operation with 8kV (CH1: voltage peaking capacitor; CH2: Voltage Stack; CH3: Voltage bank)

The energy transfer time is now within the 100ns range. The efficiency rises to 85%. This is very close to the calculated values. The magnetic assist has a hold-off time of ca 60ns. This is also within the calculated values.
During the tests no unexpected over-voltages could be measured at the stack.
To measure the voltage of the stack high voltage differential probes are used which are limited to a maximal operation voltage of 6kV peak. So the next steps have to be done with high voltage probes, which are less accurate and not available for floating voltages.
The stack voltages could be calculated by the difference of the peaking capacitors and bank capacitors.

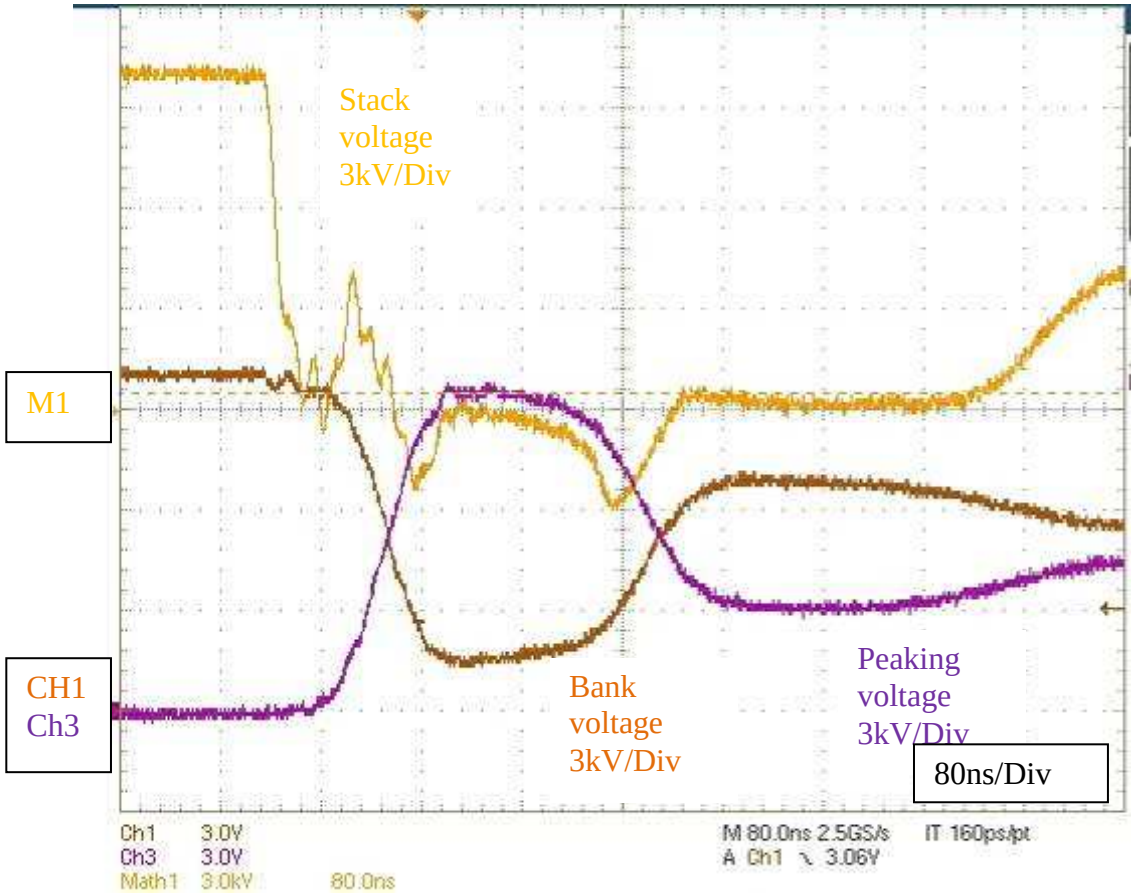

Fig. 72: Operation with 10kV (CH1: Voltage Bank; CH3: Voltage Peaking; M1: Voltage Stack)

The results are very encouraging. The energy transfer time is somewhat less than 100ns and the efficiency is 89%.

Very typical for this kind of circuit is that the bank is not completely discharged, this is a result of the damping of the circuit. The situation looks worse than it actually is. Ca 1.5 kV voltage remains after discharge in the bank. Compared to the 10kV operation it is only 2% of the total energy hence is negligible.

After these tests the components of the stack were checked. It showed out that all diodes have a short circuit. This result was not expected because no measurement shows that there is any over voltage across the entire stack. It is clear that the voltage distribution for the diodes is not well distributed.

Also, it is clear that the efficiency is not as high as measured because the drop of voltage of the diode was completely gone. Up to this point all calculations could be confirmed. Next step is to test the stack with dynamic voltage sharing.

6.3 High voltage test with dynamic voltage sharing

The stack has now a dynamic and static voltage sharing. The dynamic voltage sharing has also snupper feature with the damping resistor.
The current shunt is replaced by a more sensitive device enabling current measurements.
The operation voltage of the stack is now negative as required in the application. In the previous measurements it was positive due to an assembling error.

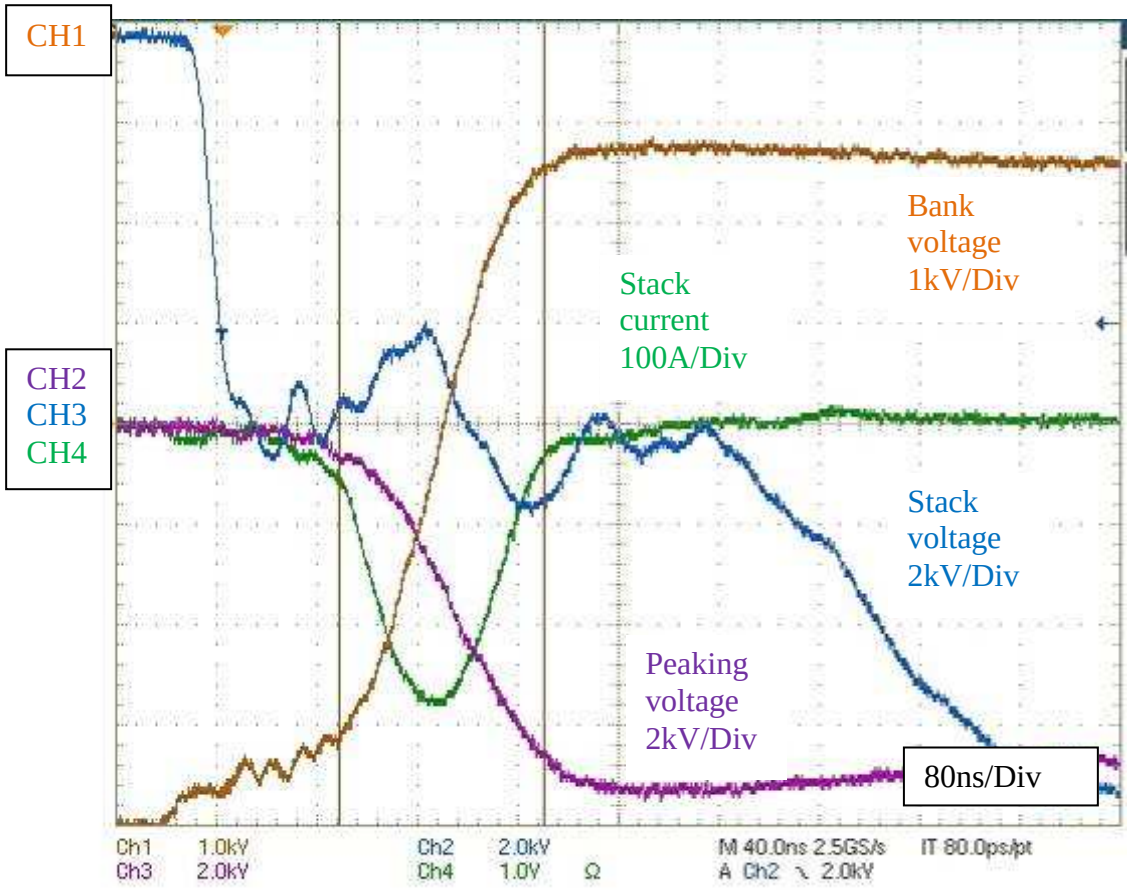

Fig. 73: Operation with 8kV (CH1: voltage bank capacitor; CH2: Voltage Stack; CH3: Voltage peaking capacitor; CH4: Stack current)

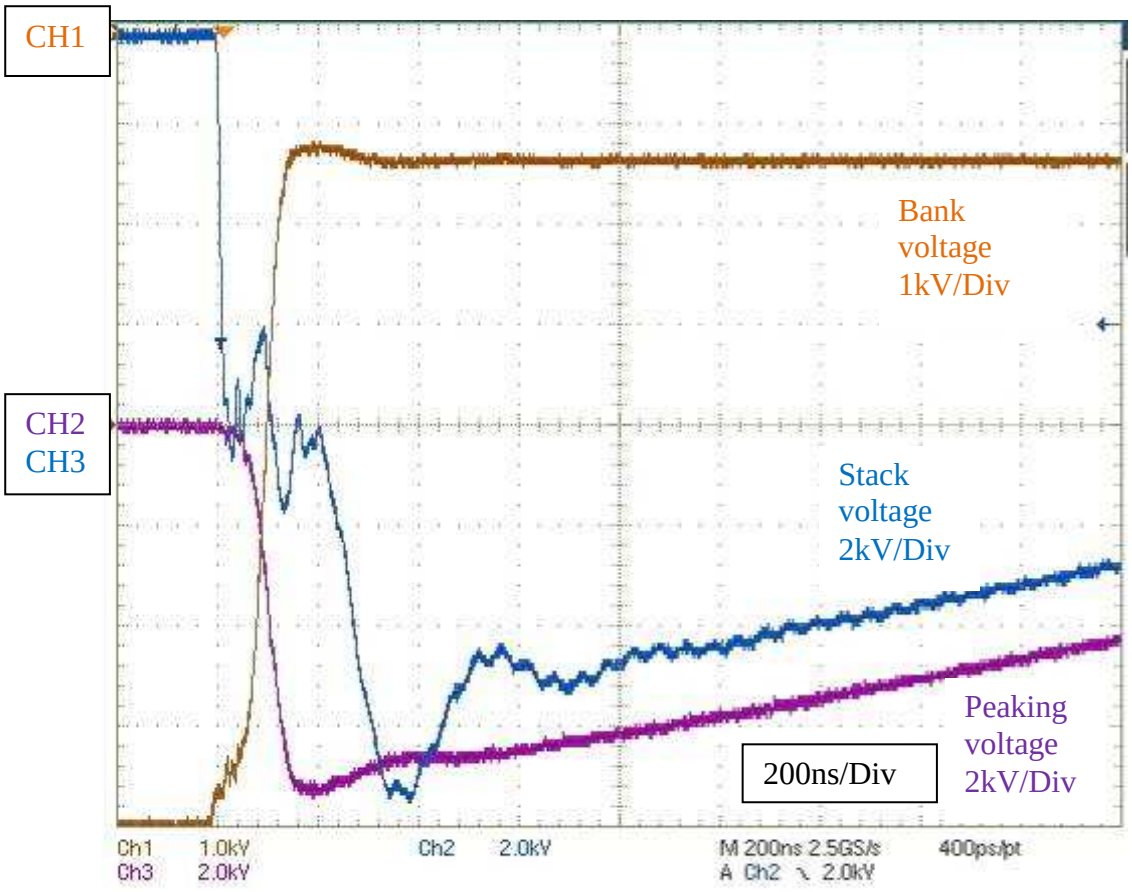

Fig. 74: The identical measurement as in Fig 73 but on a longer time scale (CH1: voltage bank capacitor; CH2: Voltage Stack; CH3: Voltage peaking capacitor)

The stack works as calculated (Fig. 73 and Fig. 74). The overall inductivity is approximately 40% smaller than calculated. The inductivity of the stack is remarkably low. With the measured voltage drop during the current rise it could be calculated to be ca 150nH. This is ca 10nH for each semiconductor component. This value is also given by the suppliers. The meander-like current flow seems to reduce the stray inductivity very effectively to the absolute minimum (the inductivity of the components).

The saturated inductivity of the magnetic assist is approximately 250nH plus 150nH of the stack plus 200nH for the rest of the circuit (Bank current returns) summarized to total 600nH.To reduce the stress of the components a doubling of the inductivity of the magnetic assist is possible. Only 1 row (instead of two) is used. Hence the total inductivity should be in the range of 900nH which is closed enough. This modification is tested in the next chapter.

Even the energy balance is still very good. The back is charged up to 7,8kV this is energy of 67mJ.

The peaking capacitor charged up to 7,2kV, which is 57mJ, hence transfer is 85%.

The stored energy of the MOSFETS and the snupper capacitors are not included in the calculation. This was already calculated, it is in the range of 2% of the total energy. So the efficiency is still above 80%. The simulation of the stack at 8kV shows an efficiency of 85%.

With higher voltages a raise of the efficiency to the calculate level (90%) is expected. Due to the limitation of the pure capacitor load it is risky to raise the voltage above the 8kV, because the allowed voltage reversal of the stack is reached.

Next steps are the measurements with a real laser head. Given the more complex load efficiency measurements are no longer sufficient accurate.

Measurements with the laser low repetition rate

The circuit is already designed in that way that it could be easily attached to the laser head.
The load behavior of the laser head is much more complex than a pure capacitor. The used capacitors have high losses compared to the dummy load. The losses are in the range of 5%.
There are also additional loads due to the pre-ionization tubes. Two tubes with ca 100pF each are in the laser. The behavior is that of a high loss capacitor. Also the onset of the laser discharge limits the peaking voltage.

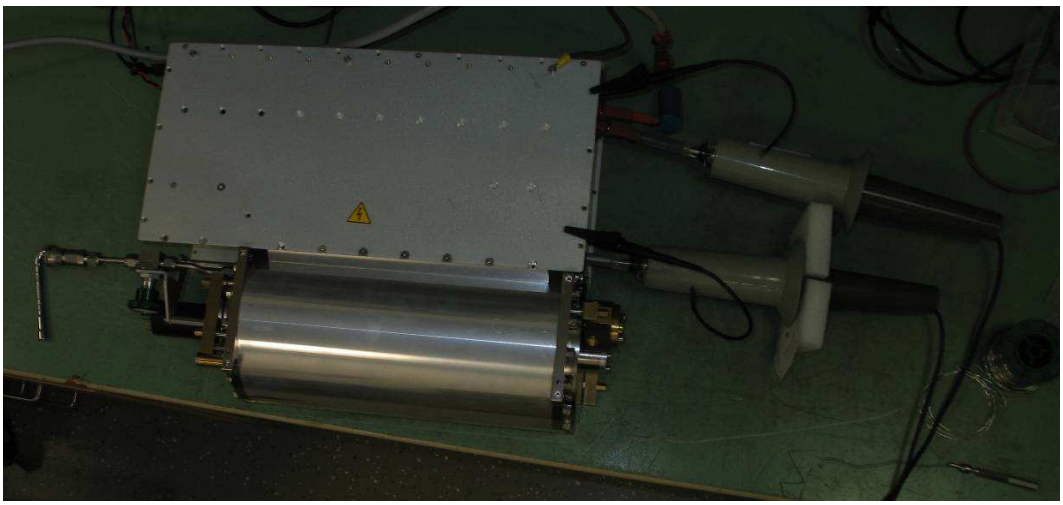

Fig. 75: Laser head and stack with attached high voltage probes

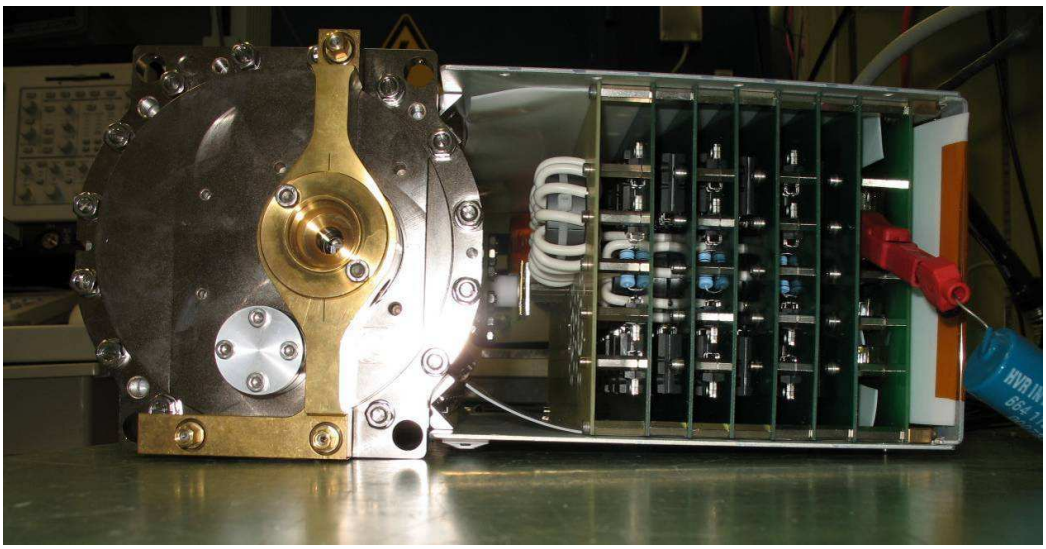

Fig. 76: Laser head front view

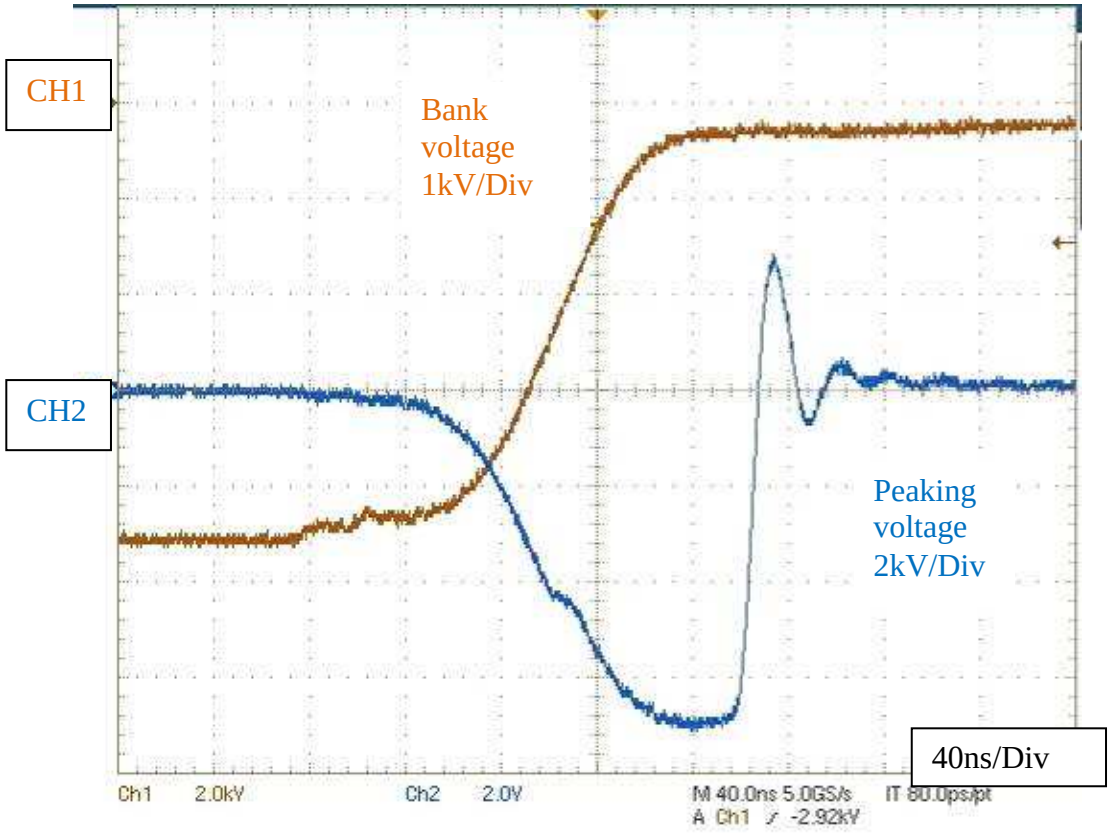

Fig. 77: Operation with 9kV Bank voltage (CH1: Voltage bank capacitor; CH2: Voltage peaking capacitor)

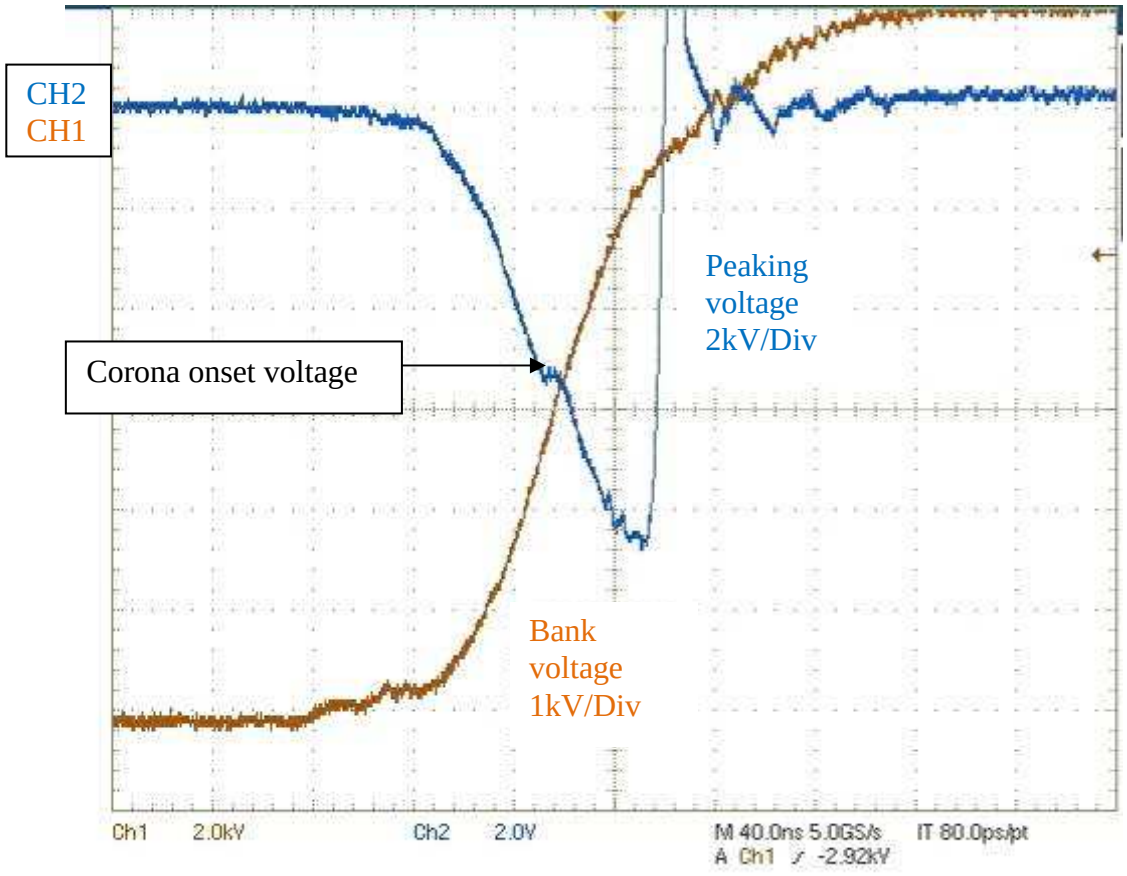

Fig. 78: Operation with 12kV Bank voltage (CH1: Voltage bank capacitor; CH2: Voltage peaking capacitor)

The step in the voltage raise of the peaking capacitor is the voltage where the corona starts to ignite.
At 12 kV bank voltage it can be seen that some energy is reflected which leads to a positive charge of the bank capacitor. For this reflected energy the diodes have to block the current to prevent ringing. This energy could be recovered. The laser starts with lasing at approximately 10kV bank voltage.

6.4 Measurements with the laser head high repetition rate

For operation with higher repetition rate a special power supply is needed. For capacitor charging normally switched constant current power supplies are used. The challenge in this application is that an operation beyond 2 kHz repetition rate is wanted. To achieve sufficient charging accuracy (every switch cycle has a certain amount of energy) very high switching frequencies are needed (to get sufficient small energy pulses). So this technique is limited for frequencies less that approximately 2 kHz.

6.4.1 High repetition rate power supply for low voltages

To overcome this limitation a resonant charge power supply is developed (Fig.79). The basic idea is to transfer the energy to the load in a single step. By the on-time of the main switch the voltage is controlled.

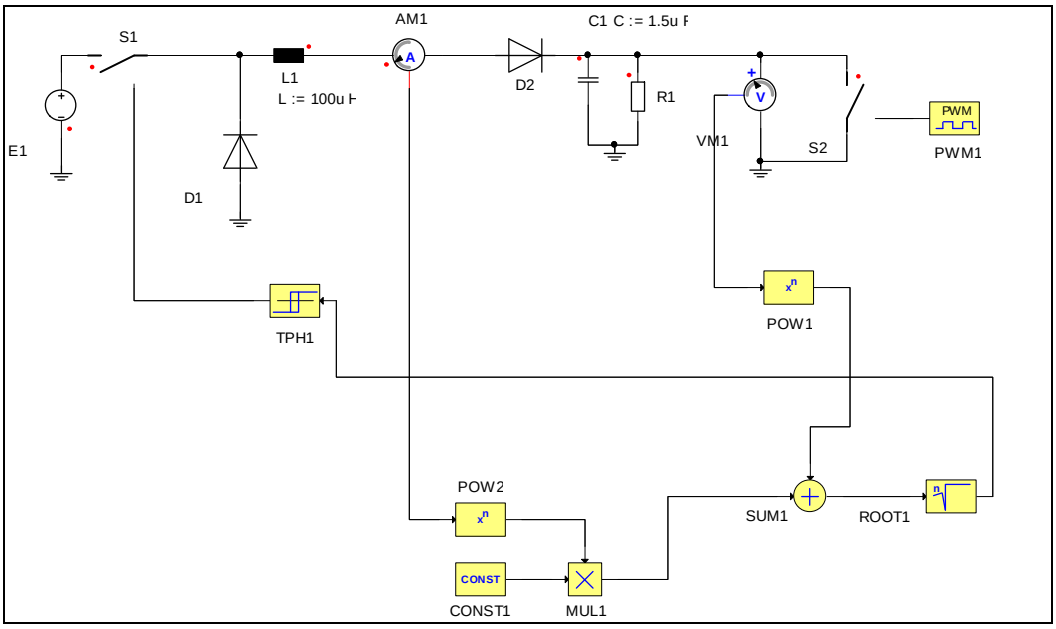

Fig. 79: Basic schematic of a resonant charge power supply

During the swing a portion of the energy is stored in the inductor the other is stored in the load. To control the final voltage a continuous calculation of the energy is necessary. If the total energy is enough to achieve the programmed voltage the switch (S1) is opened. The current is maintained by the diode (D1) until the inductive stored energy is transferred to the load.
The calculation is based on energy conservation in the circuit. The energy which is already stored in the load capacitor and the energy which is stored already in the inductivity is the total energy. The output voltage is the voltage of the output capacitor which contains the total energy of the circuit (Figure 80).

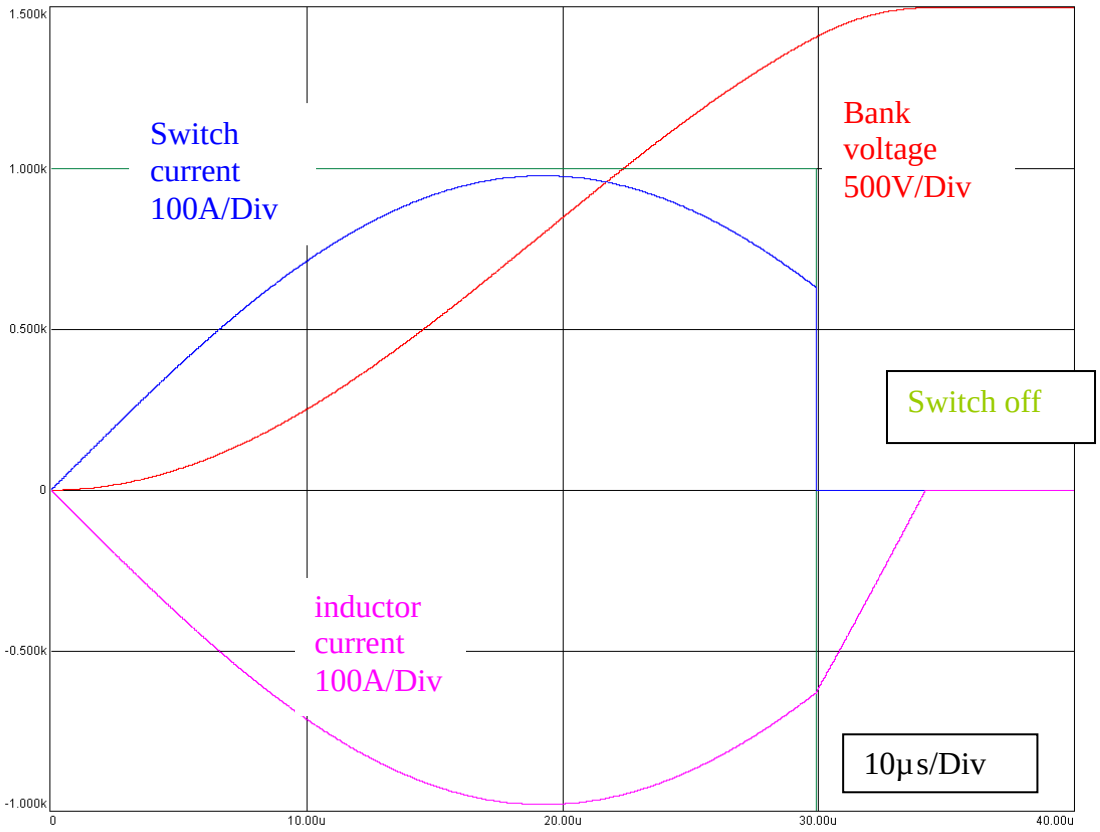

Fig. 80: simulated current and voltage of the circuit

This kind of power supplies are used in Excimer laser for high repetition rate in the semiconductor industry. It is obvious that it is limited to a maximum of 1kV because there is only a voltage gain of two (maximum) in the circuit.
In this application a maximum voltage of 15kV is needed. In this case a pulse transformer raises the voltage to the needed level.
In such a configuration it must be ensured that the saturation of the core of the transformer is avoided.

6.4.2 High repetition rate power supply high voltage first prototype

The design of the power supply is made together with a supplier experienced with high voltage power equipment. Basic concept (Figure 81) and calculations are supplied by the author the prototypes are built by the contractor.
One of the possible schematic is the two switch forward converter. The benefit of the converter is that the input stage is always clamped and only a single primary winding is necessary.
A fraction of the energy which is stored into the loop L1 and the energy of the stray inductivity of the transformer is directly transferred to the main bus; hence do not complete contribute to the output voltage after the switch turned off. The particular value depends of the contribution of the inductors in the loop.
The transformer enables the necessary voltage gain. The stray inductivity has to be small to enable a fast energy transfer. In this case lower than 200µH (referred to the primary winding). The final tuning is made with L1.
The step up ratio of the transformer is calculated

$$\beta = \frac{U_{C1}}{U_{E1}} * \frac{1}{2}$$

The factor ½ is due to the relation of the capacitors. It is a resonant charge transfer form a big bank capacity to the relative small load (C_1). In this case a voltage doubling occurs. In reality this factor is much less. The one reason is the unavoidable damping of the circuit; the other is the voltage recovery of the load. Due to this recovery the gain is additionally reduced. A factor of approximately 0.7 is chosen.
D10 and L10 is the recovery network which turns the voltage of the capacitor (C1) to recovery the energy. This is necessary because the reflected energy of the laser is stored as an opposite voltage in the C1 (Bank of the circuit).

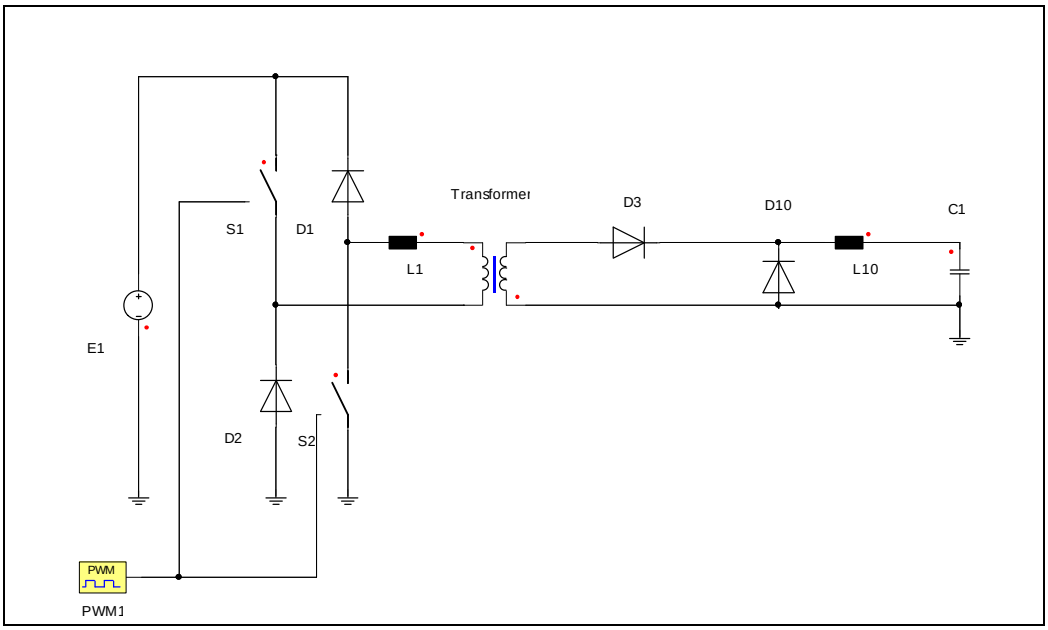

Fig. 81: Schematic of a two step forward converter

One challenge of the design is to design the transformer and L10 with very low stray capacity to avoid parasitic oscillation. The basic calculations are the same as described in the previous chapter.

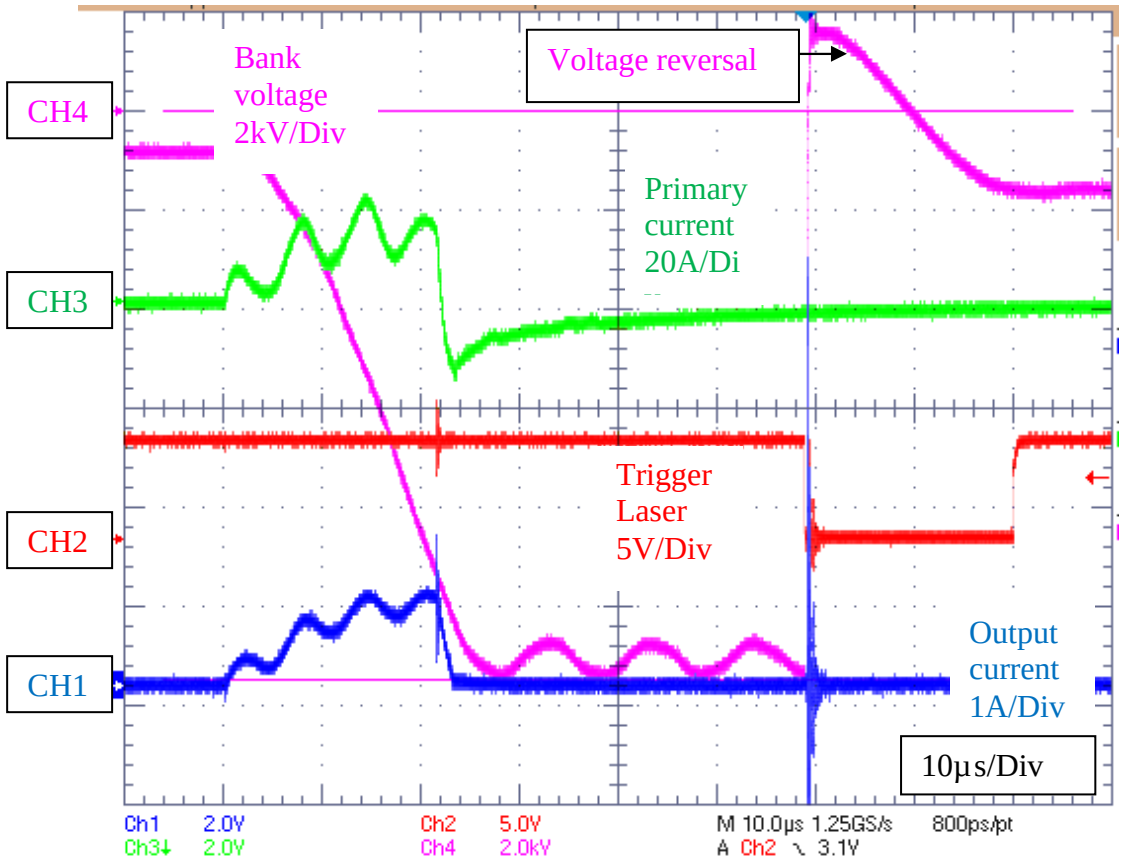

Fig. 82: Waveforms of the first power supply prototype (CH1: Output current; CH2: Trigger Laser head; CH3: current primary side; CH4: Bank voltage)

The ringing of all traces is a result of the parasitic capacity of the inductors and transformer. This ringing has to be avoided to get better output stability and efficiency.

The first results are very encouraging. With this power supply it is possible to charge the load within of 30µs. So charging time is nearly no limiting factor for repetition rate.

6.4.3 High repetition rate power supply high voltage improved prototype

In the improved prototype the stray inductivity of the inductors has been reduced to a factor of 1/10 from the original value. Also the internal controls have been improved.
The traces now look much smother. There is still some ringing of the output voltage. The reason is not completely clear. Maybe the currently long high voltage output cable induced this ringing. The reverse recovery of the high voltage diodes might contribute to the ringing, too.
The design runs now with 6 kHz and shows no sign of overheating neither in the power supply nor in the laser.

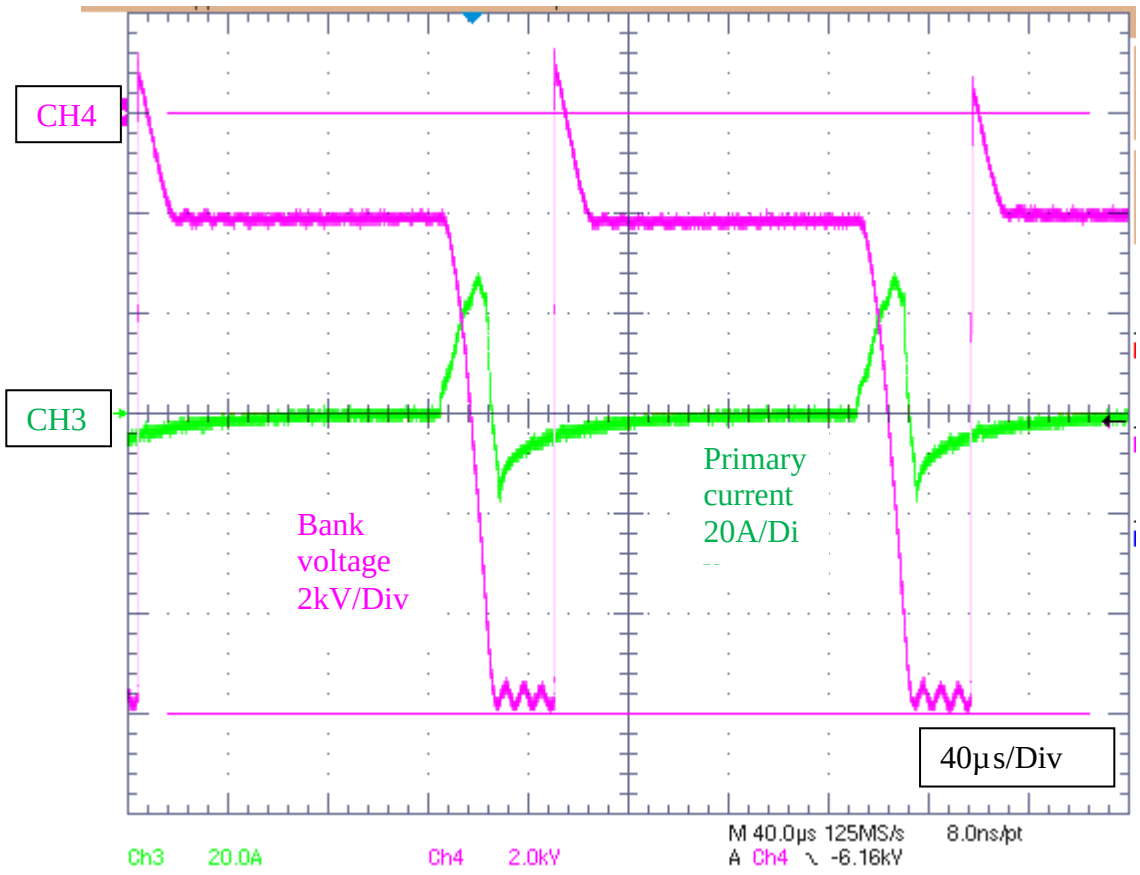

Fig. 83: Waveforms of the improved power supply prototype 6 kHz (CH3: Current primary side ; CH4: Output voltage)

The problem with the high repetition rate measurements was that the laser works only properly up to 3 kHz. With higher repetition rate the laser starts to arc und tents to discharge the peaking capacitor before the nominal voltage are achieved. This leads to additional dissipation in the circuit and a very unstable operation.
Even under these conditions the circuit works without failure or damage to the semiconductors.

Measurement	Temperature in [°C]
Ambient	30
Magn. Assist	58
Mosfets	74
Dioden	76

Tab. 20: Measurements of temperatures in the circuit at 6 kHz and 12 kV operation voltages

The temperatures are higher than expected. One reason is the pre-firing of the discharge. This causes additional reflections and hence more current. The low airflow through the circuit due to the compact design and the quite high ambient temperature during the tests tends to cause an additional rise in temperature.

7 Conclusion

In this thesis it is turned out that it is feasible to build a high efficiency fast high voltage modulator for Excimer laser.
This new design overcomes the limitation of the previous designs. Due to the lack of bulky pulse compression cores losses are considerably reduced. This open the way to very high repetition rate excimer lasers.
Due to the lack of reliable models for the components in the required application the components were tested and simulation models were developed. One focus in this work is also the losses of the passive components.
Simple straight forward models were developed which give the basis of the simulation of the complete stack.
The passive components generally are a source of unexpected high losses. Especially the very common class II capacitors dissipate up to 5% of the stored energy. This source of losses could be overcome by using class I (NP0) ceramic capacitors which unfortunately have low energy densities.
For the switches it shows that the IGBT are not feasible for application in the required timeframe. The losses are amazingly high. MOSFET switches however show superior switching properties.
For the stack also diodes are needed. In the application only SiC Schottky diodes are feasible. In the tests they show excellent dynamic behavior. The availability of this kind of diodes enables this circuit.
The parallel switching of the semiconductors is crucial for the reliable operation of the circuit. In this work a pulse transformer provide the gate drive. These gate transformers have to insulate each stage of the stack and also enable tight timing control.
The voltage sharing is also an essential point for reliable operation of the stack. The static voltage sharing is made with parallel resistors. Snubber like RC networks enables dynamic voltage sharing.
To operate the stack a novel resonant charge power supply was developed. This power supply enables charging times of less than 30µs. The use of such a power supply is not limited to this particular application. It enables a new class of capacitor charger for capacitor banks in high repetition rate applications.
The efficiency of the circuit is in the range of 80% to 90% and enables so high repetition rate operation with air cooling.
The circuit is an economical and practical solution for small high repetition rate Excimer laser with light pulse energy in the range of some mJ.
The next step is to reduce the temperature of the semiconductors to improve cooling. Bigger fans are available to ensure a higher air flow in the circuit. Also wider distances between the PCB boards are useful for better cooling. Less semiconductor temperatures also reduces losses of the circuit. This is also important for long term stability of the circuit even under harsh conditions in the application.
Long term tests are necessary to confirm the stability of the circuit. This long term tests are normally done under full load conditions and needs several months.
The tests showed that the development of the circuit regarding the high repetition rate is more advanced than the laser chamber. To enable higher repetition rate it is necessary to improve the gas flow in the laser discharge.
Long term testing and improvement of the gas flow is not part of this study, and is planned during the product development phase of this circuit.

8 References

[1] Einstein, Albert. *Zur Theorie der Strahlung*. Zürich 1916. Mitteilungen der Physikalischen Gesellschaft.
[2] N. G. Basov, V. A. Danilychev, Y. Popov, D. D. Khodkevich. Laser *Operating in the Vacuum Region of the Spectrum by Excitation of Liquid Xenon with an Electron Beam*. In: Journal of Experimental and Theoretical Physics Letter. Nr. 12, S. 329. 1970
[3] Houtermans F. G. In: Zeitschrift für Physik. 41. S. 933. 1927
[4] Konovalov et al. *Electron-beam-excited XeBr laser*. In: Sov. J. Quantum Electron. 9, 242-243
[5] Questek, *Magnetic Pulse Compression for Excimer Lasers*. Technical Note No. 1 and No. 2, May 1983
[6] Claudia Hartmann. *Entwicklung eines Hochspannungs- Mosfet- Schaltkreises*, Diplomarbeit TuiLaser AG Fachhochschule München FB06, 2001
[7] Applikationsschrift Vakuumschmelze, *NANOKRISTALLINES VITROPERM / EMV PRODUKT, Hanau, 2006*
[8] Boll Richard, *Weichmagnetische Werkstoffe* , 4. Auflage, 1990, ISBN 3-8009-1546-4
[9] Claus F. Strowitzki, *Losses in Magnetic switches*, Power Modulator Conference, 2002
[10] FERROXCUBE, Soft Ferrites and Accessories, Sep. 2004, S 41
[11] Claus F. Strowitzki, *Losses in Magnetic switches*, Power Modulator Conference, 2002
[12] Claus F. Strowitzki, *A SIMPLE METHOD TO SIMULATE MAGNETIC PULSE COMPRESSION*, Power Modulator Conference, 2004
[13] Claus F. Strowitzki, *A SIMPLE METHOD TO SIMULATE MAGNETIC PULSE COMPRESSION,* Power Modulator Conference, 2004
[14] Markus Erdorf, *Verlustanalyse in Festkörperschaltkreisen,* Diplomarbeit TuiLaser AG, Fachhochschule München FB06, S. 57 -61, 2004
[15] Markus Erdorf, *Verlustanalyse in Festkörperschaltkreisen,* Diplomarbeit TuiLaser AG, Fachhochschule München FB06,S. 61 -62, 2004
[16] Markus Erdorf, *Verlustanalyse in Festkörperschaltkreisen,* Diplomarbeit TuiLaser AG, Fachhochschule München FB06, S. 63, 2004
[17] Colonel WM.T. Mclyman, Transformer and Inductor Design Handbook, 3. Edition, Marcel Dekker, Inc. New York , Basel, 2004
[18] Rober M. Del Vecchio, Transformer Design Principles, Taylor &Francio, New York, 2002
[19] Manufacturer Data sheet, transistor A, transistor B, transistor C
[20] Manufacturer Data sheet, transistor A, transistor B, transistor C
[21] Manufacturer Date sheet, diode K, diode L, diode M
[22] Manufacturer Date sheet, diode K
[23] Patent, Cymer, US 6,240,112 B1
[24] Manufacturer Data sheet, transistor B